12/854
IN-34

# FINAL REPORT ON NASA GRANT NAG 3-634

## "COMPARISON OF UNL LASER IMAGING AND SIZING SYSTEM AND A PHASE/DOPPLER SYSTEM FOR ANALYZING SPRAYS FROM A NASA NOZZLE"

(Grant period: April 1, 1985 to August 19, 1987)

From

(NASA-CR-182437) COMPARISON OF UNL LASER IMAGING AND SIZING SYSTEM AND A PHASE/DOPPLER SYSTEM FOR ANALYZING SPRAYS FROM A NASA NOZZLE Final Report, 1 Apr. 1985 - 19 Aug. 1987 (Nebraska Univ.) 139 p    N88-16956
G3/34    Unclas 0121854

Dennis R. Alexander
Laboratory for Electro-Optical Measurements
Department of Mechanical Engineering
Room 255 WSEC
University of Nebraska-Lincoln
Lincoln, NE 68588-0525

## ABSTRACT

Research was conducted on aerosol spray characterization using a P/DPA and a laser imaging/video processing system on a NASA MOD-1 air-assist nozzle being evaluated for use in aircraft icing research. Benchmark tests were performed on monodispersed particles and on the NASA MOD-1 nozzle under identical laboratory operating conditions. The laser imaging/video processing system and the P/DPA showed agreement on calibration tests in monodispersed aerosol sprays of $\pm$ 2.6 $\mu$m with a standard deviation of $\pm$ 2.6 $\mu$m. Benchmark tests were performed on the NASA MOD-1 nozzle on the centerline and radially at one-half inch increments to the outer edge of the spray plume at a distance 2 feet (0.61 m) downstream from the exit of the nozzle. Comparative results at two operating conditions of the nozzle are presented for the two instruments. For the first case studied, the deviation in arithmetic mean diameters determined by the two instruments was in a range of 0.1 to 2.8 $\mu$m, and the deviation in Sauter mean diameters varied from 0 to 2.2 $\mu$m. Operating conditions in the second case were more severe which resulted in the arithmetic mean diameter deviating from 1.4 to 7.1 $\mu$m and the deviation in the Sauter mean diameters ranging from 0.4 to 6.7 $\mu$m.

Contents

List of Figures

List of Tables

## NOMENCLATURE

| Symbol | Description |
|---|---|
| A/D | Analog to Digital |
| AMD | Arithmetic mean diameter |
| CPM | Continuous pulse mode |
| D(10) | Arithmetic mean diameter |
| D(20) | Area mean diameter |
| D(30) | Volume mean diameter |
| D(32) | Sauter mean diameter |
| $D_d$ | Drop diameter |
| $D_b$ | Drop diameter at background |
| f | Disturbance frequency |
| GL | Gray level |
| $\lambda$ | Wavelength |
| MAGL | Measured average gray level |
| PBG | Particle boundary gradient |
| $\phi$ | Relative phase shift associated with P/DPA signals |
| PSP | Particle sizing program |
| q | Liquid flow-rate |
| SD | Standard deviation |
| SMD | Sauter mean diameter |
| SPM | Single pulse mode |
| T | Image threshold |
| $T_b$ | Image threshold just above background |
| $\vec{v}$ | Droplet velocity vector |

Section 1

# INTRODUCTION

Spray characterization is essential in many technologies. Improved cloud simulation for icing studies, increased efficiency for combustion technology, and design optimization of applicator nozzles for industry and agriculture are only a few areas which benefit from accurate spray measurements. The lack of a universally accepted calibration/verification standard and operating characteristics of sizing instrumentation has left the questions of accuracy and repeatability in spray measurements unanswered. Recently, various groups (e.g., ASTM Subcommittee E29.04 on Characterization of Liquid Particles, 1986 Droplet Technology Workshop, etc.) have addressed the question of accuracy and calibration in drop-size instrumentation, however no agreement has been reached with regard to methods or apparatus for standardizing drop-size measurement instruments [1]. The following work involves the evaluation of two instruments based on different drop-sizing techniques in side-by-side benchmark tests under identical operating conditions.

The non-intrusive nature of laser/optical techniques have shown the most promise in spray characterization. Of the three major types of laser/optical techniques (i.e., imaging, doppler anemometry, and laser-diffraction), the laser-diffraction method is most widely used, and probably the best known system is the Malvern instrument [2]. Doppler anemometry, however, is receiving more attention due to the recent development of Aerometric's P/DPA, which has an increased sizing range (35:1) [3,4], in comparison to the (10:1) range for visibility dependent Doppler anemometers [5]. With the use of real-time digital image processing to perform focus discrimination without correction, the University of Nebraska - Lincoln (UNL) laser imaging system [6-10] has shown the capability for true volumetric analysis. Previously, imaging systems, e.g., Weiss et al. [11], and others, have used depth of field corrections based on the maximum measured drop-size to "back-out" the number of smaller particles in a normalized volume. Processing time can be saved using this method, however the assumptions may lead to errors in obtaining accurate size characteristics. The above techniques vary in several areas; 1) sampling method (e.g., spatial vs. temporal), 2) probe volume (e.g., line of sight averaging, crossed beams, vs. focus volume), 3) instrument drop-size range and resolution, and 4) calibration and/or verification (e.g., reticles, monodisperse droplets, or polydispersions). Similarities shared by the imaging technique and the laser-diffraction method are that both are spatial sampling methods which allows for similar calibration (i.e., calibration reticle [7,12]). The similarity in probe volume of Doppler anemometers and imaging systems allow for verification and comparison with minimal correction. In this work, a P/DPA and a laser imaging system were evaluated by concurrently performing a set of baseline benchmark tests.

According to Tishkoff [13], chairman of ASTM Subcommittee E29.04 on Characterization of Liquid Particles, the four major areas of concern in spray characterization are instrumentation, sampling, data processing, and terminology. In the following work, the emphasis of the evaluation was placed on instrumentation (i.e., the setup and operation of the P/DPA, a temporal sampling instrument in ideal conditions, and the UNL laser imaging system, a true spatial sampling instrument). The difference in data acquisition or sampling method was minimized by overlapping the probe volumes of the two systems [14] and analyzing a spray under steady-state conditions (i.e., spray characteristics remain constant with respect to time). Data processing and terminology of the two systems closely follow the standard practices established by ASTM [15]. Taking into account the above criteria, the comparison of the P/DPA and the UNL laser imaging system was accomplished with minimal reduction of drop-size data.

The comparison of the P/DPA and the UNL laser imaging system is discussed in the following order; 1) experimental apparatus including the droplet sizing instruments, 2) procedure and operating conditions for the benchmark tests, 3) results obtained from the benchmark tests, and 4) conclusions as to the operation, data representation, and comparability of the two instruments.

Section 2

# EXPERIMENTAL APPARATUS AND PROCEDURE

The apparatus, used in the benchmark tests, consisted of a P/DPA [3,4], a laser imaging/video processing system (LI/VPS) [6-10], a MOD-1 nozzle [16], air and water supply systems (AWSS), and the measurement instrumentation used to monitor the operating conditions of the nozzle. Verification tests were performed using a Berglund-Liu vibrating orifice aerosol generator (VOAG) [17,18]. Operating conditions of the tested apparatus and the setup parameters for the sizing instruments are detailed.

## 2.1 P/DPA

Phase/Doppler Particle Analyzer theory and operation are described by Bachalo et al. in several references [3,4], therefore, only a brief description of the P/DPA components and operation follows. Setup features specific to this research are detailed with special attention given to the selection of appropriate photo-multiplier tube (PMT) gain voltage.

The P/DPA is a crossed beam laser Doppler anemometer (Fig. 2.1). The P/DPA transmitter utilizes a 10 mW He-Ne laser. The transmitter beam is split and the resulting beams are focused to a point by a convex lens. The Doppler fringes, formed at the crossed beam intersection, are relayed to the P/DPA receiver by the refracted light from a droplet passing through the crossed beam intersection. The P/DPA receiver uses a pair of convex lens to collect and focus the Doppler fringes from the passing droplet onto three PMTs, aligned parallel to the droplet's velocity vector ($\vec{v}$). The PMT voltages are filtered and amplified to remove the pedestal component of the burst and increase the differentiation of Doppler frequencies in the signal (Fig. 2.2). Particle size measurements are determined from the phase shift in the filtered Doppler signal.

Velocity measurements are taken identically to the laser Doppler velocimeter, but the P/DPA is very distinct in its method of particle size measurement. Bachalo et al. [4] have shown droplet size ($D_d$) to be dependent on the relative phase shift ($\phi$) associated with a Doppler signal incident on two adjacent PMTs.

With the operating conditions of the VOAG and the MOD-1 nozzle varying, the P/DPA also required adjustment in operating parameters. The following is a brief summary of the P/DPA setup parameters (Fig. 2.3). Parameters (A) and (B) are specified for the transmitter laser supplied by the manufacturer, and do not require adjustment. Hardware parameters of the P/DPA fixed for the duration of this work, specified according to reference [19], were; (E) the focal length of the transmitter lens used, was 495 $\mu$m for a measurable size range of 1 to 300 micrometers ($\mu$m), (F) the receiver was positioned 30° off the forward axis of the transmitter for sizing water droplets, (G) the refractive index was set for water, and (T) the Direct Memory Access (DMA), which allows for the storage of approximately 16,000 concurrent raw PMT signals for processing, was switched off

ORIGINAL PAGE IS
OF POOR QUALITY

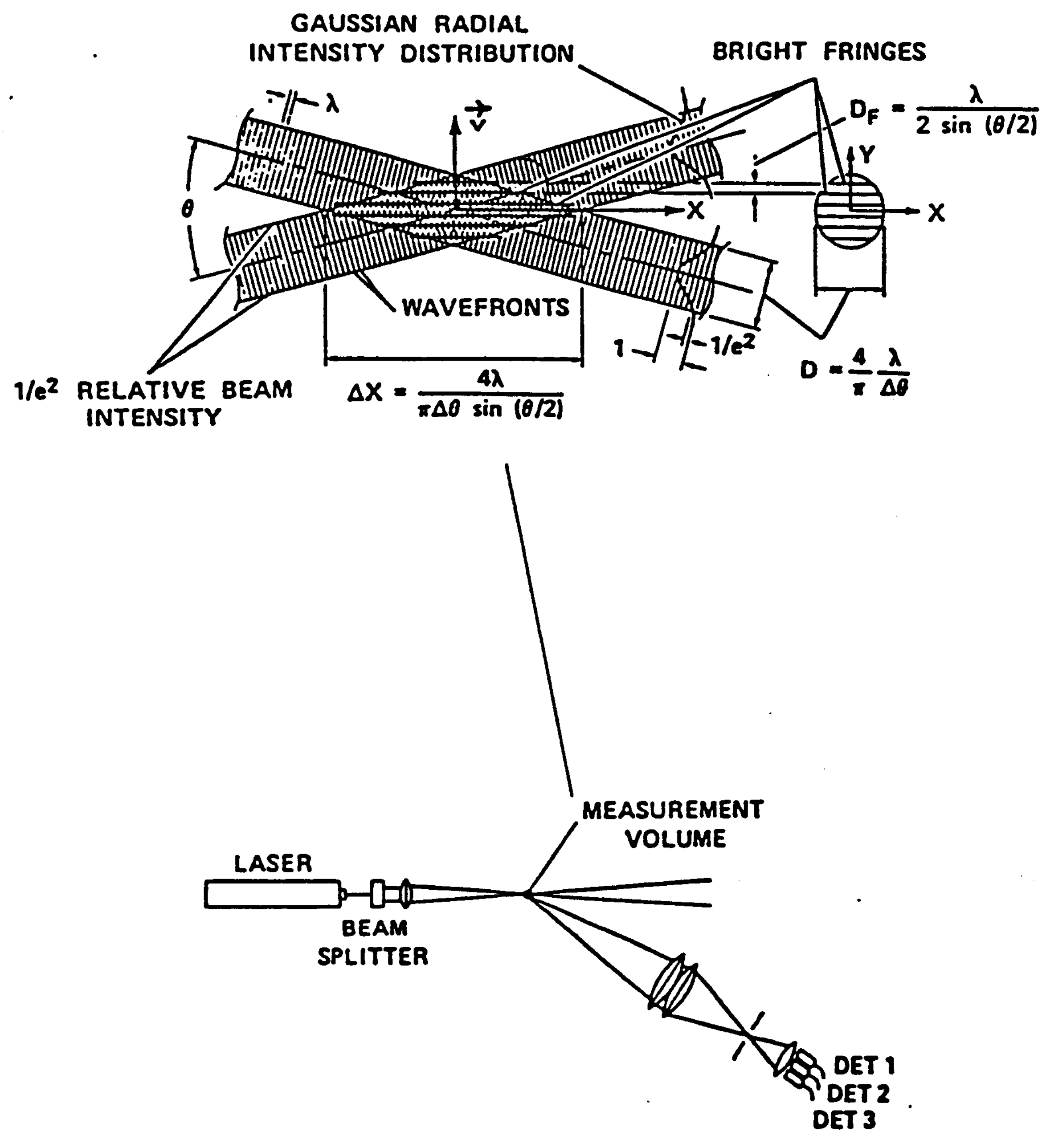


Figure 2.1: Phase Doppler/Particle Analyzer

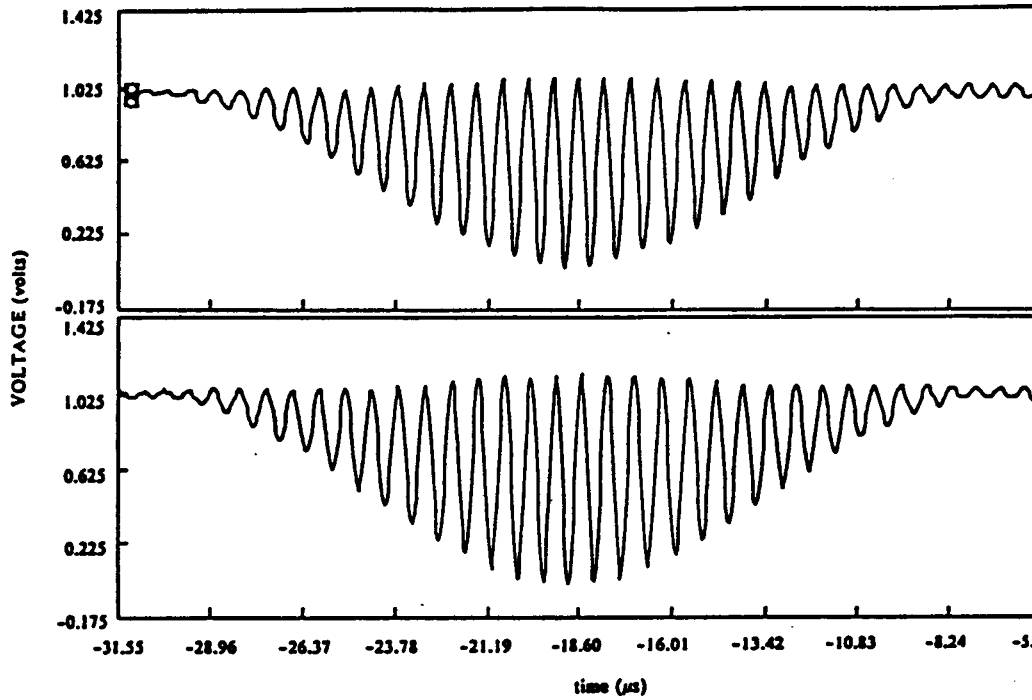


a. - Doppler Burst Signal from First Two PMTs.

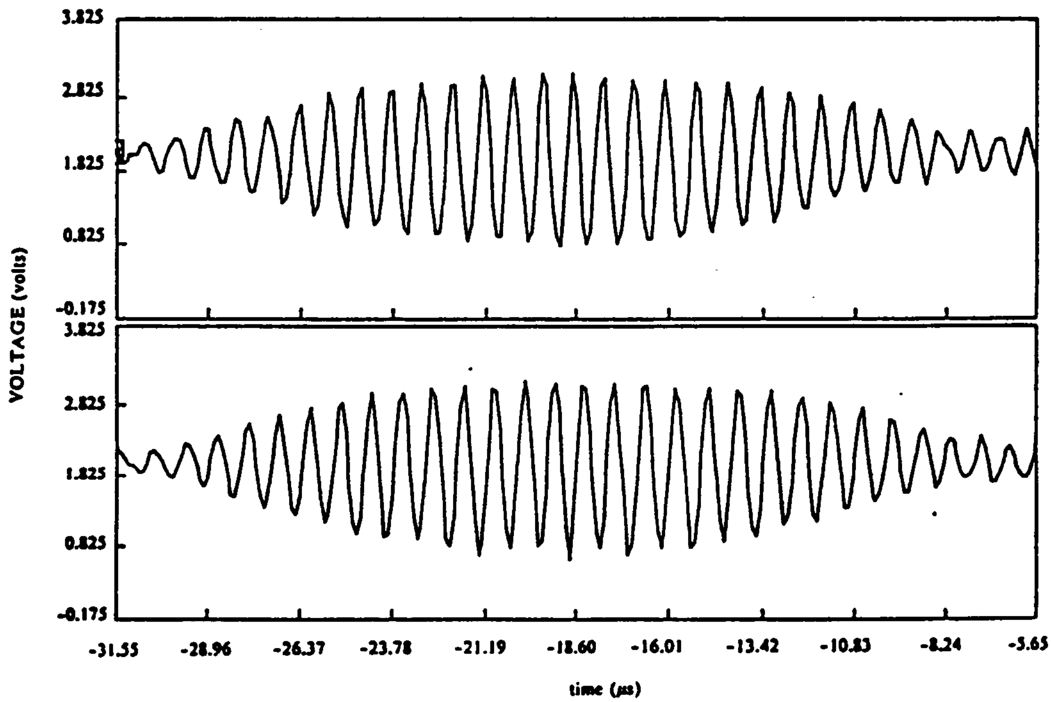


b. - Doppler Signals Filtered and Amplified.

Figure 2.2: P/DPA PMT Signals

```
(A) Wavelength= .6328 µm          P/DPA Version 2.6
(B) Beam Dia. = 2.5   mm          ~~~~~~~~~~~~~~~~~
                                  (M) High Pass Filter Increment
(D) Beam Sep. = 12.5              (N) High Pass Filter Decrement
(E) Xmit Lens = 495   mm              Filter No. 6  -  120  KHz

(F) Coll.Angle= 30    deg

(G) Refrc Indx= 1.33              (Q) Velo Max   =  7.7   m/s

(J) Size Max  =  98   µm          (R) Stop Mode = Samples
                                  (S) MaxSamples= 10000
                                  (T) DMA       = OFF

                                  (U) Data Drive= A
                                  (V) Filename  = TEMP
(L) High Volt = 300   volts       (W) Filenumber= 1
-----------------------------------------------------------------------
Current File   = A:TEMP_01.DAT    Size Span =  2.8- 360  µm
Beam Spacing   = 12.5 mm          Size Range=  2.8-  98  µm
Fringe Spacing= 25 µm
Beam Focus Dia= 159 µm            Velocity Span =  2.41 -   7.7  m/s
Nom Cycle Cnt = 6.3               Velocity Range=  2.41 -   7.7  m/s
 4  < Cycles <  19
               Parameter to change or <CR> to exit
```

Figure 2.3: P/DPA Setup Page

to facilitate the comparison with the LI/VPS. For this research, the beam separation, parameter (D), was alternated between 25 and 12.5 mm for the different spray size distributions generated (i.e., the beam separation and the transmitter lens' focal length specify the fringe spacing and number in the probe volume which, in turn, specifies a range of allowable drop-sizes to be measured). Other parameters, such as; (N) and (M) the high pass filter setting, (L) PMT voltage, (J) size, and (Q) velocity ranges are set according to the specific operating conditions droplet density, size distribution, etc.) of the VOAG or MOD-1 nozzle. The high pass filter allows only those Doppler signals with a frequency above a preset limit to pass on for further processing. The high pass filter setting is dependent on the average droplet velocity, and can be set by studying the count vs. velocity distribution. The selection of a high pass filter can be fine-tuned by using an oscilloscope to monitor the filtered PMTs for uniform signals with minimal distortion. The previous parameters are discussed in detail in the P/DPA operating manual.

The PMT gain voltage was to be set at a point just prior to PMT saturation. The above was accomplished by studying the saturation lights connected to each PMT. The saturation lights were to flash intermittently 50% of the time which implied approximately 1% saturation. Following the above procedure in performing an analysis on a high density spray, an inordinate number of large drops showed up in the analysis (Fig. 2.4). The large drops were determined to be false by concurrent studies by the LI/VPS and previous studies by NASA on the tested nozzle. According to Bachalo [20], the false drops were reflections or echoes in the PMTs caused by the high density of the spray, therefore, the PMT voltage should be set by stepping through the PMT voltage range (i.e., approximately 275 to 475 volts), and studying the number vs. size distribution for a point where little change occurs in the distribution shape (Fig. 2.5).

## 2.2 Laser Imaging/Video Processing System

The basic architecture of the LI/VPS has been described in detail by Ahlers and Alexander [8,9]. Ahlers [7] performed an analysis on static particles (e.g., polystyrene microspheres) situated in the plane of focus of the imaging optics. Further work by Wiles [10] described a technique for focus classification without depth of field corrections. The implementation of a particle sizing system capable of performing analysis on aerosol sprays has been the focus of the current research program. The following discussion is divided into sections covering: 1) components and operation, 2) drop sizing method, 3) calibration technique to minimize uncertainty due to camera tube non-linearities, 4) focus criteria, 5) modifications for dynamic measurements, and 6) software updates.

### 2.2.1 Components

The LI/VPS is divided into two subsystems, a laser imaging device and a video processor. The laser imaging device (Fig. 2.6) components are: a COHU camera system (control unit and camera), a Laser Energy Inc. (LEI) laser system (power supply unit and laser), a Laser Holography Inc. (LHI) control system (sync circuit and laser control unit), the imaging optics, a Panasonic NV-8950 or RCA VET650 VCR, a Panasonic TQ-2023 (A) laser/optical memory disk recorder (LDR), a Panasonic WJ-180 time/date generator, a Sony Trinitron monitor, a Sanyo monitor, and a back-up Molectron UV Series II Model UV12 (MUV12) $N_2$ laser. The video processor (Fig. 2.7) consists of a Recognition Concepts Inc. (RCI) Trapix 55/32 real-time image processor, a PDP 11/73 computer for control, and the processing software. A LSI-11/03 computer is also available for utility processing.

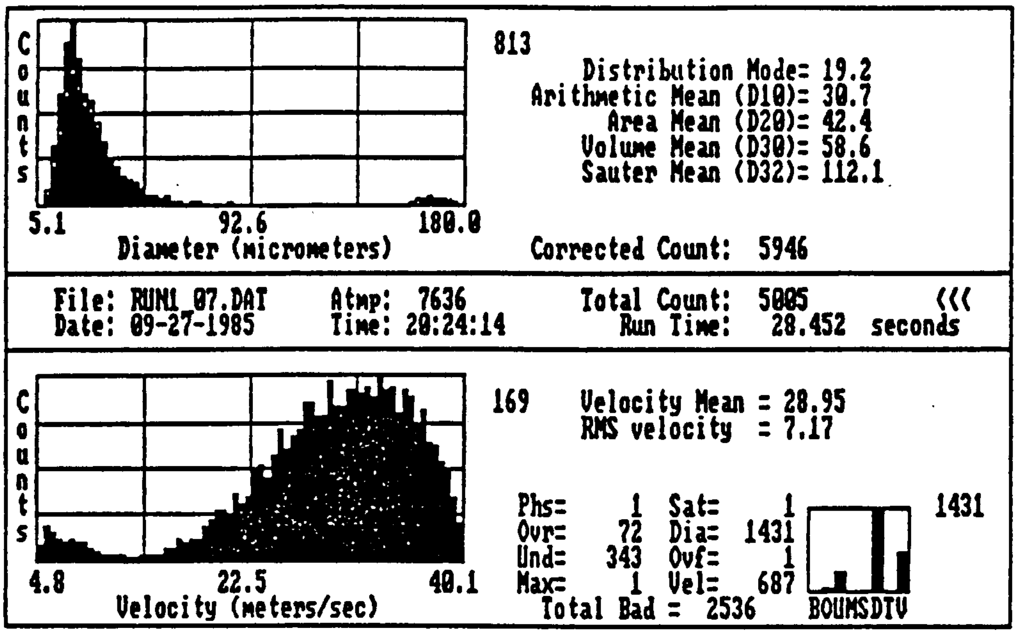


Figure 2.4: Reflections Caused by High Density Spray

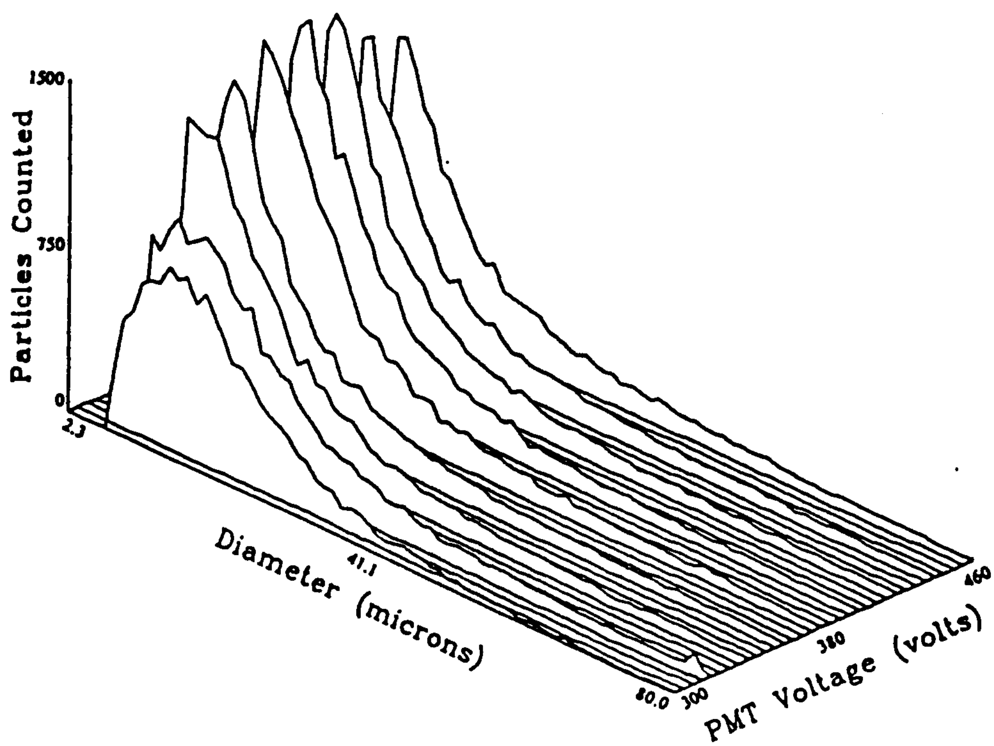


Figure 2.5: Drop Distribution Behavior with increasing PMT Voltage

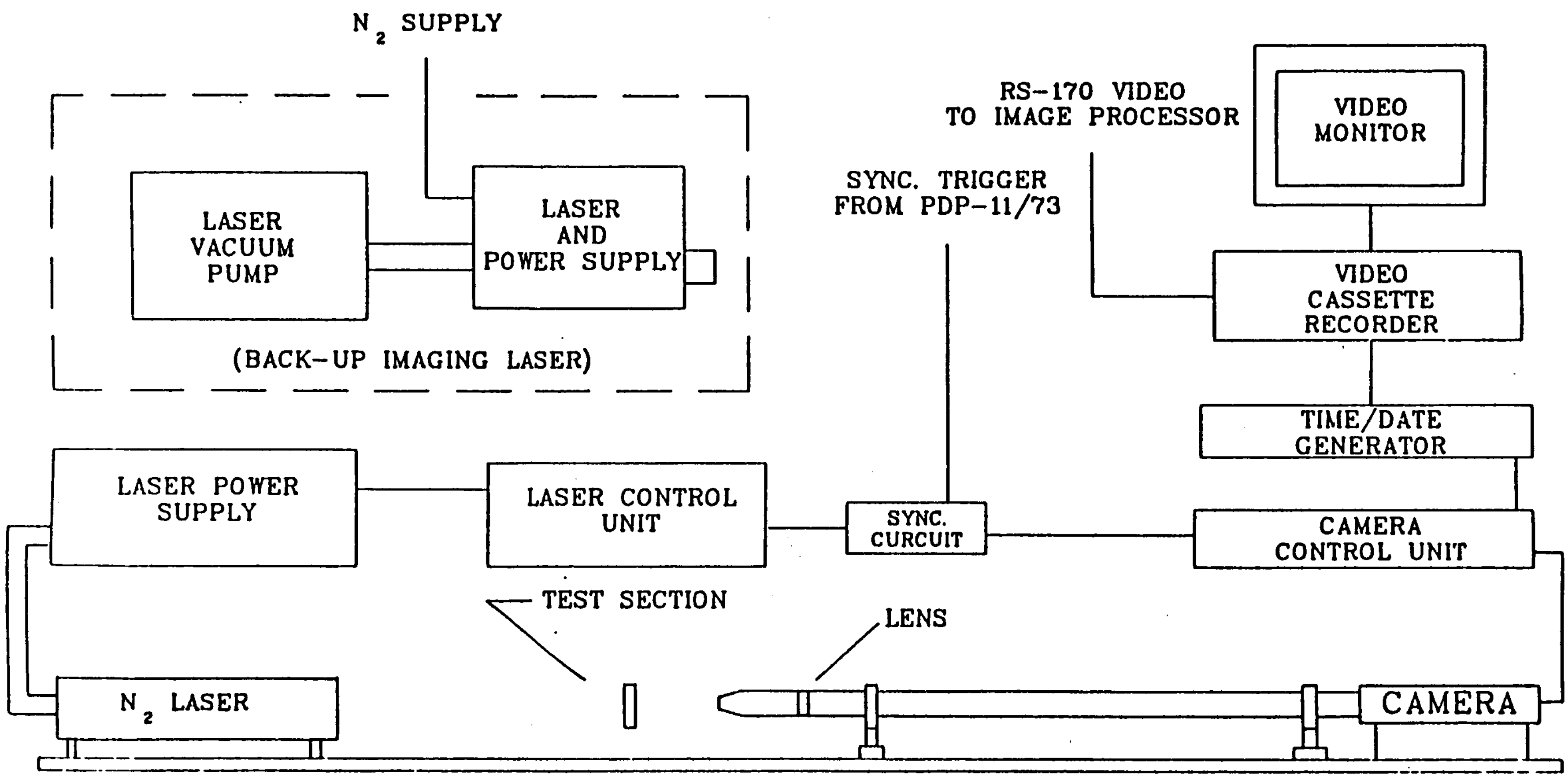


Figure 2.6: LI/VPS Laser Imaging Device

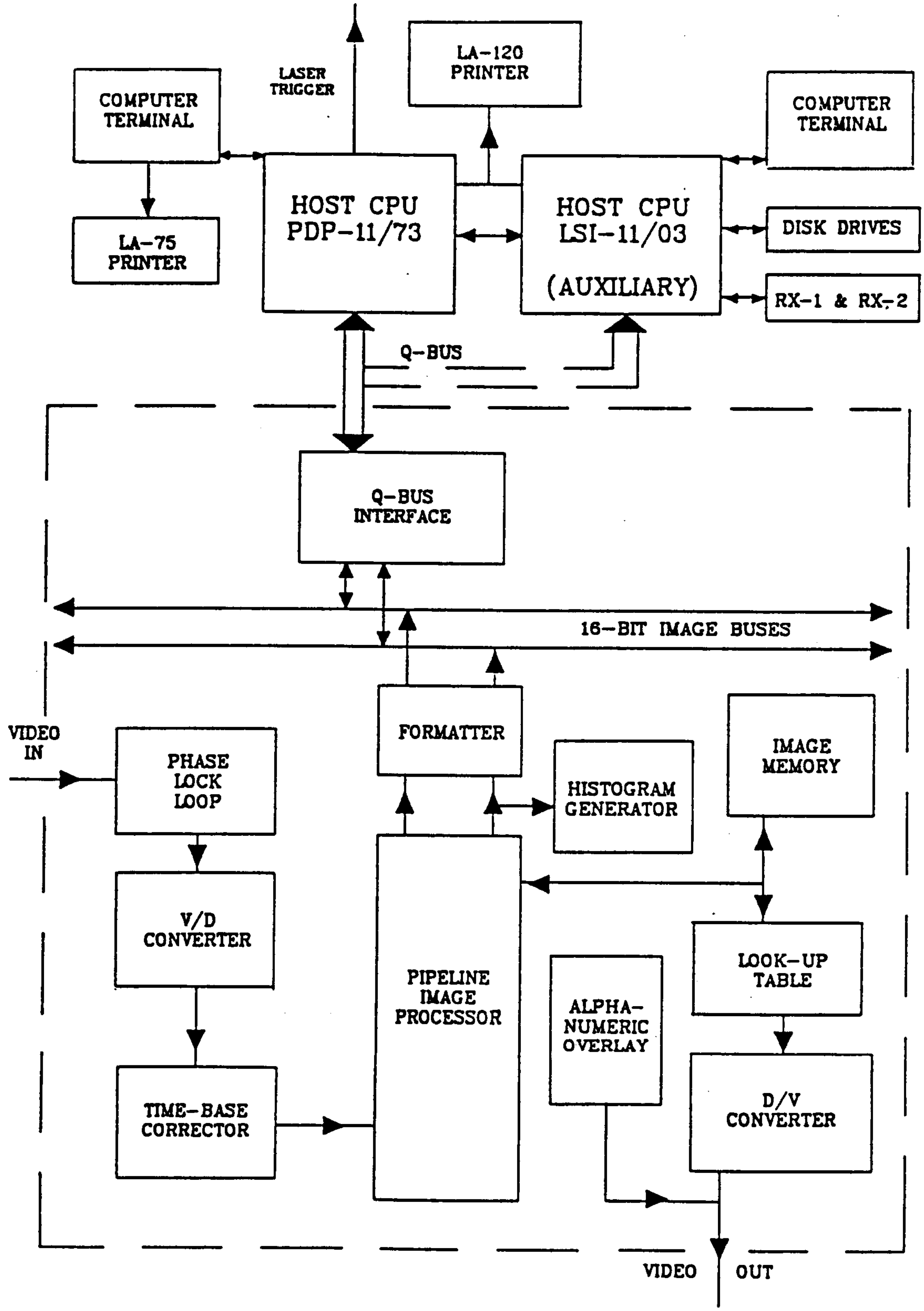


Figure 2.7: LI/VPS Video Processor Schematic

The baseline sync of the laser imaging system originates with the camera control unit (CCU). The CCU, operating on 60 Hz (line) cycle, drives the camera at video rates (i.e., one field every 16.67 milliseconds (ms) or one complete frame every 33.33 ms). The laser sync circuit (LSC); 1) receives the CCU triggering pulse, 2) uses the CCU trigger to generate a sync pulse for the laser, 3) sets the laser in sync with the camera process, and 4) sets the pulse rate of the laser to multiplies of 60 Hz (e.g., 30, 15, etc.), or allows the operator to pulse the laser manually or by computer control.

The LHI laser control unit has variable power settings with an internal sync generator. The LEI laser system consists of a Model N2-50 power supply and pulsed laser ($\lambda$ = 337 nm). The original system was operable within a range of 2-20 kW pulsed power and has been upgraded to 40 kW. By changing the mirrors in the laser tube, the pulse duration of the laser can be varied from either 3 nanoseconds (ns) or 10 ns. A second $N_2$ laser (MUV12) also contains its own internal sync generator, but the power cannot be varied. The MUV12 (laser and vacuum pump) has a peak power output of 250 kW and is limited to a pulse duration of 10 ns.

With the laser system in sync with the camera system, the object field is transferred to the camera by the imaging optics. A plano convex lens magnifies the object field before transferring the object field to the camera tube. System capabilities include a 500X and 1000X lens (i.e., 500X implies 800 by 800 micrometer ($\mu$m) field of view, and 1000X implies 400 by 400 $\mu$m field of view) for measurement. The video signal is than routed to a VCR where the images can be recorded for later viewing as a visual aid, or the images can be sent to the digital image processor. Other available options to the system are the use of the Panasonic time/date generator which overlays the time, date, and optional stopwatch capabilities on the analog video signal; and the availability of the Panasonic TQ-2023F LDR to store video frames which can provide for fast retrieval time without the tape positioning problems associated with a VCR.

The user interfaces with the LI/VPS at the PDP 11/73 console. Through the processing software, the user instructs the Trapix 55/32 to perform various logical and arithmetic operations on the images supplied by the laser imaging system. The Trapix 55/32 image processor has one megabyte of image memory which gives the processor available space to store four concurrent video frames. The PDP 11/73 computer controls the Trapix 55/32 through a parallel interface with a sub-library of control subroutines. The LSI-11/03 computer is also available for utility processing.

### 2.2.2 Sizing Method: Segmentation

The original software package developed by Ahlers [7] uses a technique called segmentation. The segmentation technique was adopted because sequential line by line processing is inherent to the camera system. The camera outputs a standard RS-170 composite video signal. The video signal is composed of 525 scan lines with interlace (i.e., odd and even scan lines interwoven into one complete frame). The segmentation technique uses the pattern recognition of the system (i.e., the conversion of the analog video signal into discrete pixels with specific intensity level and position) to analyze particles.

The premise of segmentation implies that discrete line segments, which lie adjacent to one another, can be summed into discrete two-dimensional objects. With the particles appearing as black disks on a white background in the digitized frame, the segmentation method finds the pixels upon which the particles reside and joins them into line segments (one pixel wide) in the line by line processing. The software matches the segments of the previous line to the current line until the objects are completely specified (Fig. 2.8(a)).

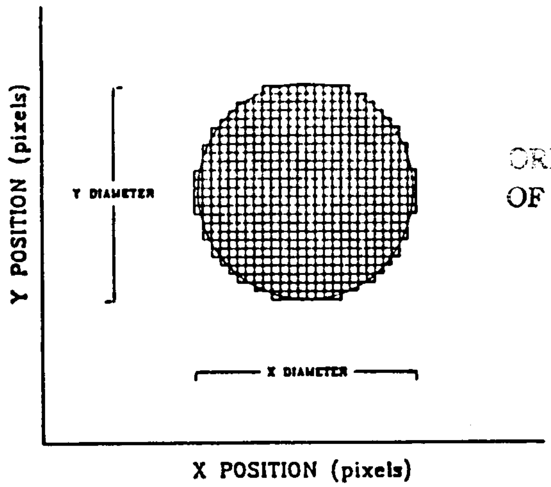




a. - Particle Characterized by Segmentation.

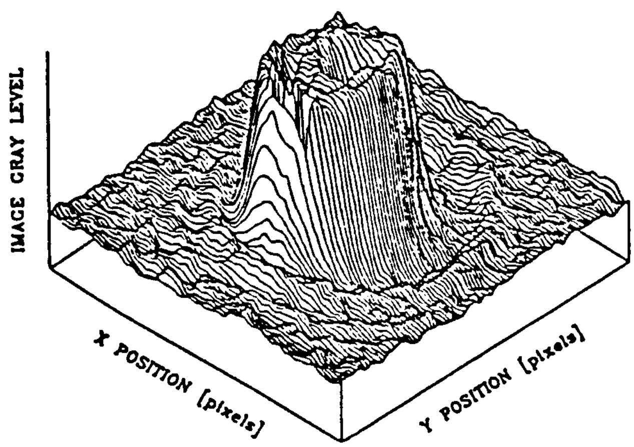


b. - Unthresholded Particle Image.

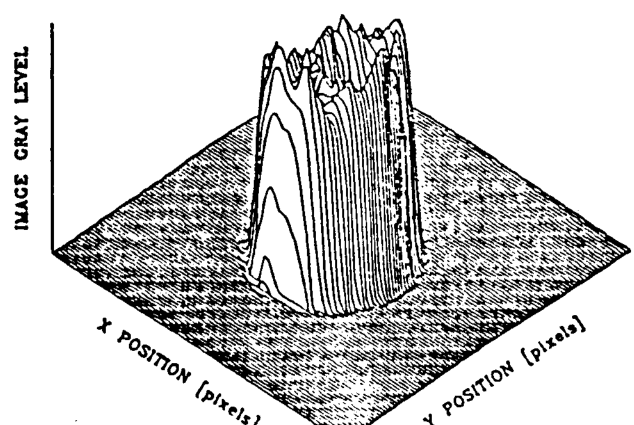


c. - Thresholded Particle Image.

Figure 2.8: LI/VPS Particle Representation

The Analog-to-Digital conversion is performed by the Trapix 55/32. The analog signal (i.e., video frame) is converted to a 512x512 array with array elements (i.e., pixels) that have eight bit precision (i.e., 256 grey levels). Ahlers showed the optimum threshold (T) was at a gray level of approximately 90 [7]. Figures 2.8(b) and 2.8(c), show the digitized particle before and after the thresholding process has been performed, respectively. After-which, with the subroutine, FINDTR, developed by Ahlers [7], the processor is able to find the transition which occurs at the 90 T. With the two transition points of a segment found, the program processes the remainder of the line until all segments are found. The above procedure is the basis for segmentation with program execution continuing in a line by line order.

### 2.2.3 Calibration

Previous work on the LI/VPS has included sections on calibration [7,10]. The initial work by Ahlers determined the qualifiers for calibration and specified an initial set of magnification correction factors (MCF). MCF qualifiers were the micron per pixel correction, the correction for non-linearities in the camera tube and the optimum value for the threshold of the image for sizing particles. The camera non-linearities initially were assumed to be dependent only on the x pixel location, this assumption required;

$$MCF = f(x). \tag{2.1}$$

Further work by Wiles showed improved accuracy by specifying MCFs with x and y dependence;

$$MCF = f(x, y). \tag{2.2}$$

In Ahlers' work, MCFs were determined by fitting experimental data points (i.e., x position, MCF) to the appropriate curve (i.e., straight line, exponential, etc.), whereas with Wiles' work, the MCFs as functions of x and y pixel position were found intuitively. In this researcher's work, calibration of the system became necessary after the COHU camera tube had to be replaced due to loss of sensitivity. Because the two-dimensional MCFs determined by Wiles were intuitive and specific to the replaced camera tube, a new method, which could be easily repeated, had to be deduced for determining the MCFs. Experimental data was discretized into 50 pixel intervals (Fig. 2.9), whereby the MCF was implied to be constant with respect to the x position in each interval;

$$MCF = \begin{cases} f1(y), & 50 \leq x < 100 \\ f2(y), & 100 \leq x < 150 \\ f3(y), & 150 \leq x < 200 \\ f4(y), & 200 \leq x < 250 \\ f5(y), & 250 \leq x < 300 \\ f6(y), & 300 \leq x < 350 \\ f7(y), & 350 \leq x < 400 \\ f8(y), & 400 \leq x < 450 \\ & \text{for } 50 \leq y < 450. \end{cases} \tag{2.3}$$

The above functions could than be found by curve- fitting the data (y position, MCF) specific to each interval. The following discussion is a description of the calibration method and procedure used.

The calibration method uses a calibration reticle (i.e., opaque disks in the form of thin metal films deposited on glass substrate) [12]. The configuration and particle size variation of the specific

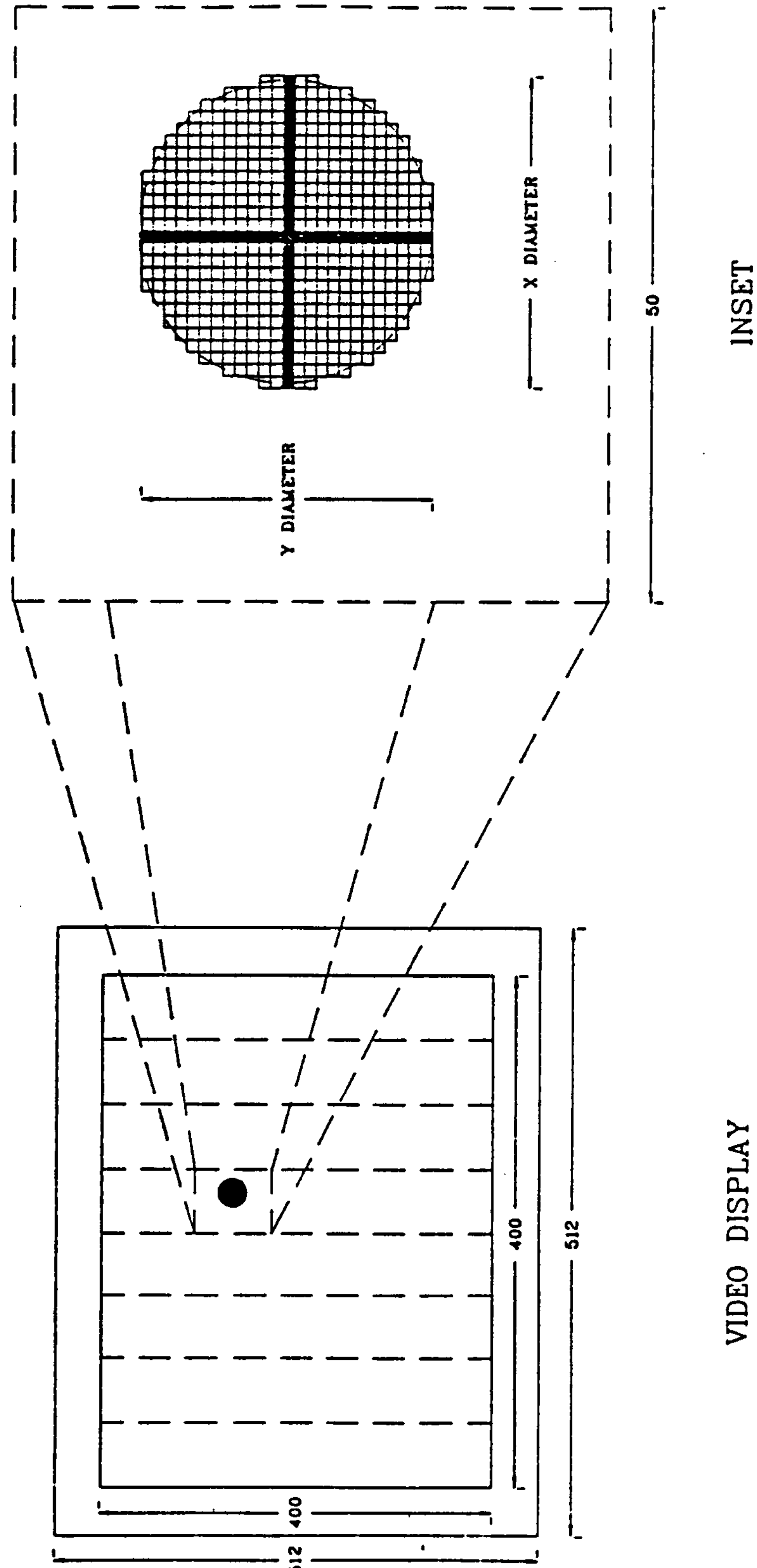


Figure 2.9: Two-Dimensional Calibration Technique

ORIGINAL PAGE IS
OF POOR QUALITY

reticle (Model #RR-50-3.0-0.08-102-CF-114) used in calibration are shown in Fig. 2.10 and Table 2.1. The range in diameter of the reticle particles is 5.29 $\mu$m to 92.75 $\mu$m. The calibration reticle is well suited for the LI/VPS because it can easily be positioned in the plane of focus of the imaging optics, eliminating the need for depth of field correction.

The calibration procedure uses a revised version of the Particle Sizing Program (PSP) developed by Ahlers [7]. The modified PSP is setup to collect data (i.e., particle position, x and y pixel diameters, etc.) for a prescribed opaque disk from the calibration reticle. With the calibration reticle in the focal plane of the imaging optics, the calibration program is started. The calibration reticle is then positioned randomly throughout plane of focus with the program storing the data simultaneously. With the known diameter, the MCFs are found by Equation (2.4);

$$MCF = \frac{\text{True diameter } (\mu m)}{\text{Measured diameter (pixels)}} \tag{2.4}$$

The calculated MCF is then specified according to the particle's center position. The data is then sorted into the perspective 50 vertical pixel intervals, and then each set of data (i.e., y pixel position, x MCF, and y MCF) is sorted according to y pixel position. With the correction factors specified as dependent variables of the y pixel position, the data can be set to the best fit curve. Figure 2.11 is a flow diagram of the aforementioned procedure. The above procedure was carried out for the 500X and the 1000X lens. The use of a different particle from the calibration reticle being the only change in the procedure. Because the MCFs are determined in the procedure as average values over the total diameter of the particle, the appropriate particle had to be chosen to avoid excessive overlapping of calibration intervals. Also, to avoid the edge effect (i.e., pixel elements being discrete implies pixels can be on or off depending on the position of the true particle's edge), the largest available particle should be chosen.

Preliminary work showed that approximate MCF for the 500X lens was 2.1 $\mu$m/pixel, and conversely, 0.98 $\mu$m/pixel for the 1000X lens. As implied above for the 50 pixel intervals, a calibration particle diameter of 25 pixels would minimize interval overlap and edge effects. Therefore, for 500X lens, the #16 particle (i.e., 52.5 $\mu$m) was used, and conversely, for the 1000X lens, the #7 particle (i.e., 23.90 $\mu$m) was used. The results of the above procedure and a comparison of previous system calibrations with the present calibration is presented in Section 3.1.

### 2.2.4 Focus Method

Ahlers [7] performed work using polystyrene micro-spheres restrained between two glass microscope slides positioned in the plane of focus of the imaging optics. The above tests verified the methodology and calibration of the LI/VPS. As with most complex systems, development occurs in stages, therefore Ahlers constructed a particle sizing system which performed analysis on static and semi-static particles in the focal plane of the imaging optics with good accuracy. Wiles [10], in the next stage in the development of the LI/VPS, defined a method of focus classification (i.e., particles unaffected by diffraction light scatter). As Fig. 2.12 shows, with a diffraction limited system, particle focus is dependent on the particle's boundary gradient and it's relative intensity as compared to background. Because of the 8-bit precision of the video processor, the particle's intensity level with respect to background could be used as a viable criteria for focus. The particle's boundary gradient (PBG) was used as a secondary test because it rejects large out of focus particles which appear as small particles in focus by the particle intensity level test [10].

With the 256 grey level resolution and the processing capabilities of the video processor, the focus parameters are determined. The particle's intensity level or measured average grey level

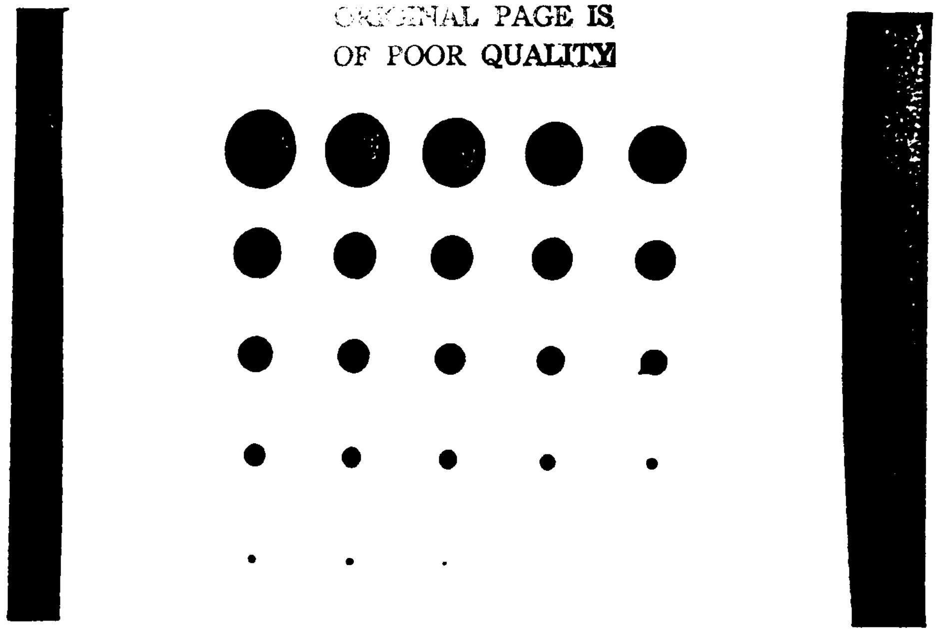

**a. - Video Image of Calibration Reticle.**

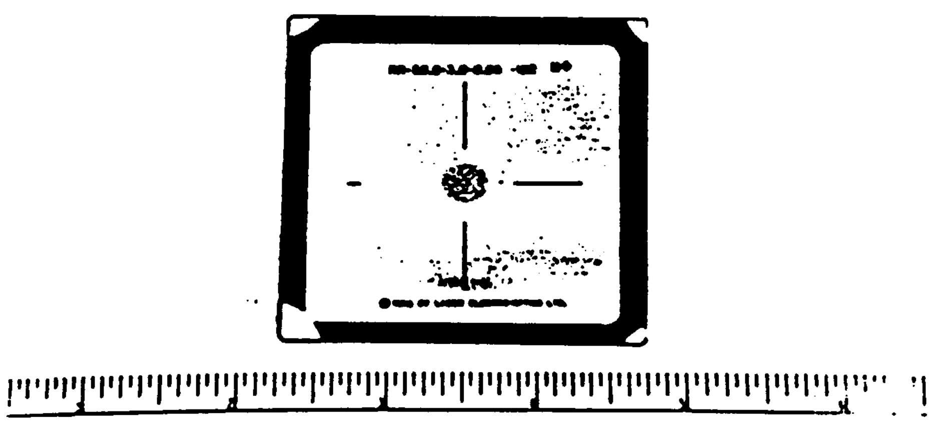

Figure 2.10: Calibration Reticle

Table 2.1: Specification Sheet for Calibration Reticle

CALIBRATION RETICLE : RR-50-3.0-0.08-102-CF - #114

FINAL DATA SHEET[1]

| | DIAMETER ($\mu$m)[2] | NUMBER | AREA FRACTION | VOLUME FRACTION |
|---|---|---|---|---|
| 1 | 5.29 | 2898 | 0.015 | 0.002 |
| 2 | 6.81 | 776 | 0.006 | 0.001 |
| 3 | 8.98 | 895 | 0.013 | 0.003 |
| 4 | 11.93 | 1171 | 0.030 | 0.009 |
| 5 | 17.20 | 1009 | 0.054 | 0.023 |
| 6 | 21.33 | 642 | 0.053 | 0.028 |
| 7 | 23.90 | 456 | 0.047 | 0.028 |
| 8 | 26.71 | 505 | 0.065 | 0.043 |
| 9 | 31.11 | 396 | 0.069 | 0.054 |
| 10 | 34.17 | 280 | 0.059 | 0.050 |
| 11 | 37.07 | 306 | 0.076 | 0.070 |
| 12 | 40.47 | 240 | 0.071 | 0.072 |
| 13 | 42.71 | 207 | 0.068 | 0.073 |
| 14 | 47.37 | 160 | 0.065 | 0.077 |
| 15 | 50.39 | 106 | 0.049 | 0.061 |
| 16 | 52.50 | 109 | 0.054 | 0.071 |
| 17 | 56.23 | 96 | 0.055 | 0.077 |
| 18 | 60.70 | 88 | 0.058 | 0.089 |
| 19 | 67.04 | 58 | 0.047 | 0.079 |
| 20 | 73.48 | 27 | 0.026 | 0.048 |
| 21 | 80.58 | 11 | 0.013 | 0.026 |
| 22 | 86.99 | 4 | 0.005 | 0.012 |
| 23 | 92.75 | 1 | 0.002 | 0.004 |
| | TOTAL | 10441 | 1.000 | 1.000 |

| | | |
|---|---|---|
| D(10) = 17.81 $\mu$m | D(20) = 23.04 $\mu$m | D(21) = 29.73 $\mu$m |
| D(30) = 27.69 $\mu$m | D(31) = 34.48 $\mu$m | D(32) = 40.01 $\mu$m |

[1] Reproduced from specification sheet supplied by the manufacturer.

[2] Diameters traceable to NBS Part. #52577, accurate to ± 2 $\mu$m (± 3% for D > 70 $\mu$m)

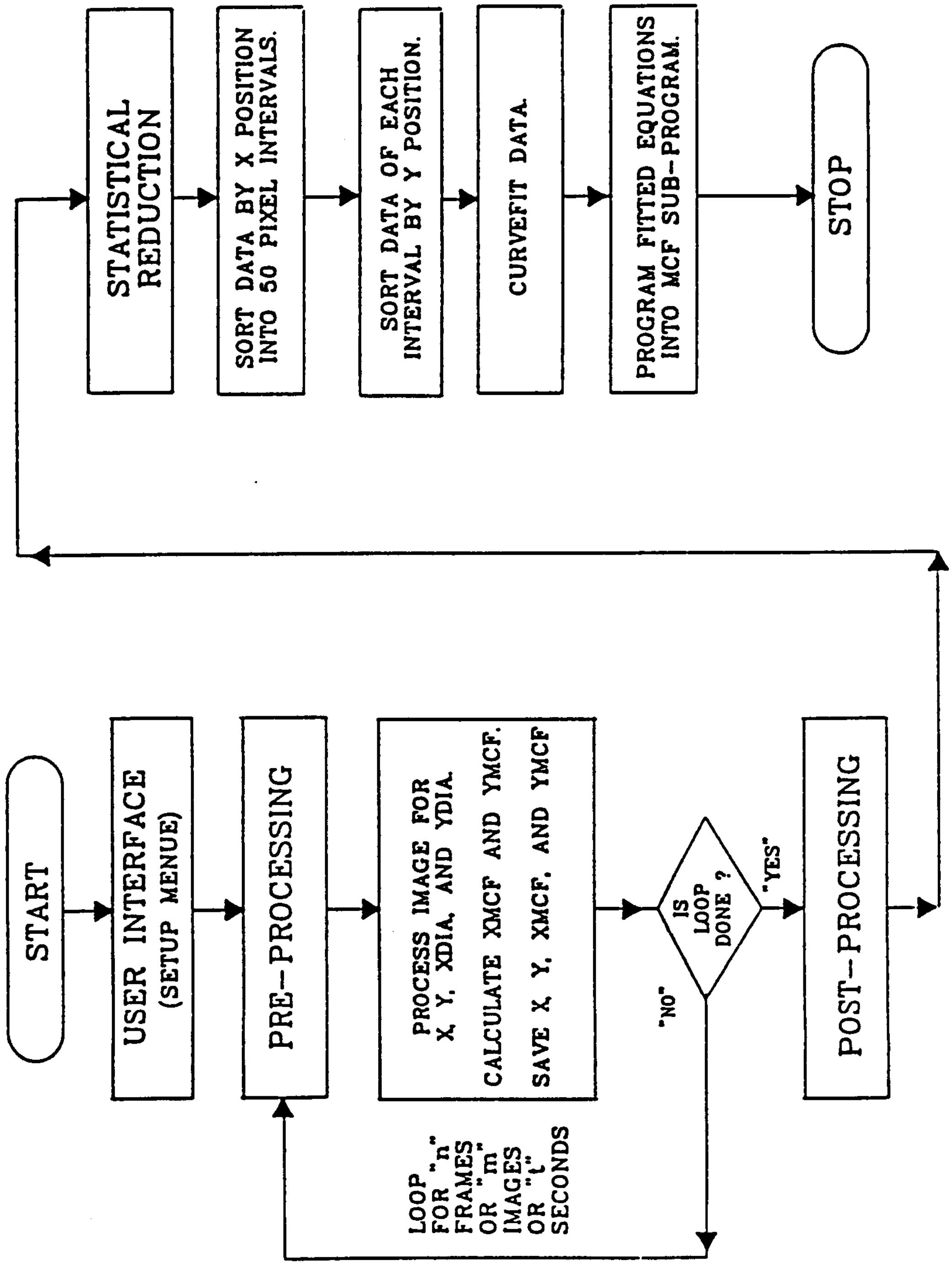


Figure 2.11: Flow Diagram for Calibration Procedure

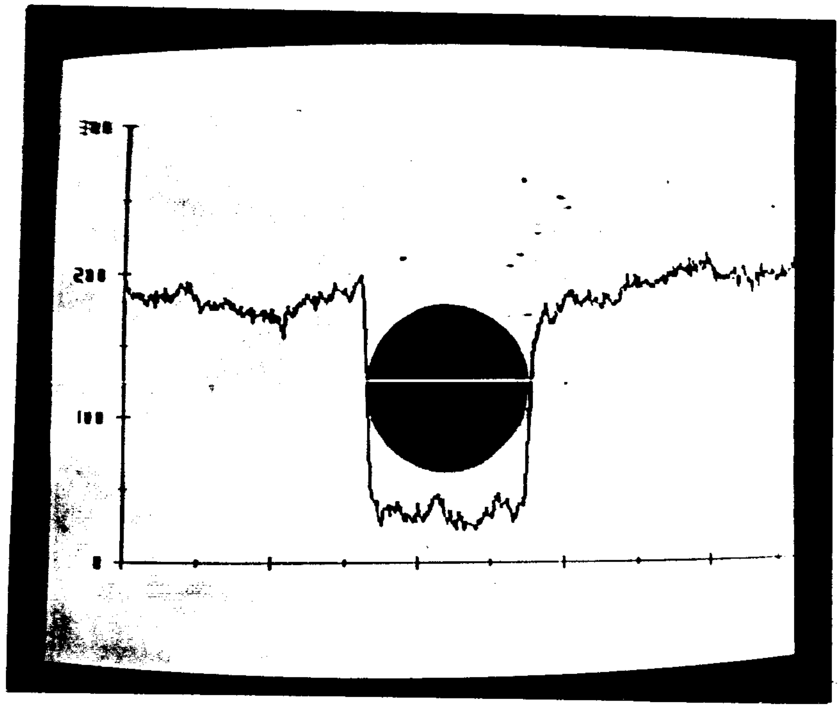

In-focus 92.75 $\mu m$ Particle.

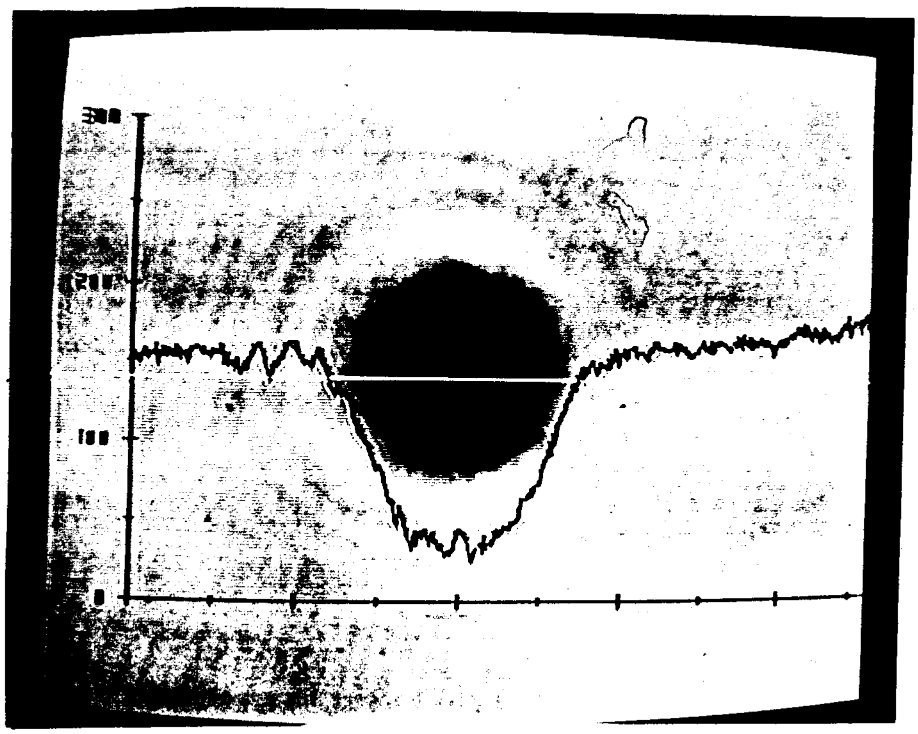

Out of Focus 92.75 $\mu m$ Particle.

Figure 2.12: LI/VPS Focus

(MAGL [10]) is calculated by thresholding the image at the optimum value (i.e., 90 T as specified by Ahlers), summing the pixel grey levels (GL) corresponding to specific particles as specified by segmentation, and dividing by the total number of pixels per particle (Equation 2.5).

$$MAGL = \frac{\sum_{i,j} GL(i,j)}{\sum_{i,j} \text{Pixel}(i,j)} \tag{2.5}$$

The PBG is determined by thresholding the image twice, once at 90 T, and the second, just below background ($T_b$). Referring to Fig. 2.12, the double threshold specifies the particle boundary gradient by:

$$PBG = D_d - D_b, \tag{2.6}$$

where $D_b$ is the particle diameter at $T_b$. With the above parameters, focus was specified for a volume centered on the focal plane of the transfer lens. First, a relation, constant with respect to focal volume, was determined for the MAGL with dependence on particle diameter, and second, the PBG was specified as a constant over the range of particle diameters specified by the MAGL criteria.

In conclusion, Wiles developed a focus criteria for the LI/VPS. In his follow-up tests, the criteria defined a depth of focus which remained fairly constant when tested with the reticle and the polystyrene spheres (i.e., 52.5 $\mu$m as specified earlier). The prescribed depth of focus was approximately 400 microns. It should be noted, Wiles' focus classification was determined and tested with the laser pulsing at 60 Hz. Thus, the focus criteria specified a depth of focus and classified particles based on grey level intensity from these operating conditions.

### 2.2.5 Modifications

The final goal of this research was the implementation of a particle sizing system capable of performing analysis on two- phase flow (e.g., aerosol sprays). The LI/VPS has been developed in stages; (1) Ahlers' initial work, hardware and software setup, (2) Wiles' work on system focus classification, and (3) the the current adaptation of the system to process truly dynamic particles in a real spray. To clarify the above statement, previous work by Ahlers and Wiles was performed with the LI/VPS operating in the continuous pulse mode (CPM), as opposed to the current work in the single pulse mode (SPM) (i.e., CPM suggests the imaging laser is pulsing at 60 Hz. in sync with the camera, and SPM implies the imaging laser is off until the video processor requires a new frame to process at which time the imaging laser is pulsed). The following discussion covers the reasoning and implementation of the SPM, and the adaptation of the previous work to function in the SPM.

All previous work on the LI/VPS was done in the CPM, therefore the system had to be converted to the SPM. The reasoning for the conversion is shown in Fig. 2.13. The two graphs were taken with the system in the CPM; the only difference being the bottom particle is dynamic whereas the top particle is stationary. As shown, there is a significant reduction in intensity for the dynamic particle as opposed to the stationary particle. The above behavior is due to the camera tube's ability to refresh between successive frames. In the CPM, the dynamic particle being frozen by the 10 ns laser pulse is present in the field of view for less than 16.67 ms (i.e., the time necessary to complete one field), but the static particle in the CPM shows greater intensity because of the cumulative effect of the particle blanking out the same area on the camera tube. The behavior being time-dependent implies the camera tube reaches a constant intensity after a sufficient amount of time. Because the software was developed for the system operating in the CPM, and all previous

ORIGINAL PAGE IS
OF POOR QUALITY

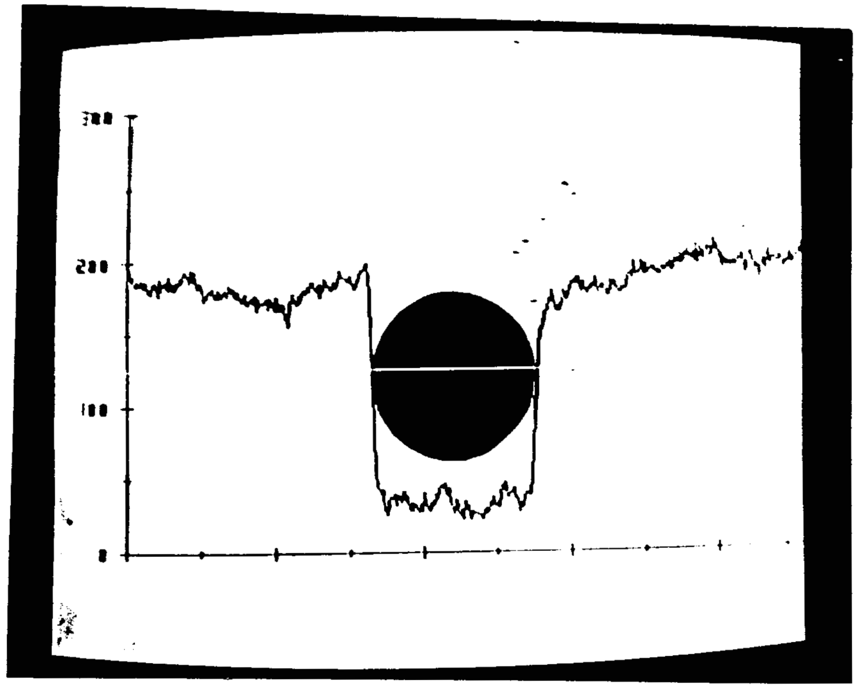


a. - Static 92.75 $\mu m$ Particle in the CPM.

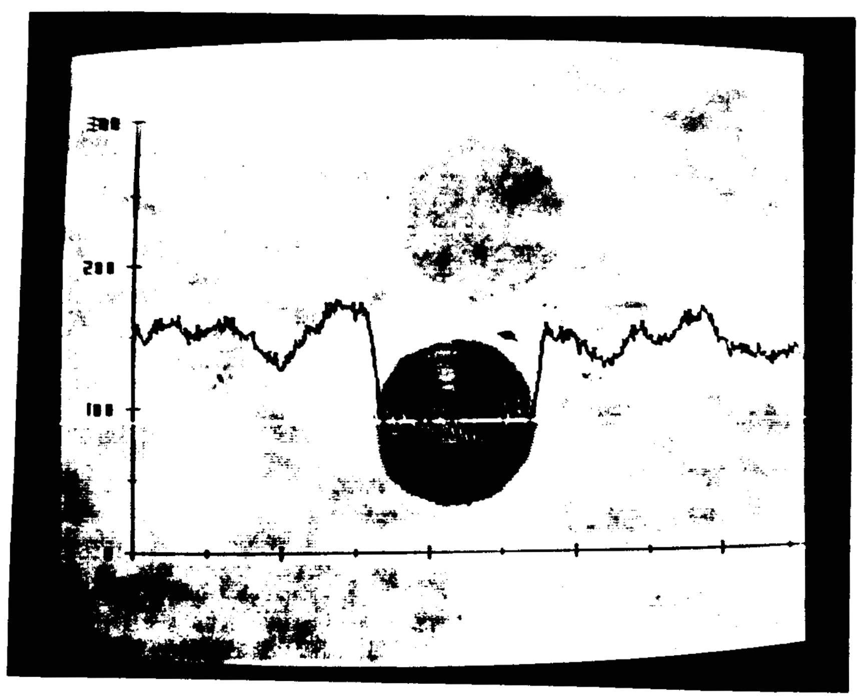


b. - Dynamic 92.75 $\mu m$ Particle in the CPM

Figure 2.13: Static vs. Dynamic Particle Representation in CPM

work was performed on static particles (i.e., particles which have motion but appear static to the system), the system had to be adapted to size dynamic particles. Revision to the system could be achieved by either changing the system software, or changing the system hardware. Figure 2.14 shows the, MAGL vs. particle size, focus classification curves. As is shown, the '*dynamic*' curve is less distinct than the '*static*' curve. Because of the added ambiguities in the '*dynamic*' curve, a method had to be determined to simulate the behavior of the stationary particles for the dynamic particles.

Because of the amount of work put into the development of the system software and the success of the focus criteria, a hardware modification was selected to accomplish the intensity contrast in dynamic particles. The SPM was found to exhibit the same characteristic intensity in the dynamic particles as found in static particles, in fact, the contrast between particle and background was greater. The SPM was accomplished by; (1) sending a trigger signal from the control computer to the LSC, (2) the LSC triggers the $N_2$ laser, (3) the laser pulses, and (4) the image processor grabs the frame just illuminated. The above procedure was accomplished by the development of a triggering circuit (APPENDIX B). The above procedure is then followed by normal program execution. The flow diagram in Fig. 2.15 shows the SPM integrated into the PSP with software modification.

The software had to adapted to handle the SPM. As stated previously, the use of the SPM produced even greater contrast between the particle image and background. Because of the greater contrast, it was necessary to redetermine the focus criteria. Using the procedure outlined by Wiles [10] (Section 2.2.4), the MAGL curve and the PBG criteria were determined in the SPM. MAGL curves for both the CPM and the SPM are represented in Fig. 2.16. As shown in the figure, the larger particles show greater contrast whereas the smaller particles contrast is unaffected by the SPM. The focus criteria was determined for both the 500X and 1000X lens. The LI/VPS, at this point, was capable of performing size measurements in a two-phase flow.

### 2.2.6 Software Updates

With PSP performing analysis on two-phase flows, the software had to be updated to allow for varying conditions in the measurement analysis. Parameters, such as the sizing window specifications, output destination, etc., were queried for before processing each time the program was executed and others, such as lens magnification, were set by changing the FORTRAN code. A menu type of setup (Fig. 2.17) was adopted to minimize setup time and to aid the operator in determining the most appropriate sizing conditions (APPENDIX C.1).

In aerosol sprays, the mean diameters (APPENDIX D) determined from the count vs. drop-size data are the most common method of characterization. Characterization by mean diameters is misleading when a single mode (i.e., Gaussian distribution) is not the case, therefore the actual count vs. drop-size distribution is also used to characterize aerosol sprays. Because of the aforementioned reasoning and the unavailability of a suitable graphics package for the LI/VPS, a graphic algorithm was developed. The algorithm was coded into a FORTRAN subroutine (APPENDIX C.2 ) for the PSP with a DEC VT240 terminal for graphic simulation (Fig. 2.18(a)) and a DEC LA75 printer for hard-copies (Fig. 2.18(b)).

## 2.3 Spray Test Facility

Figure 2.19 shows the configuration of equipment for the spray characterization tests. The tests were performed in the horizontal direction due to the positioning of the sizing instrumentation.

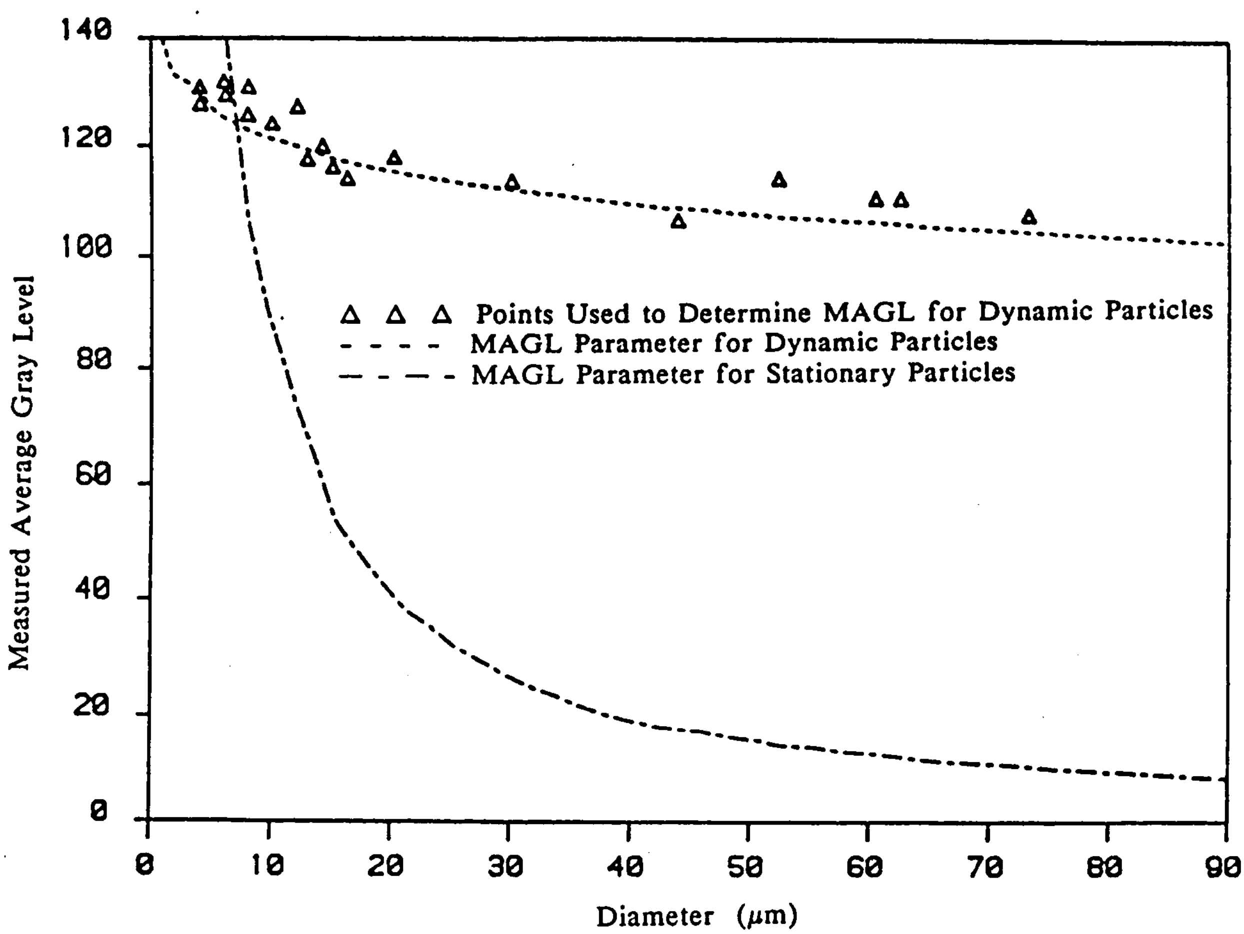


Figure 2.14: Comparison of the MAGL Parameter for Dynamic and Stationary Particles in CPM

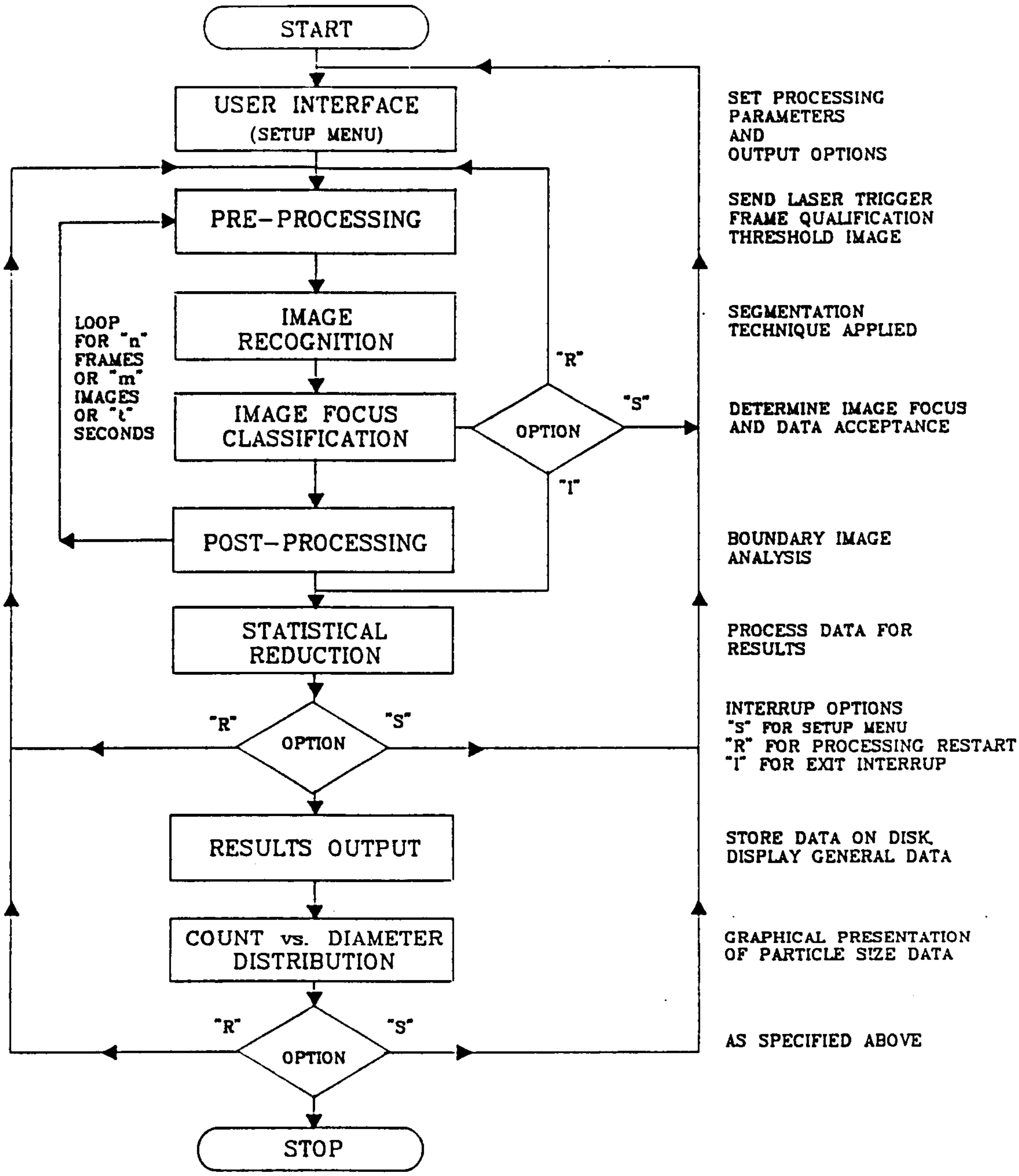


Figure 2.15: Flow Diagram for the Particle Sizing Program in SPM

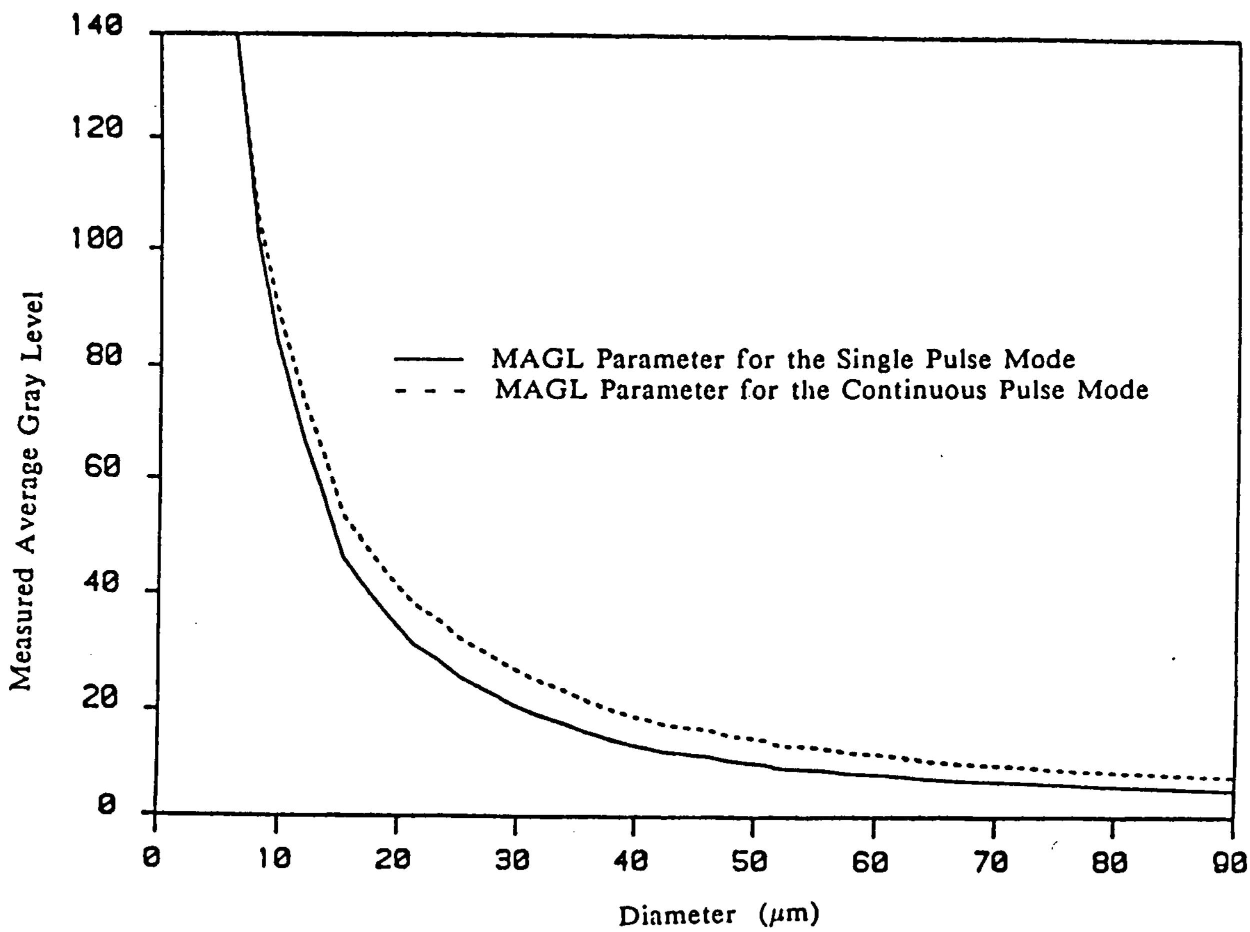


Figure 2.16: Comparison of the MAGL Parameter for SPM and CPM

ORIGINAL PAGE IS
OF POOR QUALITY

```
                                 SETUP
                      PARTICLE SIZING PROGRAM (ver. 4)
-------------------------------- PROCESSING OPTIONS ------------------------
 (A)   DYNAMC    Type of Processing           (STATIC/DYNAMIC)
 (B)   YES       Focus Criteria               (YES/NO)
 (C)   AUTO      Type of Frame Advance        (AUTO/SINGLE)
 (D)   PARTCL    Processing Limit             (TIME/FRAME/PARTICLE)
 (E)  (  1000)   Limiting Value               (seconds/frames/particles)
 (F)   REJECT    Boundary Particles           (PROCESS/REJECT)
----------------------------------- OUTPUT OPTIONS -------------------------
 (G)   YES       General Results (to PRINTER) (YES/NO)
                 WRITE TO FILE (YES/NO)       (K) FILE HEADER (4 lines)
 (H)   NO        Average Particle size data -- (L) FILE:  (TEMP01).OUT
 (I)   NO        Group Breakdown data ---------/
 (J)   YES       Per Frame data -------------> (M) FILE:  (TEMP01).DAT
---------------------------------- GENERAL OPTIONS -------------------------
 (N) Group Start =(   5)   (O) Group Width =( 5.0)   (P) # of Groups =(  68)
 (Q) X Window Start = ( 50)                   (R) X Window Width  =  (450)
 (S) Y Window Start  =  ( 50)                 (T) Y Window Width = (450)
 (U) Threshold = ( 90)     (V) Lens = HIGH    (W) Markers = NO   (YES/NO)
----------------------------------------------------------------------------
 (X) to exit SETUP menu or  (Z) to begin Partical Sizing Program ....
 Enter Letter to change specific Parameter ??
```

Figure 2.17: PSP Setup Page

ORIGINAL PAGE IS
OF POOR QUALITY

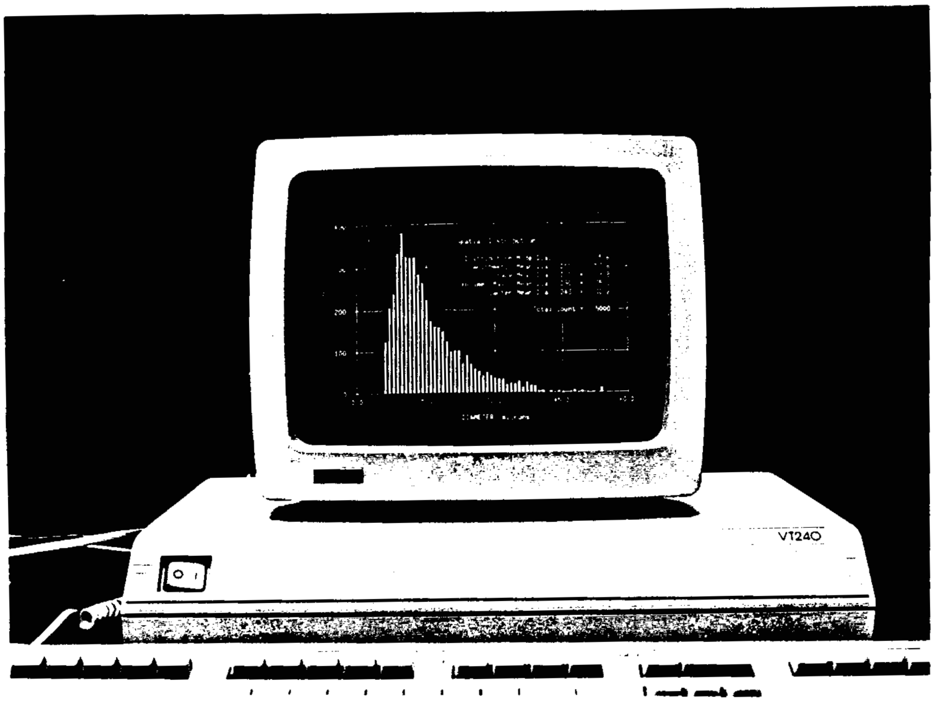


a. - DEC VT240 Terminal for Screen Emulation.

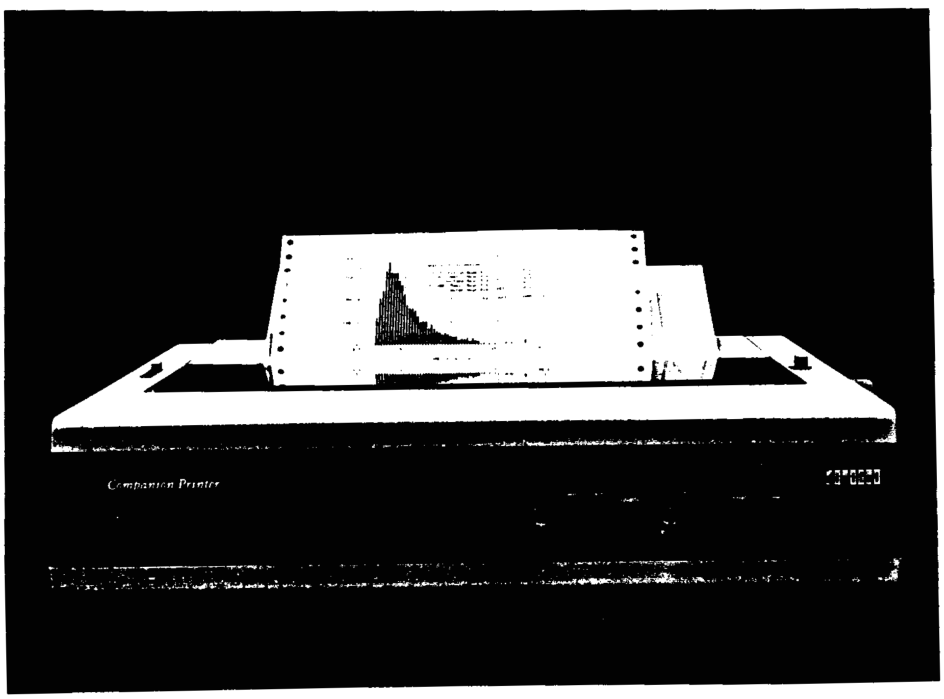

b. - DEC LA75 Printer for Hard-copys.

Figure 2.18: PSP Graphic Package

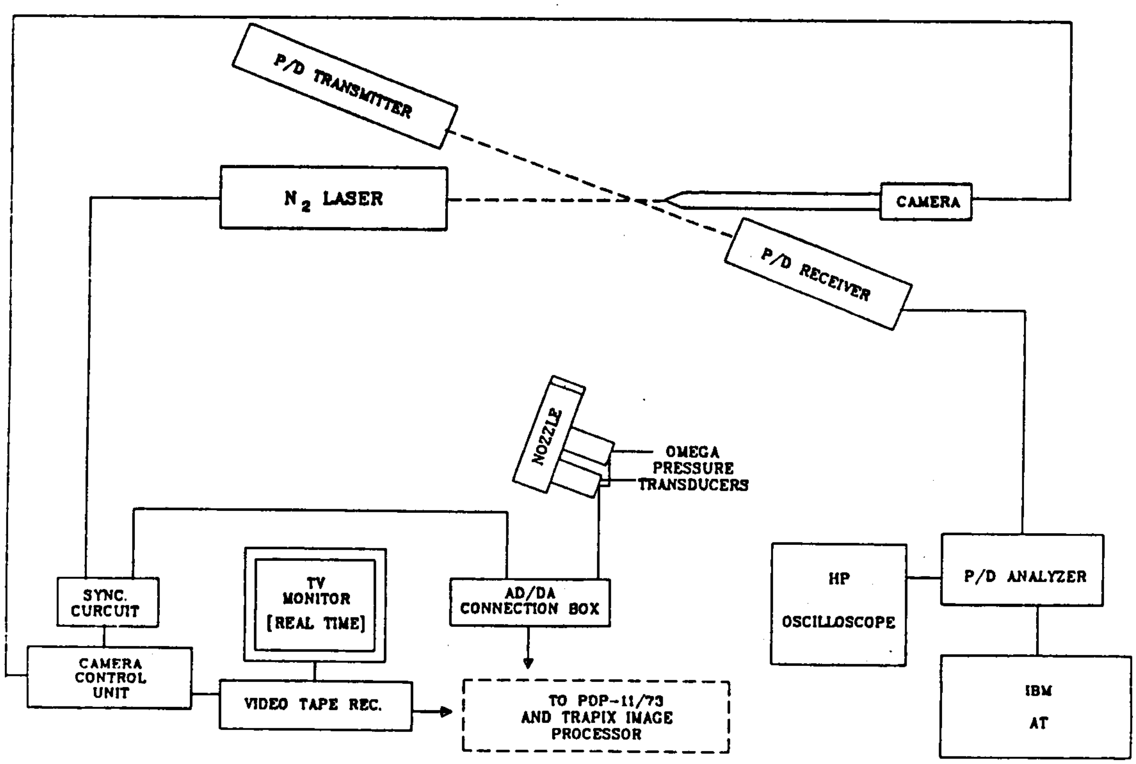


Figure 2.19: Equipment Schematic for Instrument Comparison

The experimental apparatus was situated on a Newport Research optical table equipped for isolation. The building ventilation system was used to draw off the aerosol spray after analysis. The spray characterization tests were performed on an air-assist nozzle.

### 2.3.1 MOD-1 Nozzle

Figure 2.20 shows the MOD-1 nozzle as supplied by NASA Lewis Space Research Center. The nozzle is of the atomizer type and a prototype of the nozzle proposed to be used in the NASA Altitude Wind Tunnel to simulate various cloud structures in icing studies. Variation of the drop-size in the aerosol spray produced by the nozzle is obtained by varying the input air and water pressures. The water is introduced into a 1.81 inch- by-0.368 inch diameter mixing chamber through a 0.0155 inch orifice. The air is introduced into the outer wall of the mixing chamber through twelve 0.125 inch holes. After mixing, the aerosol is expelled from the mixing chamber through a 0.125 inch orifice.

### 2.3.2 Air and Water Supply System (AWSS)

As shown in Fig. 2.21, the AWSS was constructed to supply air and water to the MOD-1 nozzle with the exception of the LI/VPS optics purge. The air for the AWSS is supplied by twin 100 hp Ingersoll-Rand turbine compressors with a delivery rate of 800 SCFM at 120 psig. Because of the high water pressure necessary for the MOD-1 nozzle, a Brunswick 20.5 liter pressure vessel was filled with water and pressurized by the supply air or for higher pressures by a regulated high pressure $N_2$ bottle. After pressurization, the water was filtered by a ADKIN spool filter. The nozzle air and water supply was regulated by a WATTS Model 2235 pressure regulator and a Cole-Palmer Model PR004-FM044-40G flowmeter, respectively. Connection lines in the supply system were YELLOW JACKET Model WPP0031A charging hose (500 max. psi.). The LI/VPS optics purge used a regulated high pressure $N_2$ bottle for a constant positive flow from the lens cover to avoid contamination.

### 2.3.3 Water Flowmeter Calibration

The Cole-Palmer flowmeter was factory calibrated. The calibration was verified by collecting and weighing the water passing through the flowmeter. The water was weighed on a HOWE model #3074131 balance scale. Twelve flow rates were measured with three samples collected at each flow rate. The experimental data and factory calibration data are presented in Table E13.1 with graphical representation shown in Fig. E.13.1 (APPENDIX E).

## 2.4 Digital Pressure Acquisition

The digital pressure system (DPS) was developed to monitor the essential input conditions of the MOD-1 nozzle. The DPS consists of two OMEGA Model PX304-150AV pressure transducers, a DEC AXV11- C analog to digital (A/D) converter board, the PDP- 11/73 micro- computer hosting the above A/D board, and a PDP RT-11 software package written to access the A/D board and store or display the resulting pressures.

ORIGINAL PAGE IS
OF POOR QUALITY

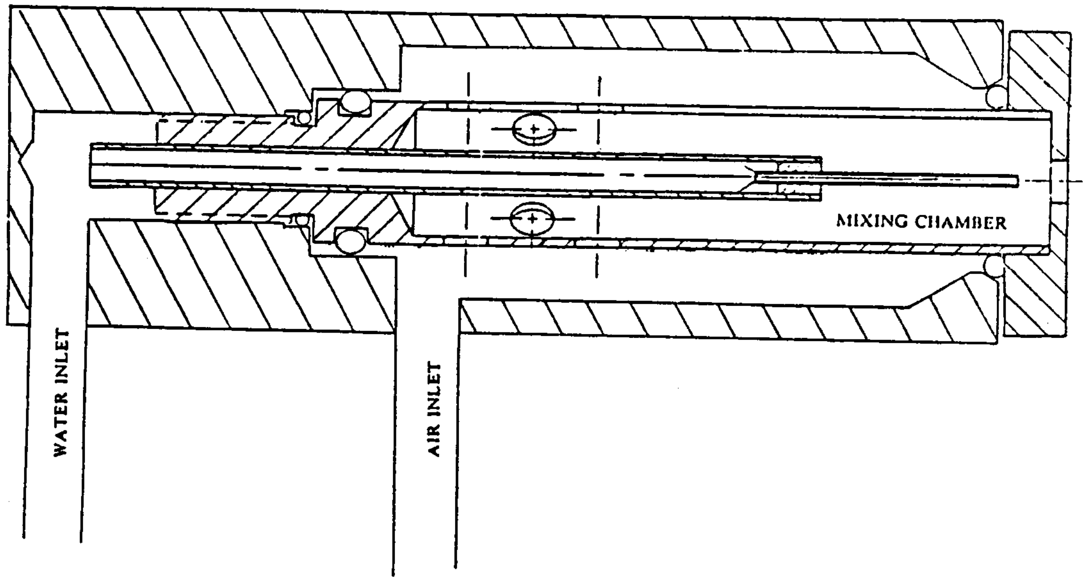


a. - MOD-1 Schematic.

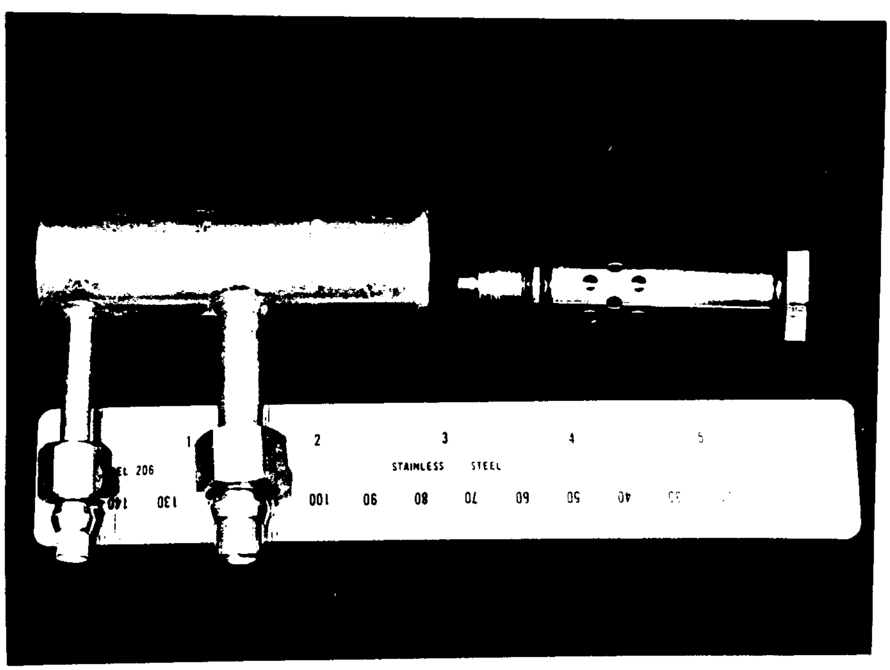

b. - MOD-1 Components.

Figure 2.20: MOD-1 Nozzle

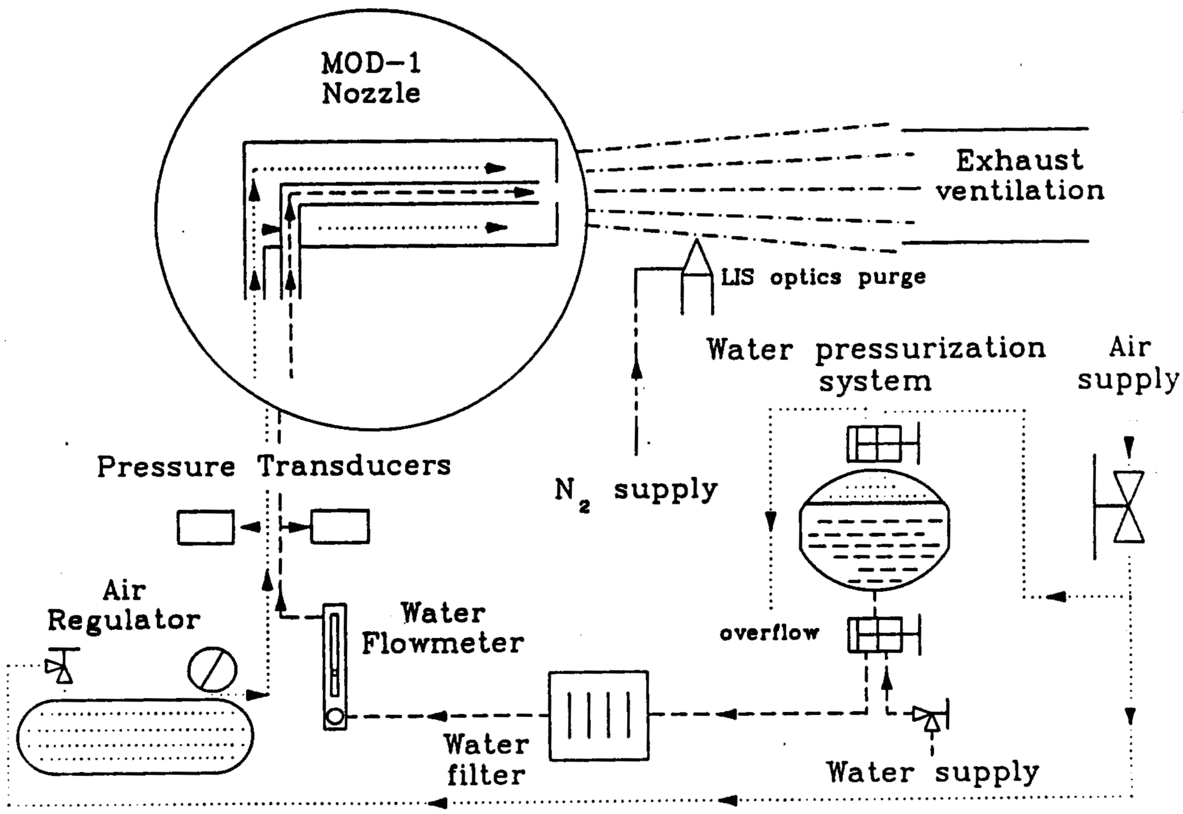


Figure 2.21: Air and Water Supply Schematic

### 2.4.1 Pressure Transducers

The OMEGA pressure transducers (Fig. 2.22) are bridge type strain gage transducers. The bridge excitation voltage was 10 VDC supplied by a Hewlett-Packard (Model Harrison 6200B) d.c. power supply with a bridge output of 0 to 100 mVDC. The transducers are specified to have an operating range of 0 to 150 psia with ± 0.75 psi accuracy.

### 2.4.2 A/D converter board

The DEC AXV11-C analog-to-digital converter board was installed in the back-plane of the PDP-11/73 microcomputer. The AXV11-C board has 12 bit digital resolution, supports up to 16 single analog input signals or 8 differential signals, A/D conversion by program, external clock, or real-time clock, and 1, 2, 4, and 8 (i.e, 10, 5, 2.5, and 1.25 volts) programmable gain settings. As recommended by the manufacturer, the 8 channel differential option was chosen to maximize analog to digital conversion, due to the 100 mV range supplied by the pressure transducers.

### 2.4.3 Analog-to-Digital Conversion

The transducer voltage signal is converted to a digital value available to the LI/VPS operator. An interface box (Fig. 2.23) was constructed to utilize the full capabilities of the AXV11-C board. The interface box has 8 A/D input ports and 2 D/A output ports using BNC connectors. The interface box is linked to the AXV11-C board by RS232 cable and connectors. The pressure measurements are made available to the analyst through the PDP-11/73 microcomputer. The RT-11 software package, written in FORTRAN subroutine form (APPENDIX C.3), allows for real-time pressure monitoring with storage and averaging capabilites for the duration of the main calling program. The A/D converter is programed for a gain setting of 8 (i.e., an effective analog input range of 0 to 1.25 volts) to optimize A/D conversion of the pressure transducer output range of 0 to 100 mV.

### 2.4.4 Digital Pressure System Calibration

The pressure transducers were calibrated for various static pressures by pressurizing the transducers and reading the A/D output after a steady equilibrium state had been attained. A laboratory grade test gage was used to measure the "*standard*" pressure. The test gage, with a range of 0 to 160 psig, was calibrated using an American Steam Gage Co. deadweight pressure gage tester. With the pressure transducer's specified input pressure range of 0 to 150 psia, the calibration data was taken within a range of 0 to 110 psig ( 14.05 to 124.05 psia). The atmospheric pressure at the time of the calibration run was measured to be 727.29 mm Hg. or 14.05 psia from a Precision Thermo & Inst Co. model #Z769 barometer. The experimental data is presented in Tables F14.1 and F14.2 with graphical representation shown in Figs. F14.1 and F14.2 (APPENDIX F).

## 2.5 Experimental Procedure

With system performance and verification as the basis for comparison, equivalent sampling was required. As discussed earlier, the P/DPA and the LI/VPS use different methods of particle sizing (i.e., temporal vs. spatial), but each instrument uses a probe volume for data collection. Therefore, system comparison was dependent on spray density, droplet size range, and user designation of the measurement volumes (i.e., the P/DPA's crossed-beam intersection volume, specified by

ORIGINAL PAGE IS
OF POOR QUALITY

Model # - PX 304-150A V

SPECIFICATIONS
Excitation: 10 VDC
Output: 0 to 100 mV
Sensitivity: 10 mV/V ±1%

Input Impedance: 1200 ohm
Output Impedance: 500 ohm

PERFORMANCE
Accuracy: ±0.5% full scale
Zero Balance: ±2.0% full scale
Operable Temperature Range:
-29 to 60° C

a. - OMEGA Pressure Transducer Data Sheet.

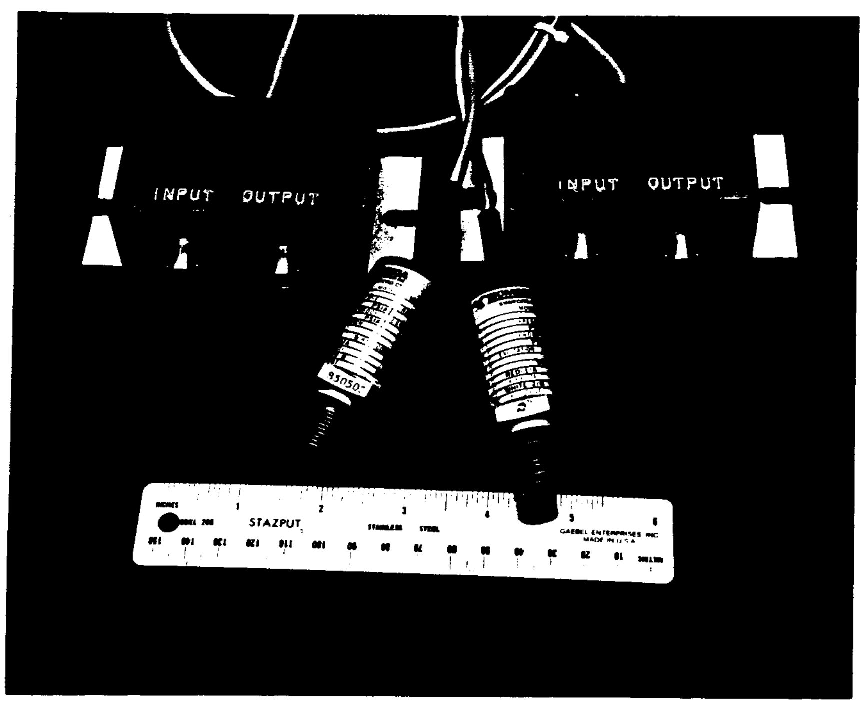


b. - OMEGA Pressure Transducers.

Figure 2.22: OMEGA Pressure Transducers

## SCHEMATIC FOR AD/DA CONNECTOR BOX

**(For Differential Setup)**

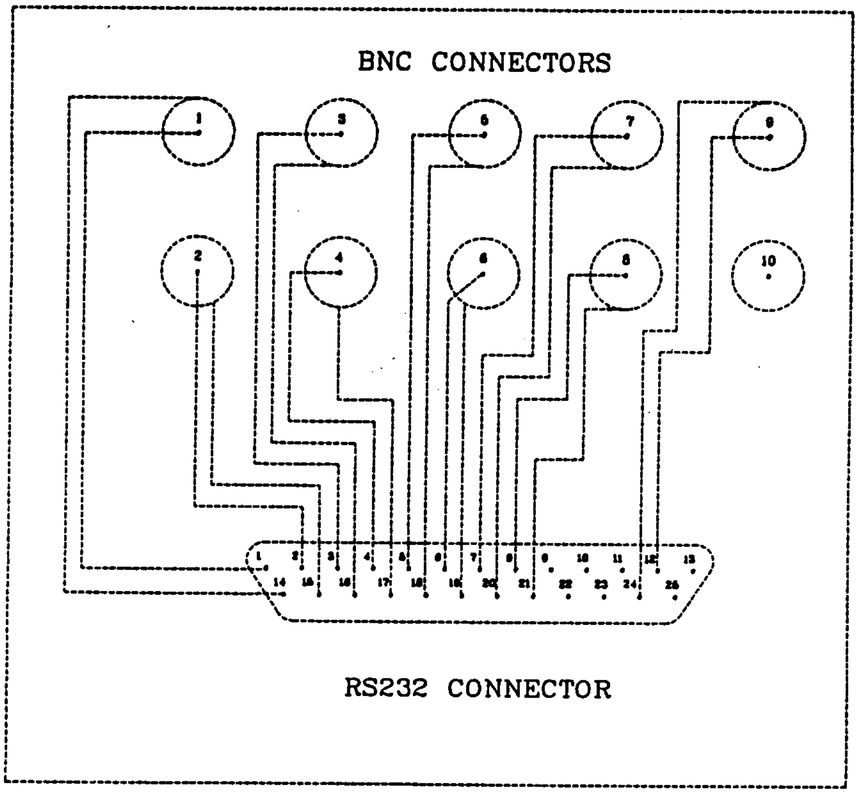


**NOTE:**
For further documentation refer to PDP-11 Microcomputer Interface Handbook page 70.

| RS232 | BNC |
|---|---|
| Pin 1 - CH. 1 | 1 |
| Pin 2 - CH. 2 | 2 |
| Pin 3 - CH. 3 | 3 |
| Pin 4 - CH. 4 | 4 |
| Pin 5 - CH. 5 | 5 |
| Pin 6 - CH. 6 | 6 |
| Pin 7 - CH. 7 | 7 |
| Pin 8 - CH. 8 | 8 |
| Pin 12 - DA #1 | 9 |
| Pin 14 - CH. 1 Return | |
| Pin 15 - CH. 2 Return | |
| Pin 16 - CH. 3 Return | |
| Pin 17 - CH. 4 Return | |
| Pin 18 - CH. 5 Return | |
| Pin 19 - CH. 6 Return | |
| Pin 20 - CH. 7 Return | |
| Pin 21 - CH. 8 Return | |
| Pin 24 - DA #1 Return | |

Figure 2.23: A/D Connector Box Schematic

the transmitter lens chosen and beam diameter, vs. the LI/VPS focus volume, specified by the imaging optics and software).

The procedure for overlapping the probe volumes is described in reference [14]. Figure 2.24 is included to show the scattered light, from drops generated by the VOAG passing through the crossed-beam intersection volume, as seen by the LI/VPS.

### 2.5.1 Verification Tests

The P/DPA and the LI/VPS probe volumes for the verification tests were specified as follows; the P/DPA transmitter lens with the 495 mm focal length and 25 mm beam separation formed a probe volume with an approximate 160 $\mu$m waist diameter, and for the LI/VPS, the 1000X lens specifies a 400x400x140 $\mu m^3$ volume with software selectable field of view for a 160x160x140 $\mu m^3$ volume (Fig. 2.25).

With the above configuration, the P/DPA and the LI/VPS were tested using a TSI Model 3450 Vibrating Orifice Aerosol Generator (VOAG). Operating conditions of the VOAG were varied to generate a size range of particles, 19.8 to 99.6 $\mu$m (Table 2.2).

Table 2.2: Verification Test Conditions

| TEST (#) | ORIFICE DIAMETER ($\mu$m) | DISTURBANCE FREQUENCY (Hz.) | WATER FEED RATE (cm$^3$/min) | THEORETICAL DIAMETER ($\mu$m) |
|---|---|---|---|---|
| 1 | 10 | 330.4 | 0.080 | 19.8 |
| 2 | 20 | 100.2 | 0.139 | 35.5 |
| 3 | 20 | 79.2 | 0.139 | 39.0 |
| 4 | 20 | 62.5 | 0.139 | 41.5 |
| 5 | 20 | 51.6 | 0.139 | 44.2 |
| 6 | 20 | 41.6 | 0.139 | 47.5 |
| 7 | 50 | 30.1 | 0.590 | 85.6 |
| 8 | 50 | 25.5 | 0.590 | 90.4 |
| 9 | 50 | 19.0 | 0.590 | 99.6 |

Each particle size generated either in single stream form or using the dispersion cup (Fig. 2.26)to generated a spray was measured using the P/DPA and the LI/VIPS system. The TSI droplet diameter ($D_d$) was calculated using the TSI theoretical equation (2.7);

$$D_d = \left[\frac{6q}{\pi f}\right]^{1/3} \tag{2.7}$$

where q is the liquid flow rate and f is the disturbance frequency. Results of the tests are presented in Section 3.2.

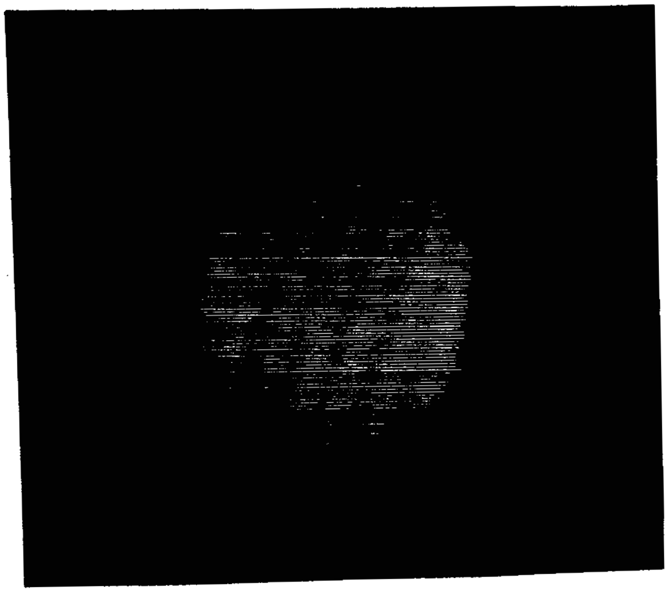

Figure 2.24: P/DPA Doppler Fringes as Seen by the LI/VPS Imaging Camera

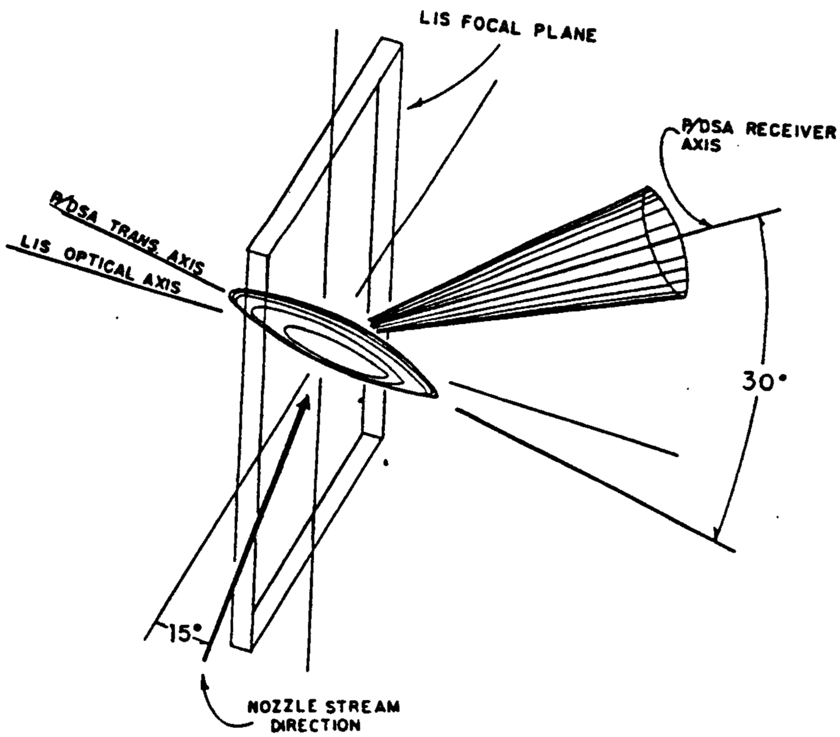


Figure 2.25: P/DPA and LI/VPS Over-lapping Probe Volumes

ORIGINAL PAGE IS
OF POOR QUALITY

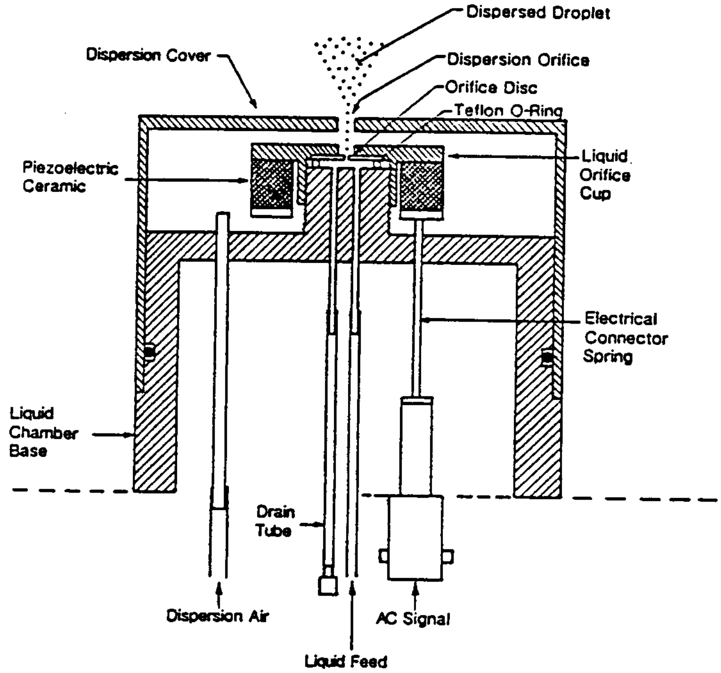


a. - VOAG Dispersion Cup.

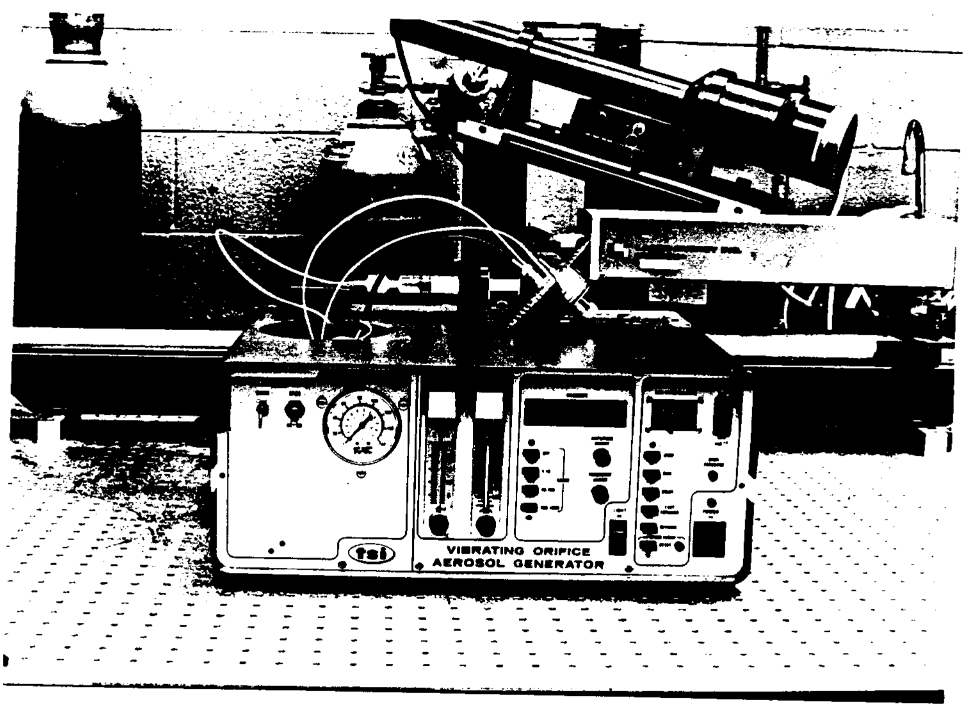


b. - TSI Vibrating Orifice Aerosol Generator.

Figure 2.26: Verification Test Apparatus

### 2.5.2 Spray Comparison

With the spray density and particle size range depending on the nozzle conditions, the benchmark tests were performed for two specific cases. Inlet nozzle conditions are shown in Table 2.3.

Table 2.3: Comparison Test Conditions

| | CASE I | CASE II |
|---|---|---|
| Pressure (water) | 115 psia | 105 psia |
| Pressure (air) | 45 psia | 65 psia |

For each case, a sample was taken on centerline two feet downstream from the nozzle with succeeding samples taken radially in 0.5 inch increments to the outer edge of the spray plume.

To avoid undue comparative data reduction, the P/DPA and LI/VPS were matched in approximate probe volume size, as previously stated, and appropriate particle size range. Assuming nozzle conditions were steady state, preliminary setup of the P/DPA and the LI/VPS was performed to optimize instrument operation. The results of the analysis are presented in Section 3.3.

Section 3

# PRESENTATION AND DISCUSSION OF RESULTS

This section will present the results of the LI/VPS calibration tests including a comparison with previous calibration tests, the verification tests with the VOAG, and the comparison tests using the MOD-1 nozzle. The major concern of these results is the accuracy of the sizing measurements with secondary interest in the comparability of the LI/VPS and the P/DPA.

## 3.1 LI/VPS Calibration Results

As was stated previously, the LI/VPS had to be recalibrated due to the replacement of the vidicon camera tube. With the new vidicon tube, the MCF became approximately 2.1 $\mu$m/pixel (i.e., for the 500X lens), as opposed to the previous factor of 1.8 $\mu$m/pixel [7,10], for the old camera tube. The new vidicon tube, therefore, reduced the LI/VPS measurement resolution. The above is mentioned to explain the increased error in determining the smaller particle sizes for the 500X lens, as well as the reasoning for the calibration of the 1000X lens. The following calibration results specify the MCFs for the 500X and the 1000X lens. Results of previous calibration tests using the calibration reticle have been compared to the new calibrations.

Using the procedure described in Section 2.2.3, the Equations (3.1) thru (3.4) represent the MCFs as functions of x and y location for the two lens;

the xMCF for the 500X lens;

$$MCF(y) = \begin{cases} 2.21 + y * 0.803E - 04 \text{ for } 50 \leq x < 100 \\ 2.20 + y * 0.290E - 04 \text{ for } 100 \leq x < 150 \\ 2.16 + y * 0.679E - 04 \text{ for } 150 \leq x < 200 \\ 2.16 + y * 0.442E - 07 \text{ for } 200 \leq x < 250 \\ 2.16 - y * 0.947E - 04 \text{ for } 250 \leq x < 300 \\ 2.11 - y * 0.306E - 07 \text{ for } 300 \leq x < 350 \\ 2.10 - y * 0.124E - 03 \text{ for } 350 \leq x < 400 \\ 2.07 - y * 0.135E - 03 \text{ for } 400 \leq x < 450, \end{cases} \tag{3.1}$$

the yMCF for the 500X lens;

$$MCF(y) = \begin{cases} 2.10 - y * 0.183E - 03 \text{ for } 50 \leq x < 100 \\ 2.11 - y * 0.240E - 03 \text{ for } 100 \leq x < 150 \\ 2.12 - y * 0.314E - 03 \text{ for } 150 \leq x < 200 \\ 2.13 - y * 0.313E - 03 \text{ for } 200 \leq x < 250 \\ 2.15 - y * 0.397E - 03 \text{ for } 250 \leq x < 300 \\ 2.18 - y * 0.484E - 03 \text{ for } 300 \leq x < 350 \\ 2.19 - y * 0.505E - 03 \text{ for } 350 \leq x < 400 \\ 2.18 - y * 0.509E - 03 \text{ for } 400 \leq x < 450, \end{cases} \tag{3.2}$$

the xMCF for the 1000X lens;

$$MCF(y) = \begin{cases} 0.977 + y * 8.09E - 05 \text{ for } 50 \leq x < 100 \\ 0.974 + y * 2.60E - 05 \text{ for } 100 \leq x < 150 \\ 0.967 - y * 8.12E - 07 \text{ for } 150 \leq x < 200 \\ 0.961 + y * 4.73E - 06 \text{ for } 200 \leq x < 250 \\ 0.961 - y * 5.46E - 05 \text{ for } 250 \leq x < 300 \\ 0.948 - y * 3.72E - 05 \text{ for } 300 \leq x < 350 \\ 0.943 - y * 6.80E - 05 \text{ for } 350 \leq x < 400 \\ 0.920 - y * 2.58E - 05 \text{ for } 400 \leq x < 450, \end{cases} \tag{3.3}$$

and the yMCF for the 1000X lens;

$$MCF(y) \begin{cases} 0.977 - y * 9.17E - 05 \text{ for } 50 \leq x < 100 \\ 0.981 - y * 1.24E - 04 \text{ for } 100 \leq x < 150 \\ 0.981 - y * 1.19E - 04 \text{ for } 150 \leq x < 200 \\ 0.990 - y * 1.63E - 04 \text{ for } 200 \leq x < 250 \\ 1.000 - y * 1.96E - 04 \text{ for } 250 \leq x < 300 \\ 1.014 - y * 2.19E - 04 \text{ for } 300 \leq x < 350 \\ 1.027 - y * 2.63E - 04 \text{ for } 350 \leq x < 400 \\ 1.029 - y * 2.69E - 04 \text{ for } 400 \leq x < 450. \end{cases} \tag{3.4}$$

With the above equations, a software algorithm was setup in subroutine form to determine the correction factors as functions of particle location and for the magnification lens installed (APPENDIX C.4).

Figures 3.1 - 3.4 show the variation of the MCFs with respect to x and y location. The similarity in Figs. 3.1 and 3.3, as well as the similarity in Figs. 3.2 and 3.4 show the MCFs' variation is mainly due to the geometric non-linearities in the vidicon tube. The procedure developed to determine the MCFs as functions of both x and y screen location is easy to use, straight-forward, and not time consuming. The implementation of the MCFs in PSP is easily facilitated by the use of the FORTRAN subroutine format.

The following comparison represents LI/VPS accuracy studies by this investigator and the previous investigators [7,10]. The basis for the comparison was the utilization of the calibration reticle with the 500X lens. Table 3.1 shows the results for the 500X lens by this investigator. Table 3.2 represents the equivalent results for the 1000X lens under similar test conditions.

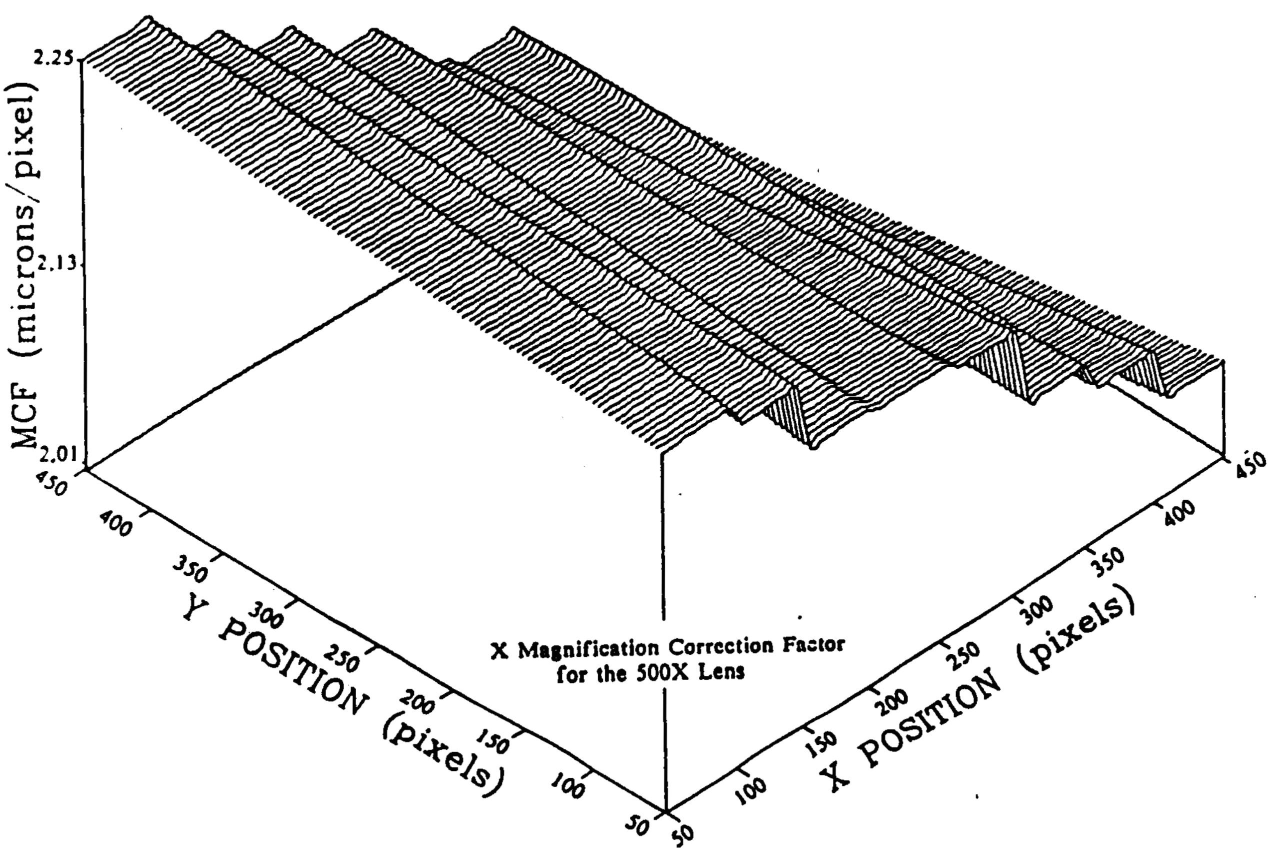


Figure 3.1: Magnification Correction Factor Behavior

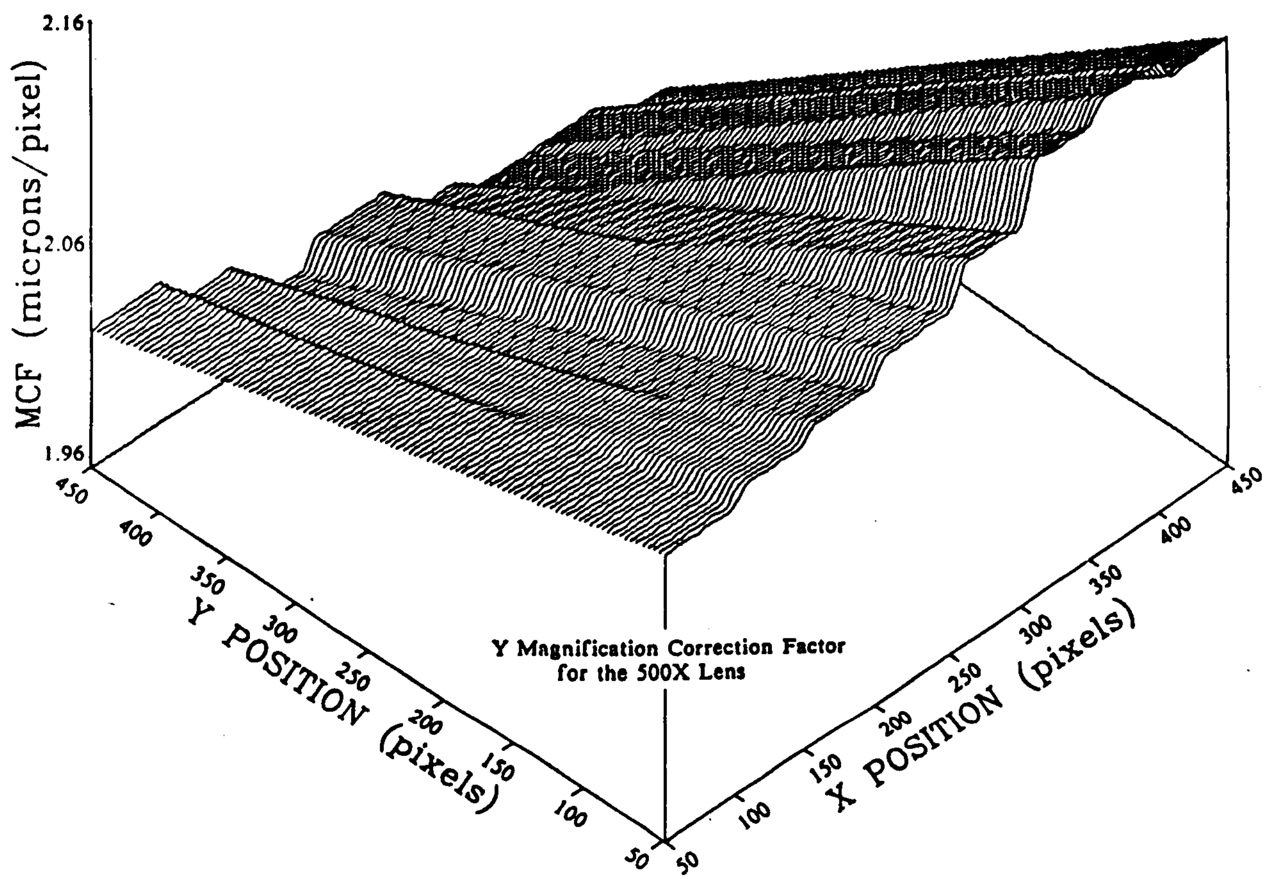


Figure 3.2: Magnification Correction Factor Behavior

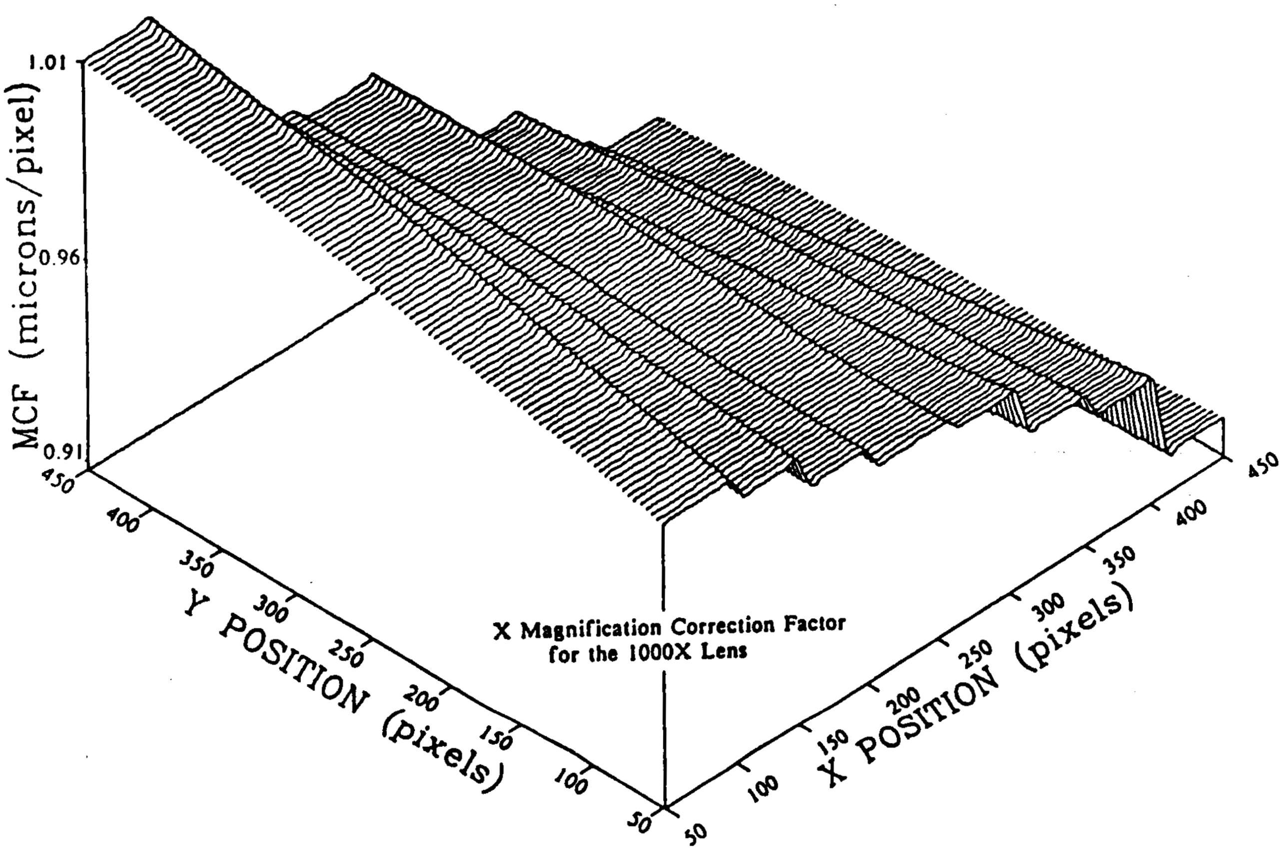


Figure 3.3: Magnification Correction Factor Behavior

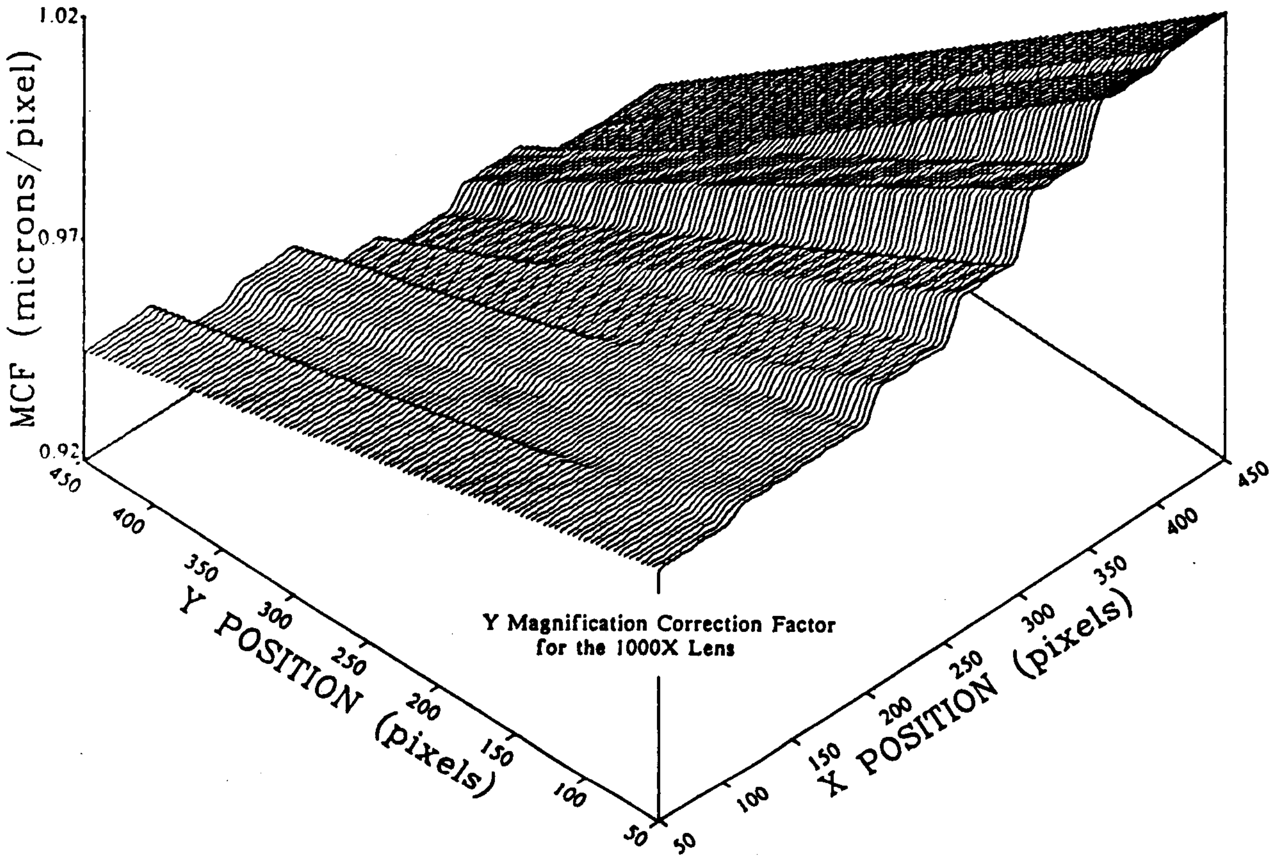


Figure 3.4: Magnification Correction Factor Behavior

#114 CALIBRATION RETICLE
CALIBRATION FOR THE 500X LENS
DATA TAKEN: 26-MAR-86 19:36:22
CONSTANT THRESHOLD LEVEL = 90

Number of Frames in Analysis: 30 Particles Counted: 660

| Particle (#) | Counts (#) | Actual Dia. | Average Dia. | Std. Dev. | Diameter Size Range | Average Error | Error Std. Dev. | Avg. % Error |
|---|---|---|---|---|---|---|---|---|
| 1 | 0 | 5.29 | 0.00 | 0.00 | 0.0 - 0.0 | 0.00 | 0.00 | 0.00 % |
| 2 | 30 | 6.81 | 5.45 | 0.81 | 4.2 - 7.9 | 1.81 | 0.51 | 26.58 % |
| 3 | 30 | 8.98 | 8.80 | 0.58 | 7.7 - 9.8 | 0.78 | 0.58 | 8.68 % |
| 4 | 30 | 11.93 | 10.03 | 0.33 | 10.4 - 11.9 | 0.33 | 0.43 | 2.77 % |
| 5 | 30 | 17.20 | 16.40 | 0.79 | 15.7 - 17.0 | 1.79 | 0.78 | 10.41 % |
| 6 | 30 | 21.33 | 20.46 | 0.45 | 20.0 - 21.2 | 1.23 | 0.45 | 5.77 % |
| 7 | 30 | 23.90 | 23.51 | 0.90 | 22.9 - 24.1 | 1.34 | 0.59 | 5.61 % |
| 8 | 30 | 26.71 | 27.18 | 0.71 | 26.3 - 27.8 | 0.81 | 0.61 | 3.03 % |
| 9 | 30 | 31.11 | 29.81 | 0.45 | 29.0 - 30.6 | 0.65 | 0.92 | 2.09 % |
| 10 | 30 | 34.17 | 35.51 | 0.37 | 34.2 - 35.9 | 0.67 | 0.47 | 1.86 % |
| 11 | 30 | 37.07 | 36.75 | 0.57 | 36.0 - 37.7 | 0.52 | 0.57 | 1.40 % |
| 12 | 30 | 40.47 | 40.01 | 0.67 | 39.3 - 41.1 | 0.67 | 0.47 | 1.66 % |
| 13 | 30 | 42.71 | 43.91 | 0.71 | 40.9 - 42.7 | 0.51 | 0.61 | 1.19 % |
| 14 | 30 | 47.37 | 48.31 | 0.56 | 47.3 - 49.8 | 0.69 | 0.66 | 1.41 % |
| 15 | 30 | 50.39 | 50.28 | 0.39 | 48.9 - 51.0 | 0.39 | 0.56 | 0.77 % |
| 16 | 30 | 52.50 | 51.98 | 0.50 | 49.8 - 52.8 | 0.54 | 0.34 | 1.03 % |
| 17 | 30 | 56.23 | 56.25 | 0.23 | 55.0 - 57.1 | 0.25 | 0.29 | 0.44 % |
| 18 | 30 | 60.70 | 60.85 | 0.70 | 60.0 - 63.5 | 0.63 | 0.57 | 1.04 % |
| 19 | 30 | 67.04 | 67.24 | 0.84 | 65.3 - 70.0 | 0.44 | 0.54 | 0.66 % |
| 20 | 30 | 73.45 | 73.35 | 0.38 | 71.4 - 76.1 | 2.82 | 0.36 | 3.84 % |
| 21 | 30 | 80.58 | 80.69 | 0.48 | 79.0 - 82.2 | 3.45 | 0.48 | 4.28 % |
| 22 | 30 | 86.99 | 87.10 | 0.57 | 86.2 - 88.3 | 1.57 | 0.37 | 1.80 % |
| 23 | 30 | 92.75 | 93.26 | 0.65 | 90.8 - 95.3 | 0.65 | 0.65 | 0.70 % |
| Averages: | | | | 0.57 | | 1.02 | 0.53 | 3.96 % |

Table 3.1: Calibration Accuracy Test

#114 CALIBRATION RETICLE
CALIBRATION FOR THE 1000X LENS
DATA TAKEN: 29-MAR-86 04:15:24
CONSTANT THRESHOLD LEVEL = 90

Number of Frames in Analysis: 30    Particles Counted: 690

| Particle (#) | Counts (#) | Actual Dia. | Average Dia. | Std. Dev. | Diameter Size Range | Average Error | Error Std. Dev. | Avg. % Error |
|---|---|---|---|---|---|---|---|---|
| 1 | 30 | 5.29 | 4.93 | 0.89 | 3.3 - 7.2 | 1.78 | 1.03 | 33.65 % |
| 2 | 30 | 6.81 | 5.76 | 0.81 | 4.2 - 7.8 | 1.21 | 0.31 | 17.77 % |
| 3 | 30 | 8.98 | 8.67 | 0.58 | 7.7 - 9.9 | 0.38 | 0.28 | 4.23 % |
| 4 | 30 | 11.93 | 11.40 | 0.33 | 9.9 - 13.1 | 0.63 | 0.33 | 5.28 % |
| 5 | 30 | 17.20 | 16.67 | 0.29 | 15.5 - 19.4 | 0.79 | 0.58 | 4.59 % |
| 6 | 30 | 21.33 | 21.03 | 0.15 | 19.7 - 23.2 | 0.83 | 0.25 | 3.89 % |
| 7 | 30 | 23.90 | 23.69 | 0.24 | 21.3 - 24.6 | 0.74 | 0.19 | 3.10 % |
| 8 | 30 | 26.71 | 26.78 | 0.32 | 25.8 - 27.3 | 1.11 | 0.31 | 4.16 % |
| 9 | 30 | 31.11 | 30.67 | 0.27 | 28.7 - 33.7 | 1.02 | 0.42 | 3.28 % |
| 10 | 30 | 34.17 | 34.33 | 0.29 | 31.4 - 36.5 | 0.77 | 0.42 | 2.25 % |
| 11 | 30 | 37.07 | 37.02 | 0.50 | 36.0 - 39.3 | 0.57 | 0.17 | 1.54 % |
| 12 | 30 | 40.47 | 39.78 | 0.27 | 38.4 - 42.9 | 0.67 | 0.57 | 4.13 % |
| 13 | 30 | 42.71 | 41.87 | 0.31 | 40.3 - 43.6 | 0.45 | 0.41 | 3.39 % |
| 14 | 30 | 47.37 | 47.77 | 0.22 | 46.3 - 50.2 | 0.37 | 0.23 | 0.78 % |
| 15 | 30 | 50.39 | 49.89 | 0.30 | 47.9 - 51.2 | 0.76 | 0.36 | 1.51 % |
| 16 | 30 | 52.50 | 52.78 | 0.17 | 50.2 - 53.5 | 0.34 | 0.32 | 0.65 % |
| 17 | 30 | 56.23 | 56.02 | 0.23 | 54.5 - 57.2 | 1.25 | 0.21 | 2.22 % |
| 18 | 30 | 60.70 | 61.01 | 0.15 | 59.0 - 63.3 | 1.96 | 0.45 | 3.23 % |
| 19 | 30 | 67.04 | 67.33 | 0.13 | 65.2 - 71.4 | 0.40 | 0.42 | 0.60 % |
| 20 | 30 | 73.45 | 73.38 | 0.18 | 72.1 - 77.3 | 0.34 | 0.32 | 0.46 % |
| 21 | 30 | 80.58 | 79.88 | 0.28 | 78.3 - 83.7 | 0.43 | 0.40 | 0.53 % |
| 22 | 30 | 86.99 | 87.21 | 0.31 | 85.8 - 89.3 | 1.23 | 0.39 | 1.14 % |
| 23 | 30 | 92.75 | 92.78 | 0.25 | 90.2 - 97.3 | 0.35 | 0.28 | 0.38 % |
| Averages: | | | | 0.32 | | 1.02 | 0.38 | 4.48 % |

Table 3.2: Calibration Accuracy Test

Table 3.3 shows the average percent error for the above calibration accuracy tests with the previous work of Ahlers [7] and Wiles [10]. A comparison of the average % error for the three accuracy tests performed on the 500X lens shows a decrease in the % error from the one- dimensional MCF test (i.e., 4.04% error) to the two-dimensional MCF tests (i.e., for Wiles - 2.73% error and for this work - 3.96% error). The % error values for the test performed on the 1000X lens show an increase in LI/VPS accuracy for all the particles measured by the 500X lens tests. The inclusion of the 5.29 $\mu$m particle in the analysis shows an increased sizing range, as opposed to previous tests.

The following results represent the initial method used to compare the P/DPA and the LI/VPS. As specified earlier, the probe volumes of the two instruments were overlapped, and due to the steady state operation of the VOAG, samples by both instruments were assumed to be nearly identical. Two separate cases were performed to verify instrument operation and accuracy. The first case was performed with the VOAG producing a steady single stream of drops which passed through the concurrent probe volumes, and secondly, the dispersion cup (Fig. 2.26) was utilized to produce a spray of monodisperse droplets which randomly pass through the concurrent probe volumes. Nine separate tests were performed for each case with the instrument results represented in Figs. 3.5 thru 3.13 for the case without the dispersion cup, and Figs. 3.14 thru 3.22 for the case with the dispersion cup. Figures 3.23 and 3.24 show the TSI theoretical diameter, and the arithmetic mean diameters from the LI/VPS and the P/DPA distributions as functions of test number. Data in Table 3.4 has been plotted in Fig. 3.23 and 3.24 with the standard deviation (SD) also shown. The arithmetic mean diameters of the LI/VPS and the P/DPA agree, on the most part, with each other and the theoretical expected diameter within $\pm$ 2.6 $\mu$m. The SD of the samples is shown to illustrate the monodisperse behavior of the VOAG and the ability of the LI/VPS and the P/DPA to measure the monodisperse aerosol spray. The highest SD (i.e., 1.109 $\mu$m) determined for the LI/VPS is shown in CASE II - Test 5, and for the P/DPA, the highest SD (i.e., 2.073 $\mu$m) is shown in CASE I - Test 1.

Referring to Table 3.4, the first test in both cases show the maximum SD for P/DPA. The arithmetic mean diameters, 20.5 $\mu$m for CASE I and 21.5 $\mu$m for CASE II, are within 2.0 $\mu$m of the expected diameter, 19.8 $\mu$m. The SD of the samples may be higher than the rest, due to the high density of drops passing through the P/DPA probe volume. This phenomena was especially noticeable in CASE II test runs where the dispersion cup was used. As was expected, the SD for most of the tests increased from CASE I to CASE II. The above behavior was expected, due to the increase in number of drops passing through the edges of the probe volumes.

## 3.2 Results For the MOD-1 Nozzle Comparison

The following results represent a comparison of the LI/VPS and the P/DPA in side-by-side benchmark tests performed on a NASA MOD-1 atomizing nozzle. As previously stated, two cases (i.e., variation in the operating conditions of the nozzle) were studied. For each case, eight data runs (i.e., a data run was performed on the centerline, two feet down-stream from the nozzle with succeeding data runs performed at one-half inch increments radially outward to the edge of the dispersion) were performed by the LI/VPS and the P/DPA using a procedure similar to the VOAG analysis. Figures 3.25 - 3.32 and Figs. 3.33 - 3.40 are the results from the P/DPA and the LI/VPS for CASE I (i.e., nozzle conditions: Air pressure = 65 psia and Water pressure = 105 psia.) and CASE II (i.e., nozzle conditions: Air pressure = 45 psia and Water pressure = 115 psia), respectively.

Table 3.2: Calibration Accuracy Test

CALIBRATION RETICLE : RR-50-3.0-0.08-102-CF - #114

| | | For the 500X Lens. | | | For the 1000X Lens. |
|---|---|---|---|---|---|
| PART. (#) | DIAMETER ($\mu$m)[1] | Ahlers' TEST [7] Avg. % Error | Wiles' TEST [10] Avg. % Error | Current TEST Avg. % Error | Current TEST Avg. % Error |
| 1 | 5.29 | 0.00 | 0.00 | 0.00 | 33.65 |
| 2 | 6.81 | 17.75 | 16.06 | 26.58 | 17.77 |
| 3 | 8.98 | 7.66 | 7.40 | 8.69 | 4.23 |
| 4 | 11.93 | 12.12 | 7.53 | 2.77 | 5.28 |
| 5 | 17.20 | 3.64 | 1.52 | 10.41 | 4.59 |
| 6 | 21.33 | 3.33 | 2.04 | 5.77 | 3.89 |
| 7 | 23.90 | 2.05 | 2.19 | 5.61 | 3.10 |
| 8 | 26.71 | 3.01 | 3.89 | 3.03 | 4.16 |
| 9 | 31.11 | 5.06 | 1.66 | 2.09 | 3.28 |
| 10 | 34.17 | 3.27 | 1.66 | 3.43 | 2.25 |
| 11 | 37.07 | 2.34 | 1.21 | 1.79 | 1.54 |
| 12 | 40.47 | 1.04 | 1.91 | 1.66 | 4.13 |
| 13 | 42.71 | 1.50 | 2.50 | 1.19 | 3.39 |
| 14 | 47.37 | 3.96 | 1.52 | 1.41 | 0.78 |
| 15 | 50.39 | 3.44 | 0.94 | 0.77 | 1.51 |
| 16 | 52.50 | 2.06 | 1.21 | 1.03 | 0.65 |
| 17 | 56.23 | 1.35 | 1.09 | 0.44 | 2.22 |
| 18 | 60.70 | 0.91 | 1.33 | 1.04 | 3.23 |
| 19 | 67.04 | 4.50 | 0.83 | 0.66 | 0.60 |
| 20 | 73.48 | 3.02 | 1.25 | 3.84 | 0.46 |
| 21 | 80.58 | 2.50 | 0.76 | 4.28 | 0.53 |
| 22 | 86.99 | 1.45 | 0.88 | 1.80 | 1.41 |
| 23 | 92.75 | 0.92 | 0.67 | 0.70 | 0.38 |
| AVERAGES: | | 4.04 | 2.73 | 3.96 | 4.48 |

[1] Diameters traceable to NBS Part. #52577, accurate to ± 2 $\mu$m (± 3% for D > 70 $\mu$m)

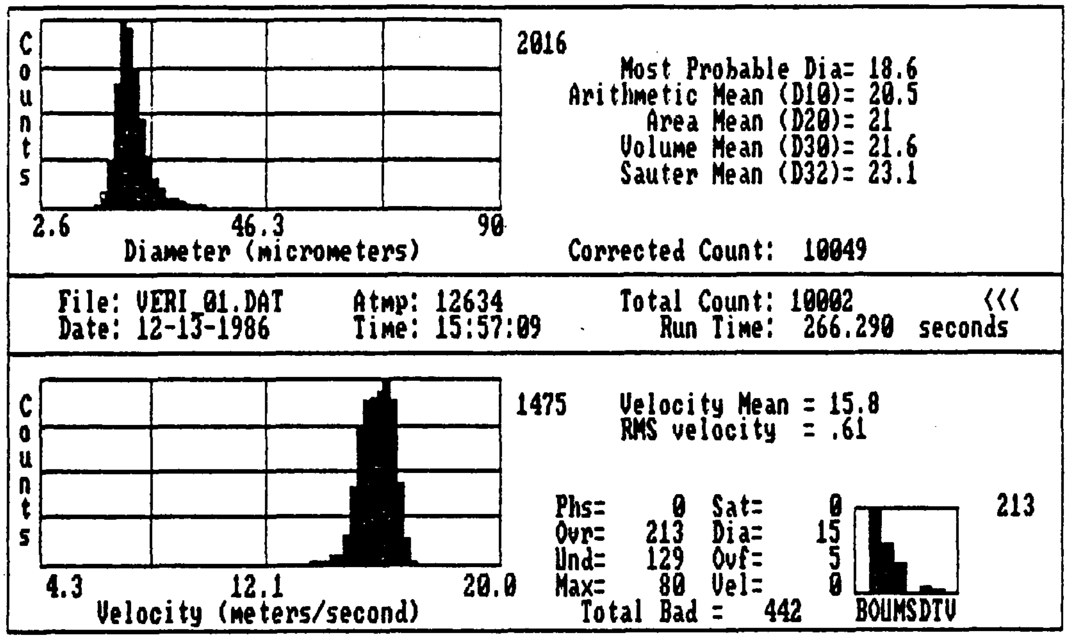


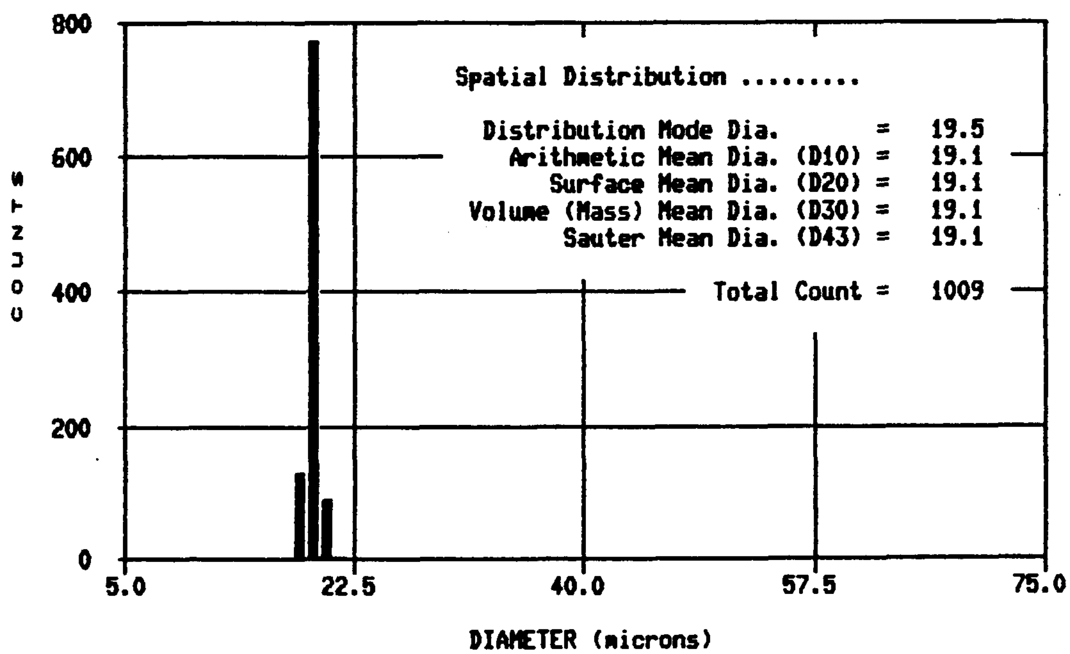


Theoretical Diameter = 19.8 $\mu$m
Diameter of Orifice = 10 $\mu$m
Liquid Feedrate = 0.08 $cm^3$/min.
Vibration Frequency = 330.4 kHz

Figure 3.5: VOAG Verification w/o Dispersion Cup



ORIGINAL PAGE IS
OF POOR QUALITY

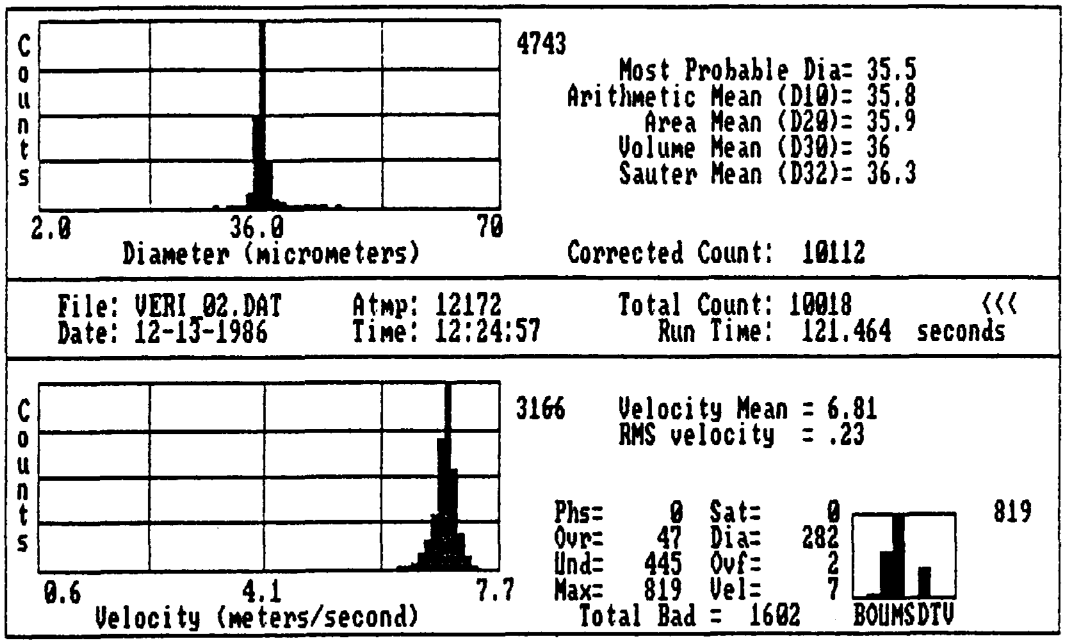


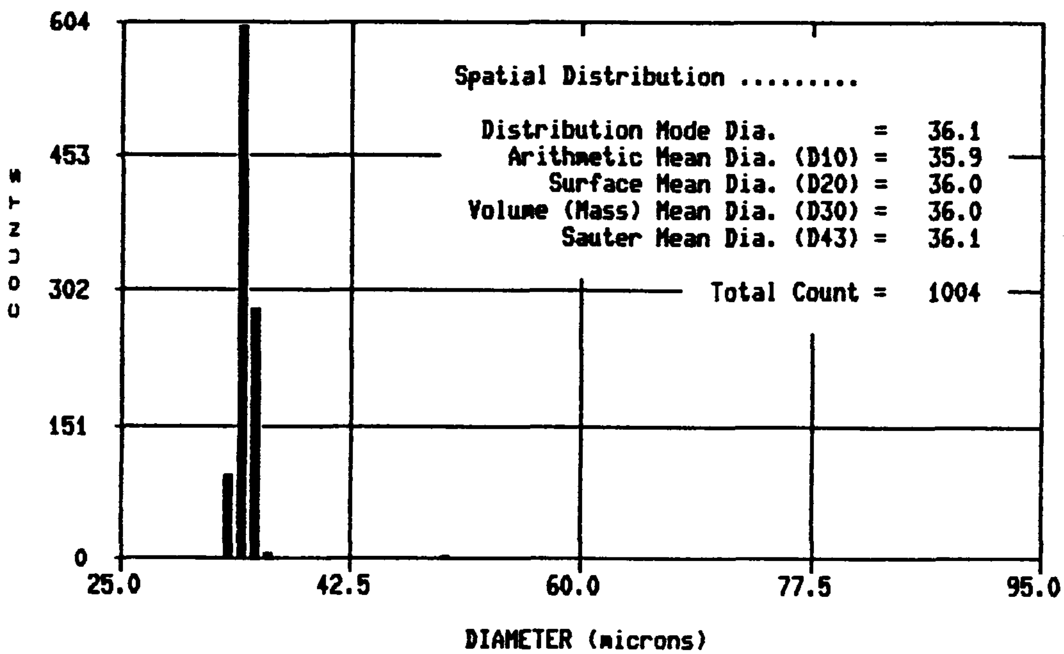


Theoretical Diameter = 35.5 $\mu$m
Diameter of Orifice = 20 $\mu$m
Liquid Feedrate = 0.139 cm$^3$/min.
Vibration Frequency = 100.2 kHz

Figure 3.6: VOAG Verification w/o Dispersion Cup

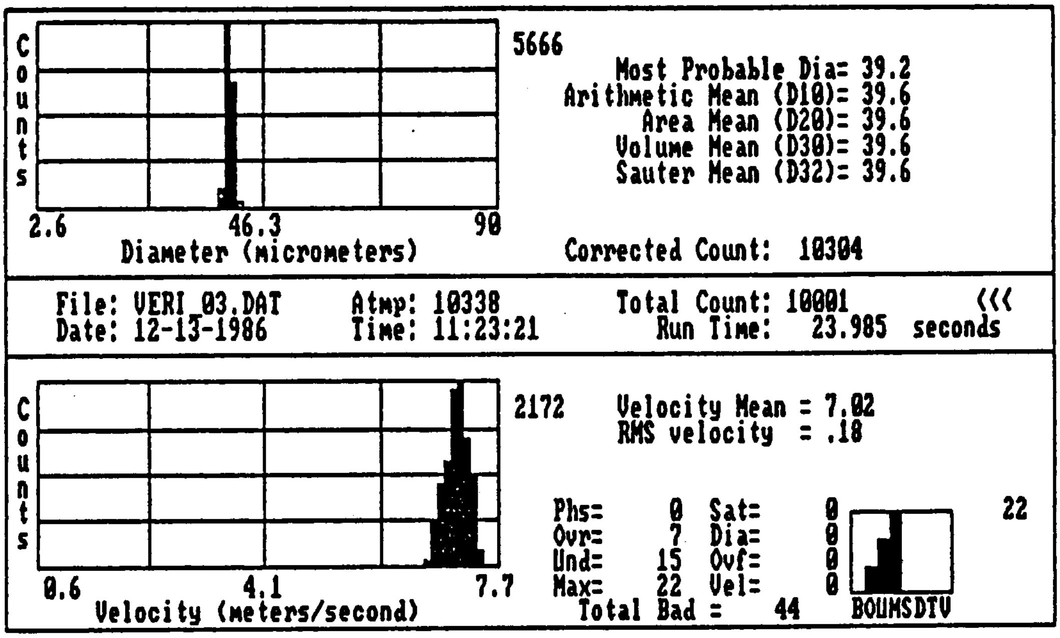


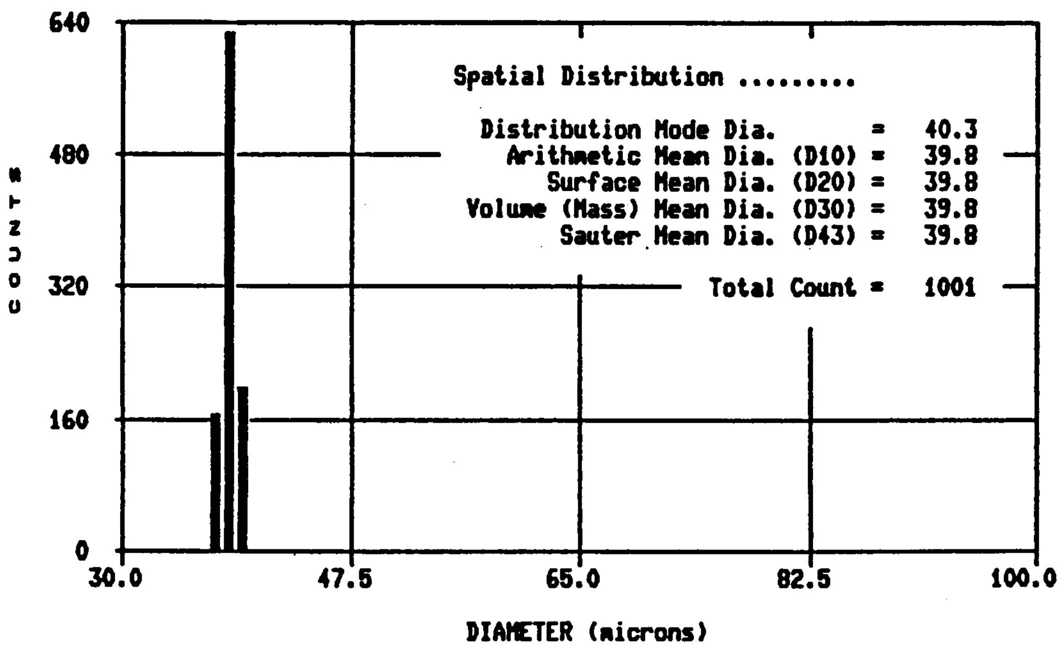


Theoretical Diameter = 39.0 $\mu$m
Diameter of Orifice = 20 $\mu$m
Liquid Feedrate = 0.139 $cm^3$/min.
Vibration Frequency = 79.2 kHz

Figure 3.7: VOAG Verification w/o Dispersion Cup

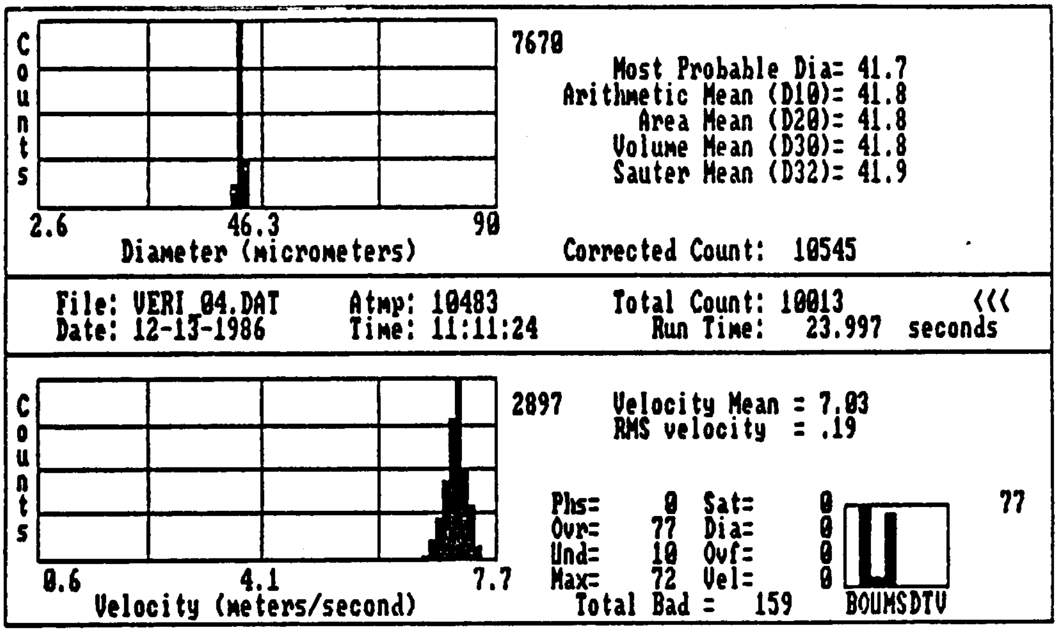


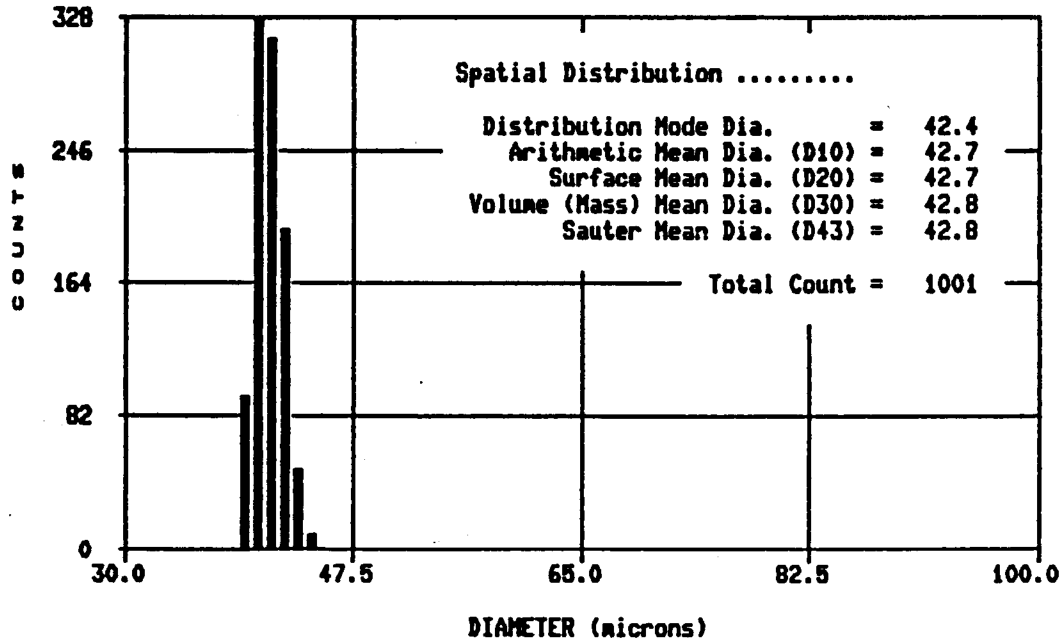


Theoretical Diameter = 41.5 $\mu$m
Diameter of Orifice = 20 $\mu$m
Liquid Feedrate = 0.139 $cm^3$/min.
Vibration Frequency = 62.5 kHz

Figure 3.8: VOAG Verification w/o Dispersion Cup

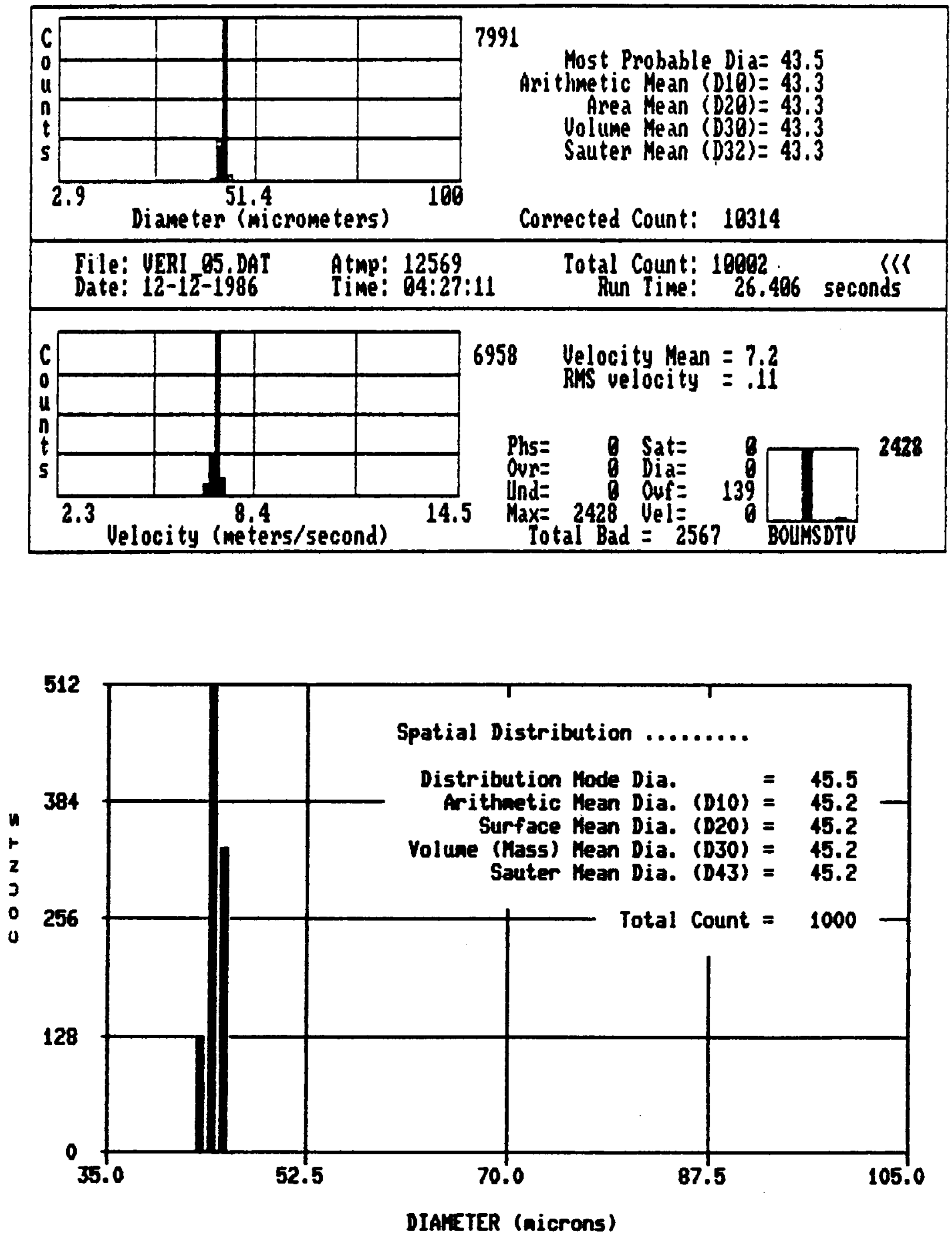


Theoretical Diameter = 44.2 $\mu$m
Diameter of Orifice = 20 $\mu$m
Liquid Feedrate = 0.139 $cm^3$/min.
Vibration Frequency = 51.6 kHz

Figure 3.9: VOAG Verification w/o Dispersion Cup

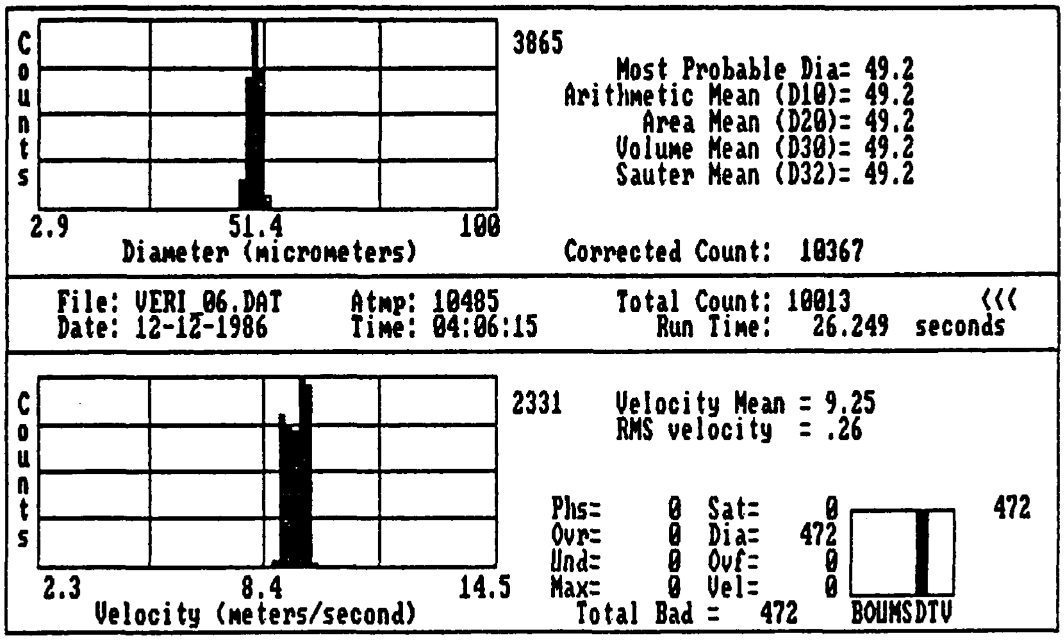


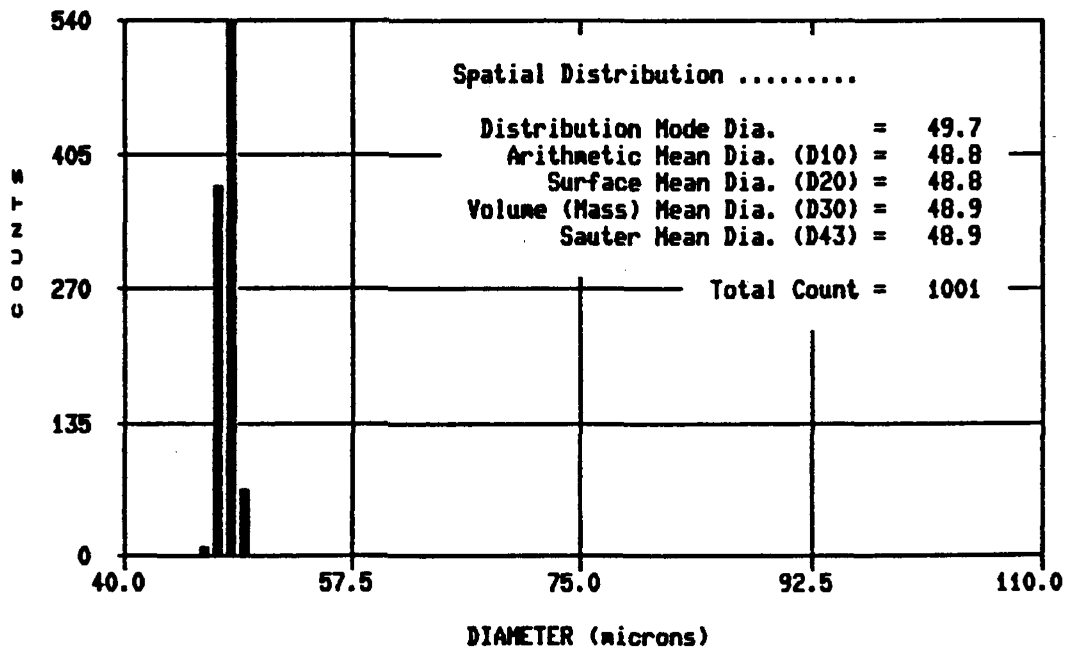


Theoretical Diameter = 47.5 $\mu$m
Diameter of Orifice = 20 $\mu$m
Liquid Feedrate = 0.139 cm$^3$/min.
Vibration Frequency = 41.6 kHz

Figure 3.10: VOAG Verification w/o Dispersion Cup

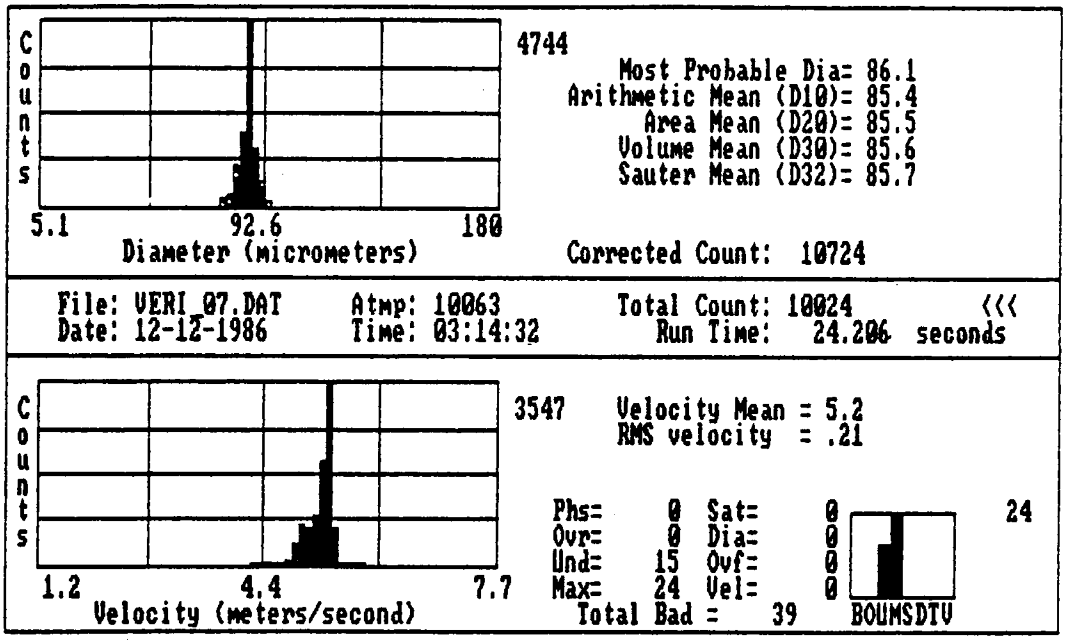


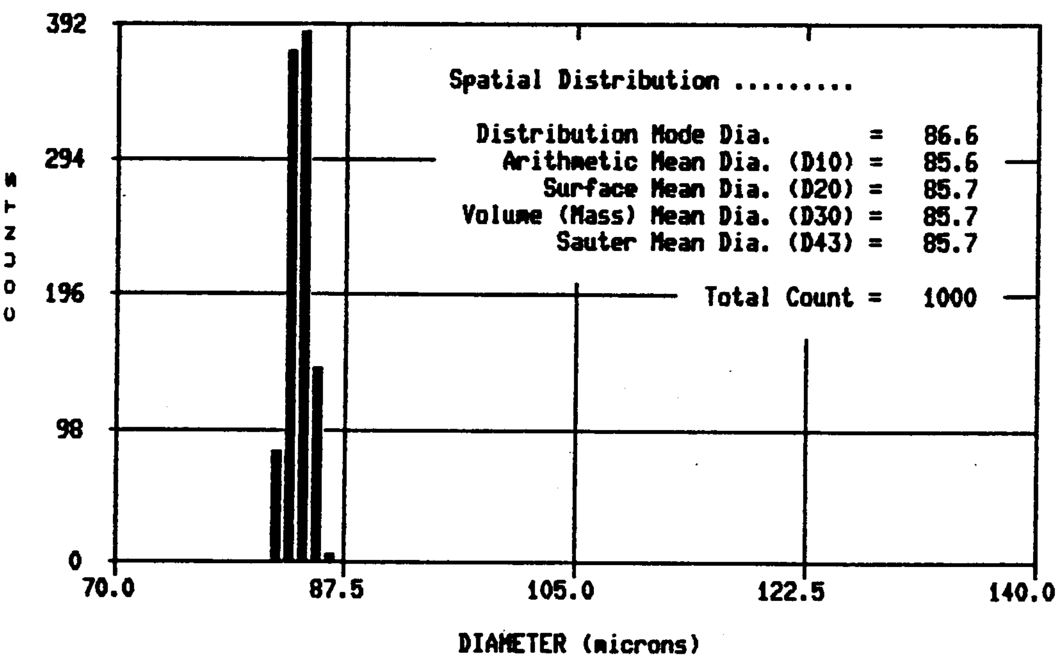


Theoretical Diameter = 85.6 $\mu$m
Diameter of Orifice = 50 $\mu$m
Liquid Feedrate = 0.59 $cm^3$/min.
Vibration Frequency = 30.1 kHz

Figure 3.11: VOAG Verification w/o Dispersion Cup

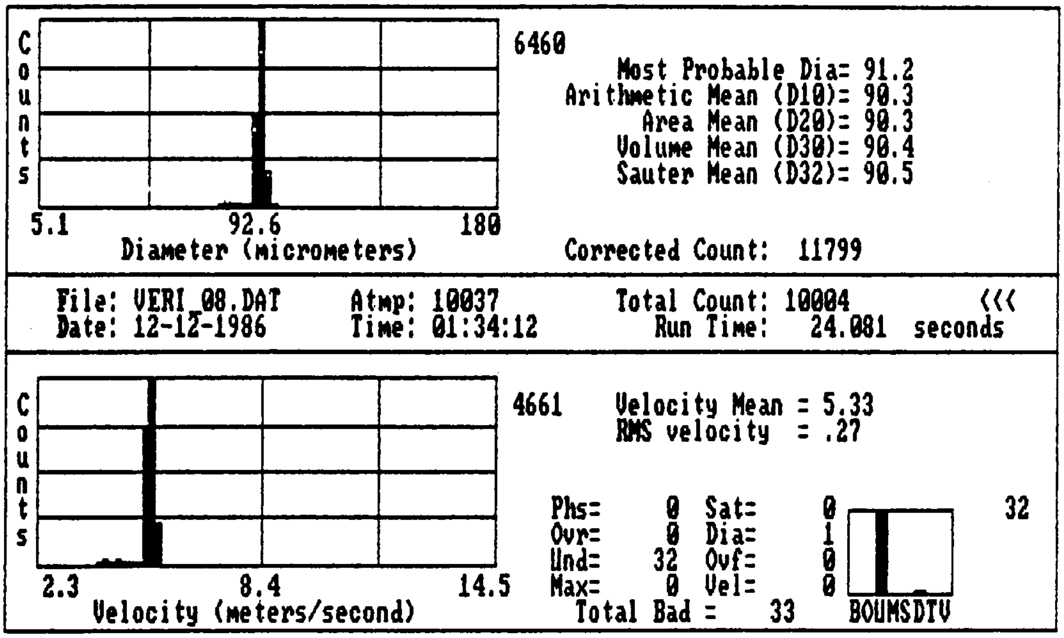


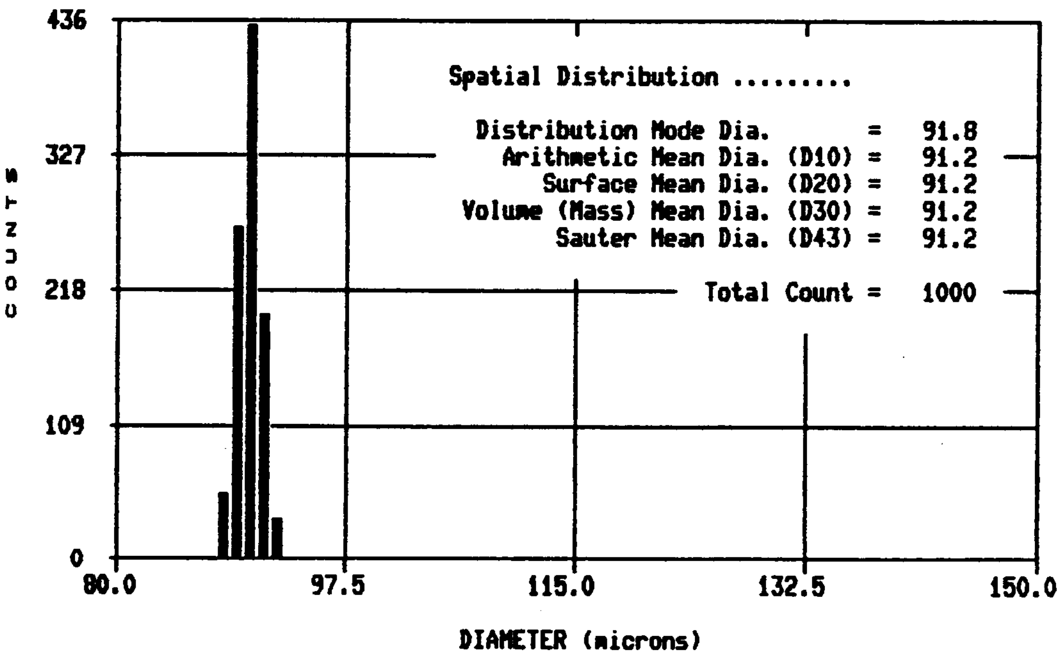


Theoretical Diameter = 90.4 $\mu$m
Diameter of Orifice = 50 $\mu$m
Liquid Feedrate = 0.59 cm$^3$/min.
Vibration Frequency = 25.5 kHz

Figure 3.12: VOAG Verification w/o Dispersion Cup

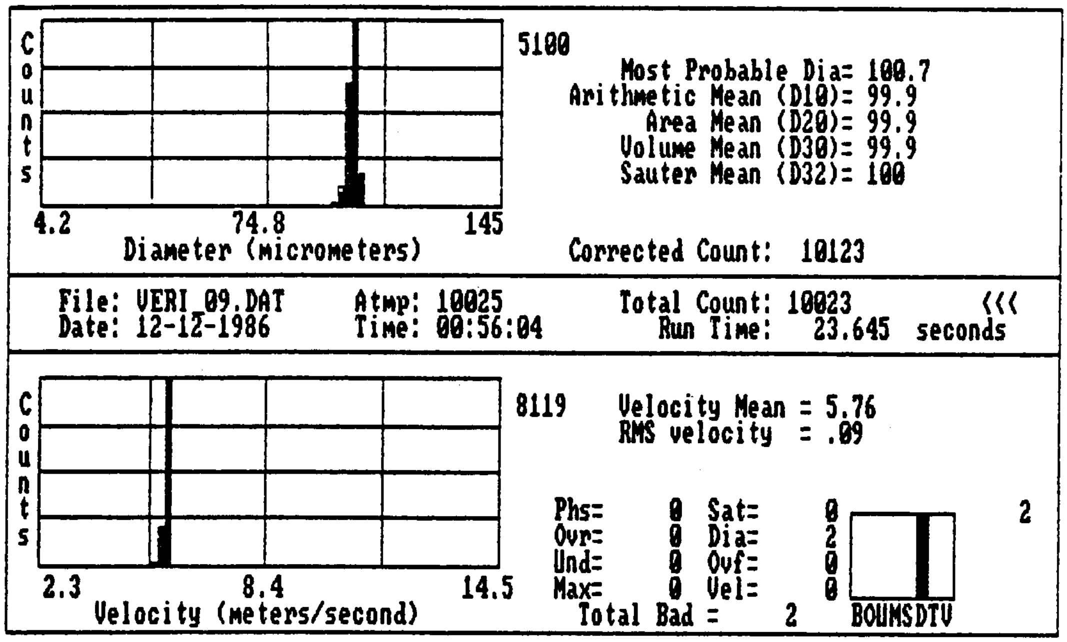


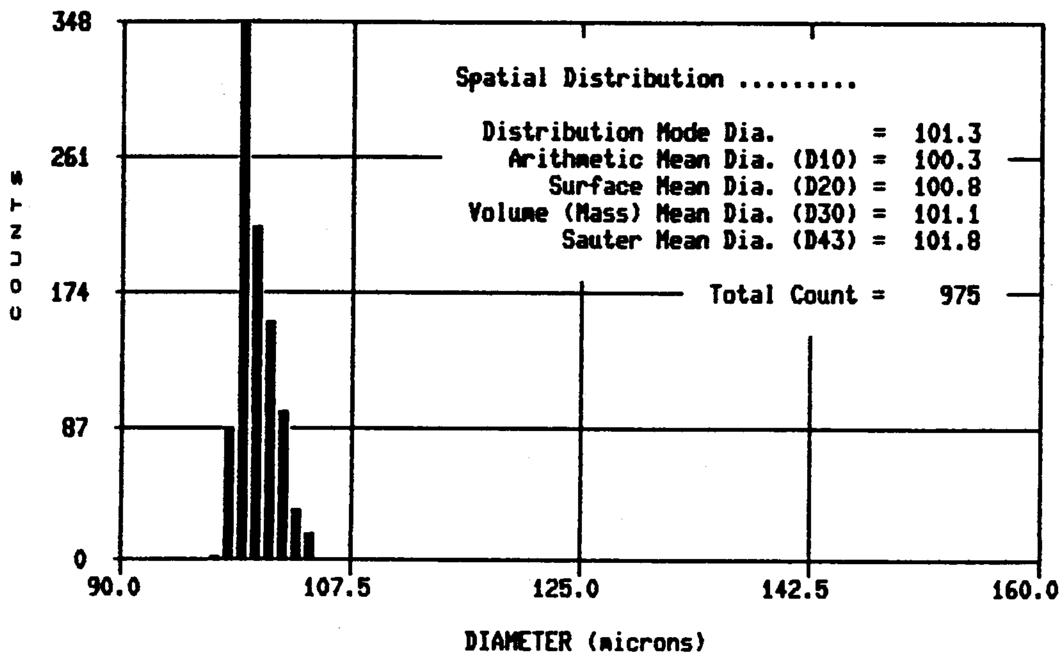


Theoretical Diameter = 99.6 $\mu$m
Diameter of Orifice = 50 $\mu$m
Liquid Feedrate = 0.59 $cm^3$/min.
Vibration Frequency = 19.0 kHz

Figure 3.13: VOAG Verification w/o Dispersion Cup

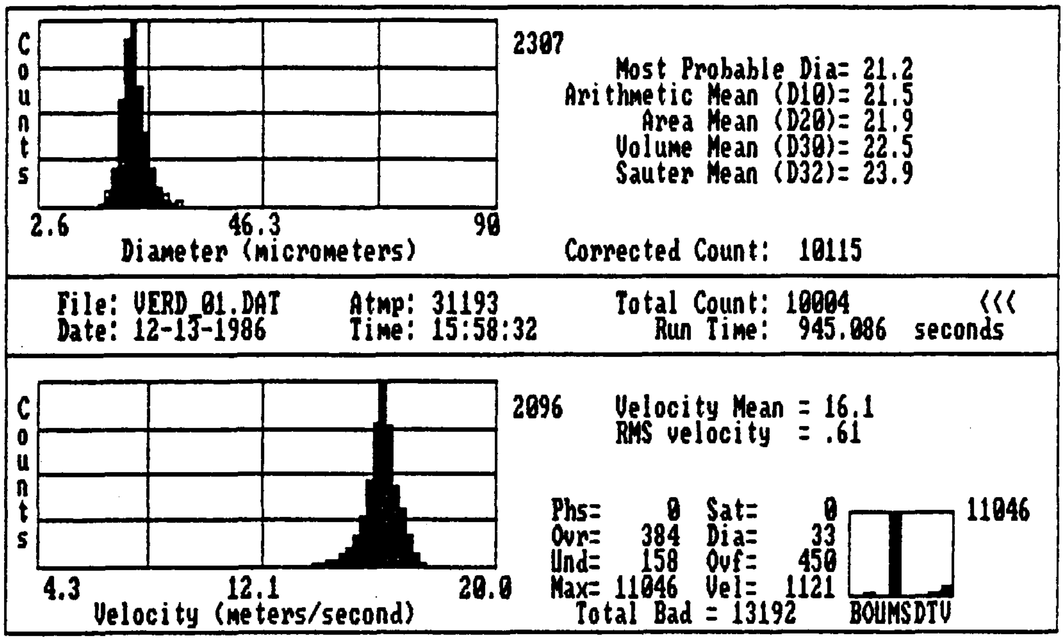


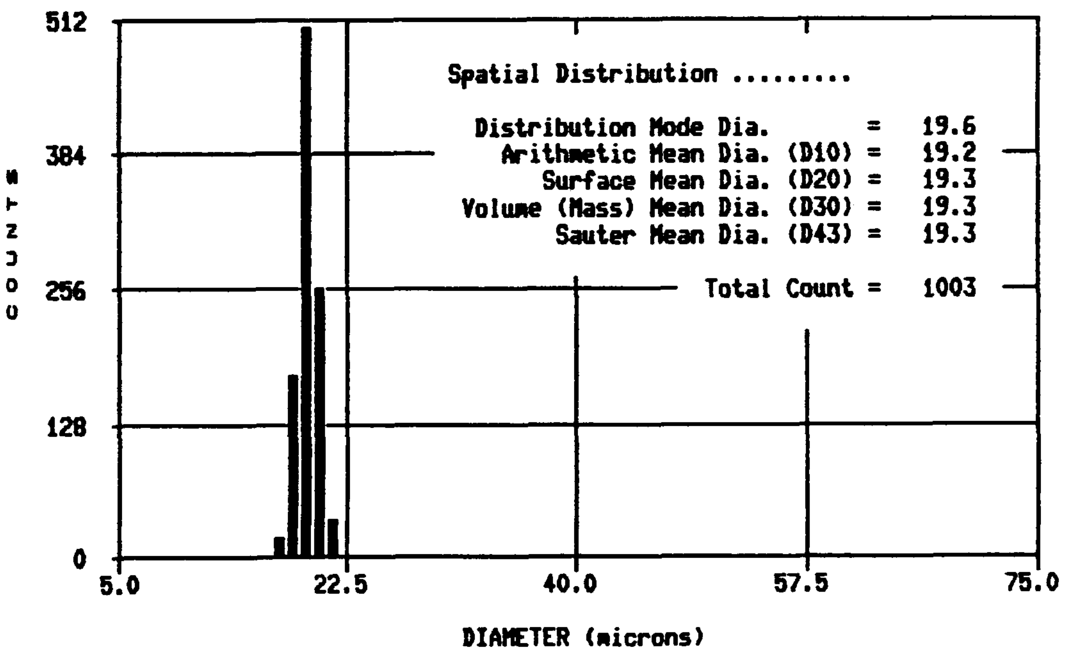


Theoretical Diameter = 19.8 $\mu$m
Diameter of Orifice = 10 $\mu$m
Liquid Feedrate = 0.08 $cm^3$/min.
Vibration Frequency = 330.4 kHz

Figure 3.14: VOAG Verification w/ Dispersion Cup

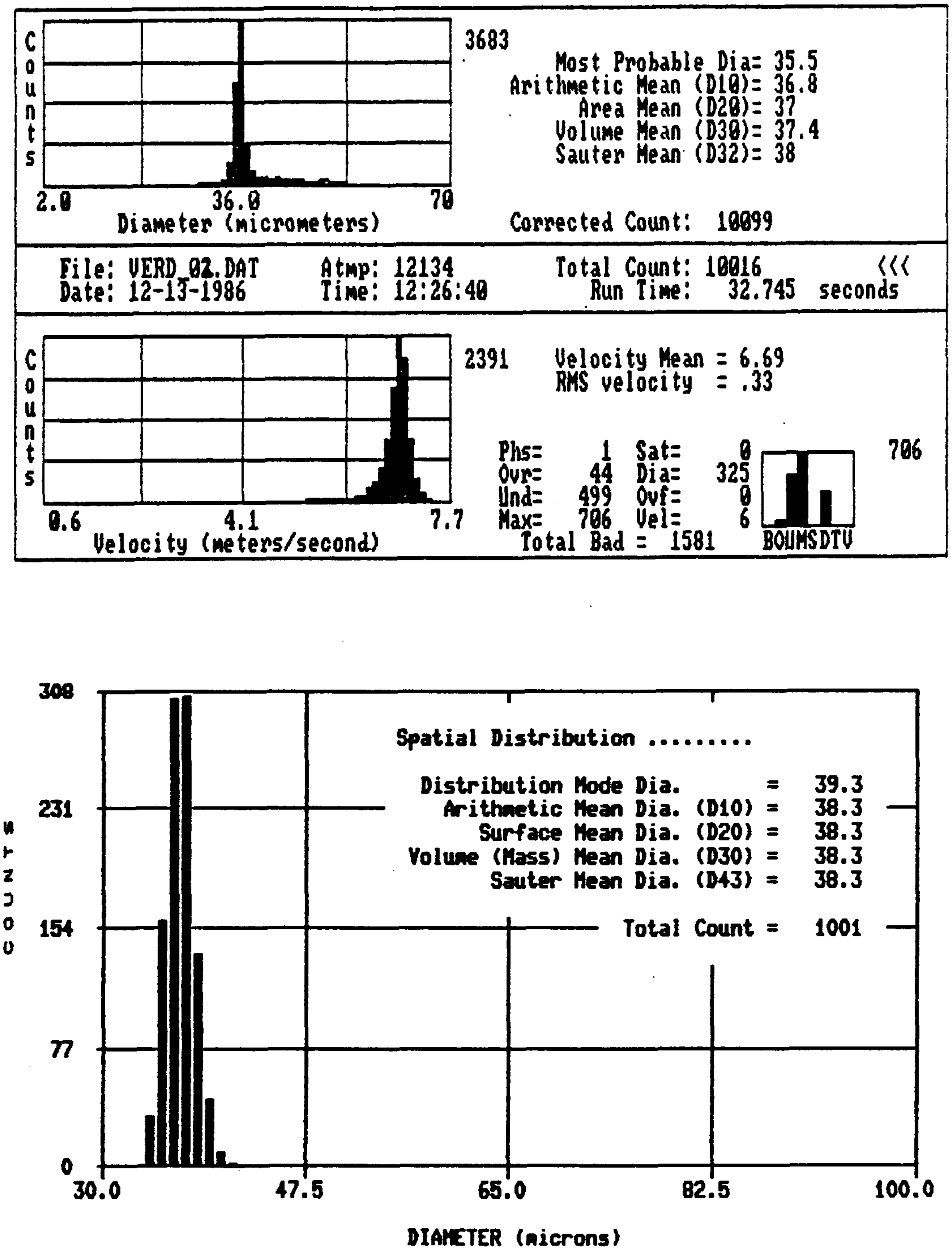


Theoretical Diameter = 35.5 $\mu$m
Diameter of Orifice = 20 $\mu$m
Liquid Feedrate = 0.139 cm$^3$/min.
Vibration Frequency = 100.2 kHz

Figure 3.15: VOAG Verification w/ Dispersion Cup

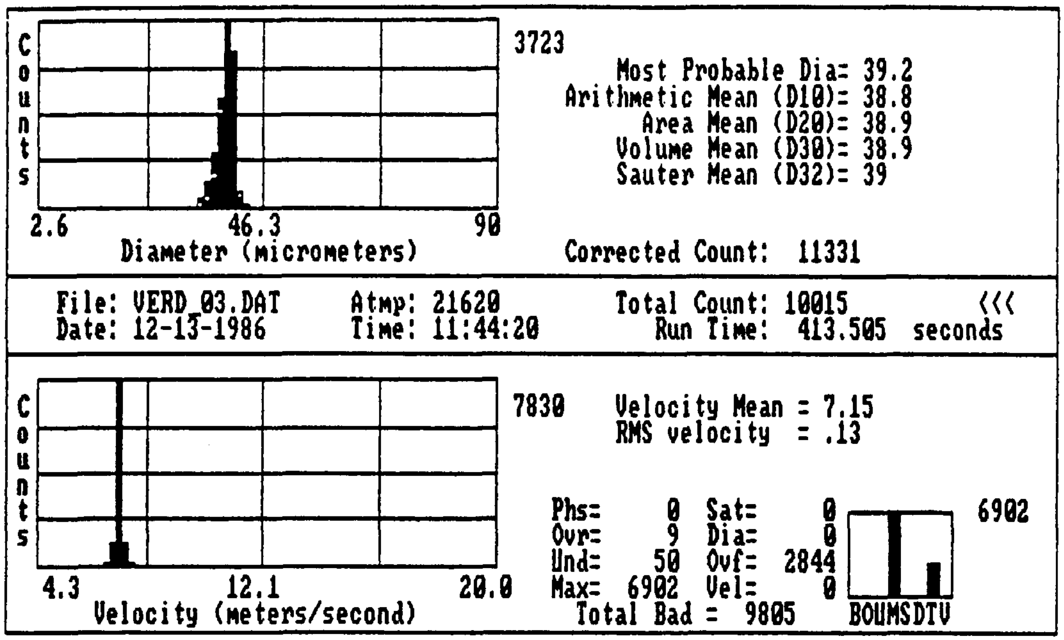


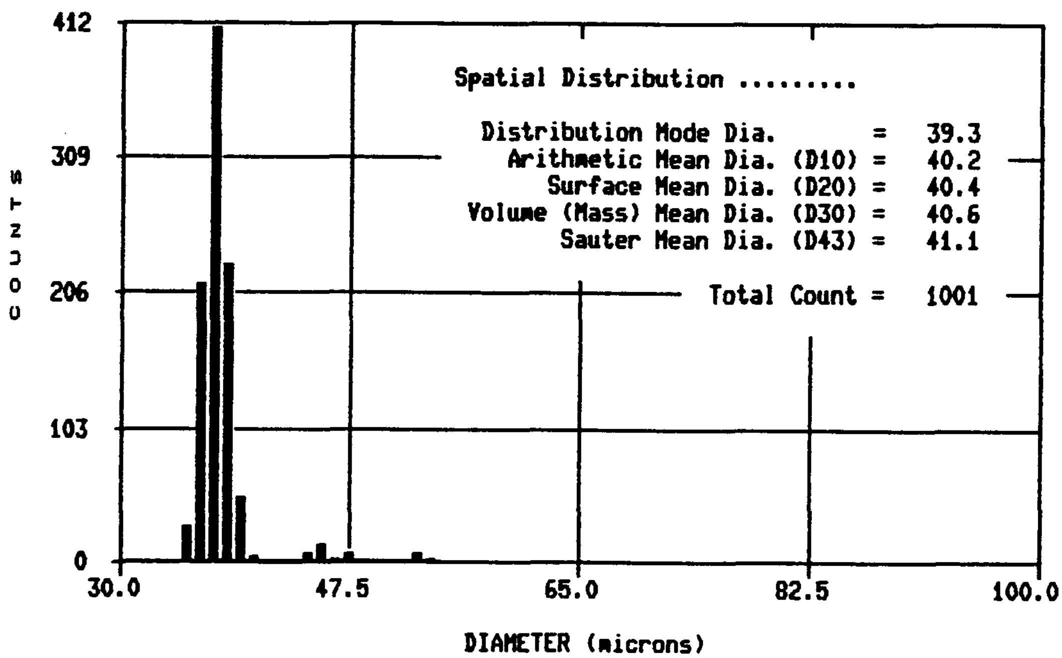


Theoretical Diameter = 39.0 $\mu$m

Diameter of Orifice = 20 $\mu$m

Liquid Feedrate = 0.139 $cm^3$/min.

Vibration Frequency = 79.2 kHz

Figure 3.16: VOAG Verification w/ Dispersion Cup

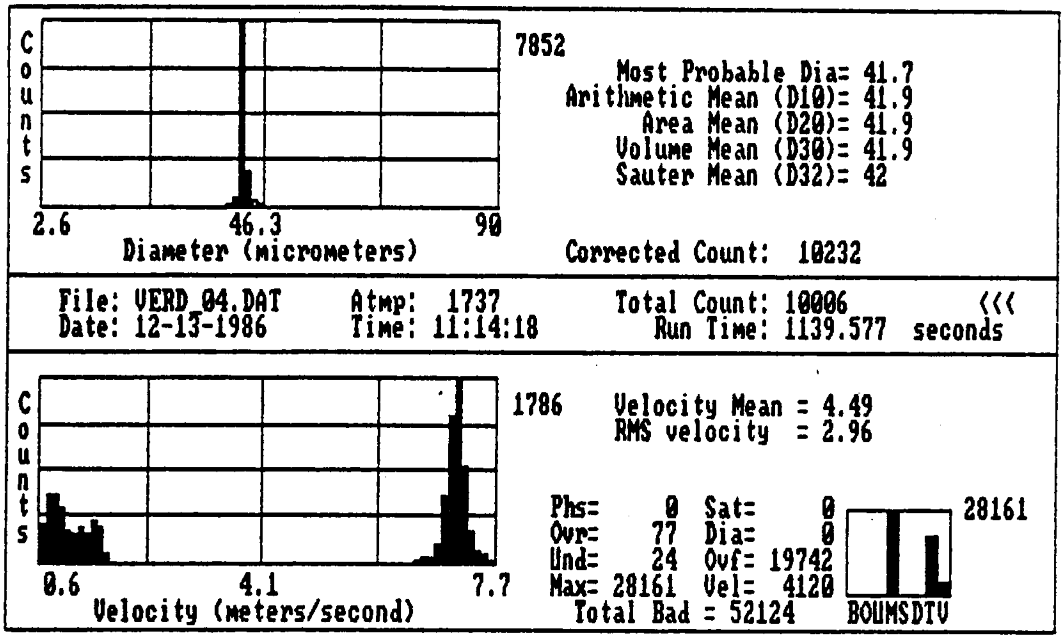


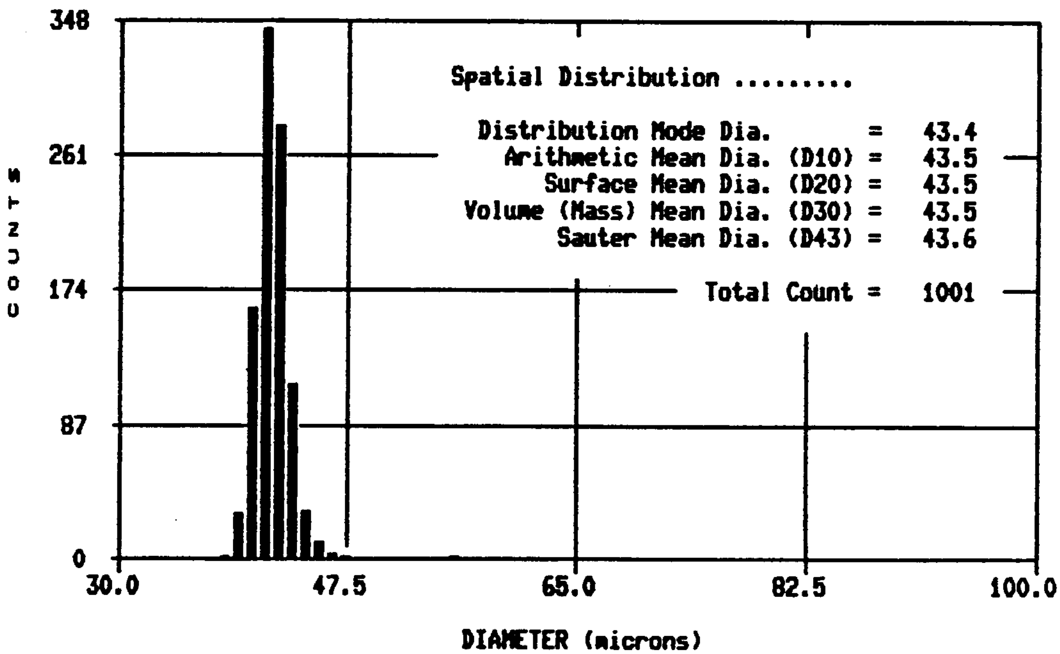


Theoretical Diameter = 41.5 $\mu$m
Diameter of Orifice = 20 $\mu$m
Liquid Feedrate = 0.139 $cm^3$/min.
Vibration Frequency = 62.5 kHz

Figure 3.17: VOAG Verification w/ Dispersion Cup

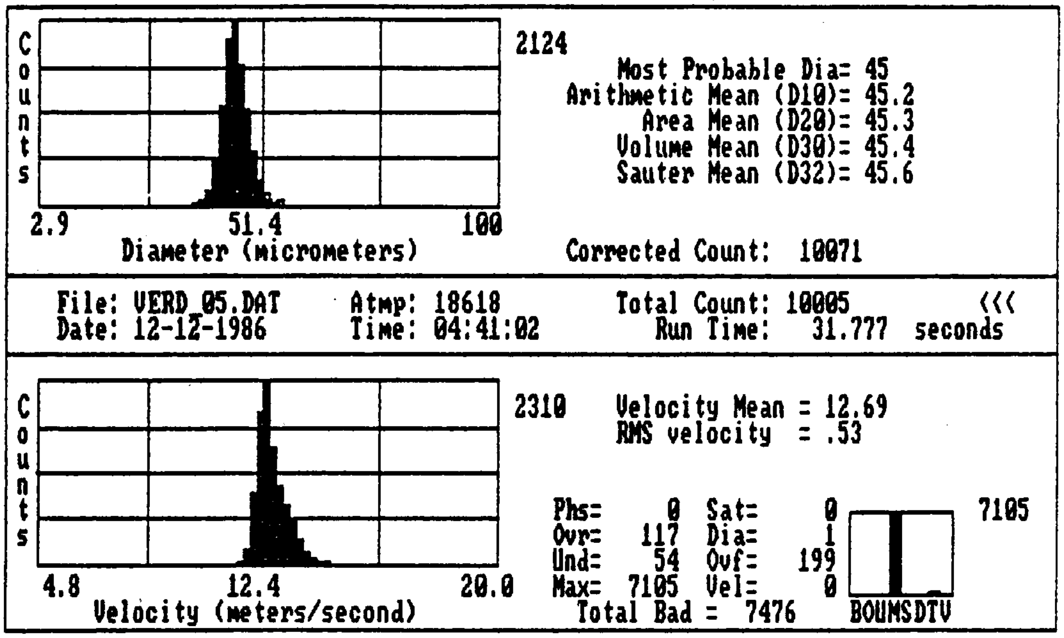


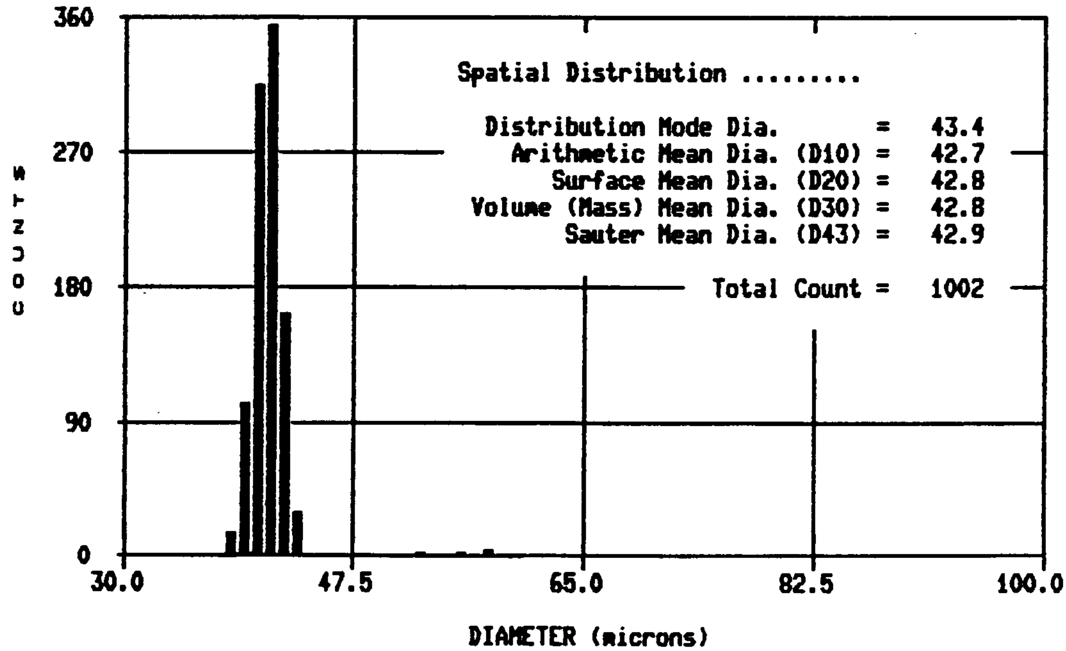


Theoretical Diameter = 44.2 $\mu$m
Diameter of Orifice = 20 $\mu$m
Liquid Feedrate = 0.139 $cm^3$/min.
Vibration Frequency = 51.6 kHz

Figure 3.18: VOAG Verification w/ Dispersion Cup

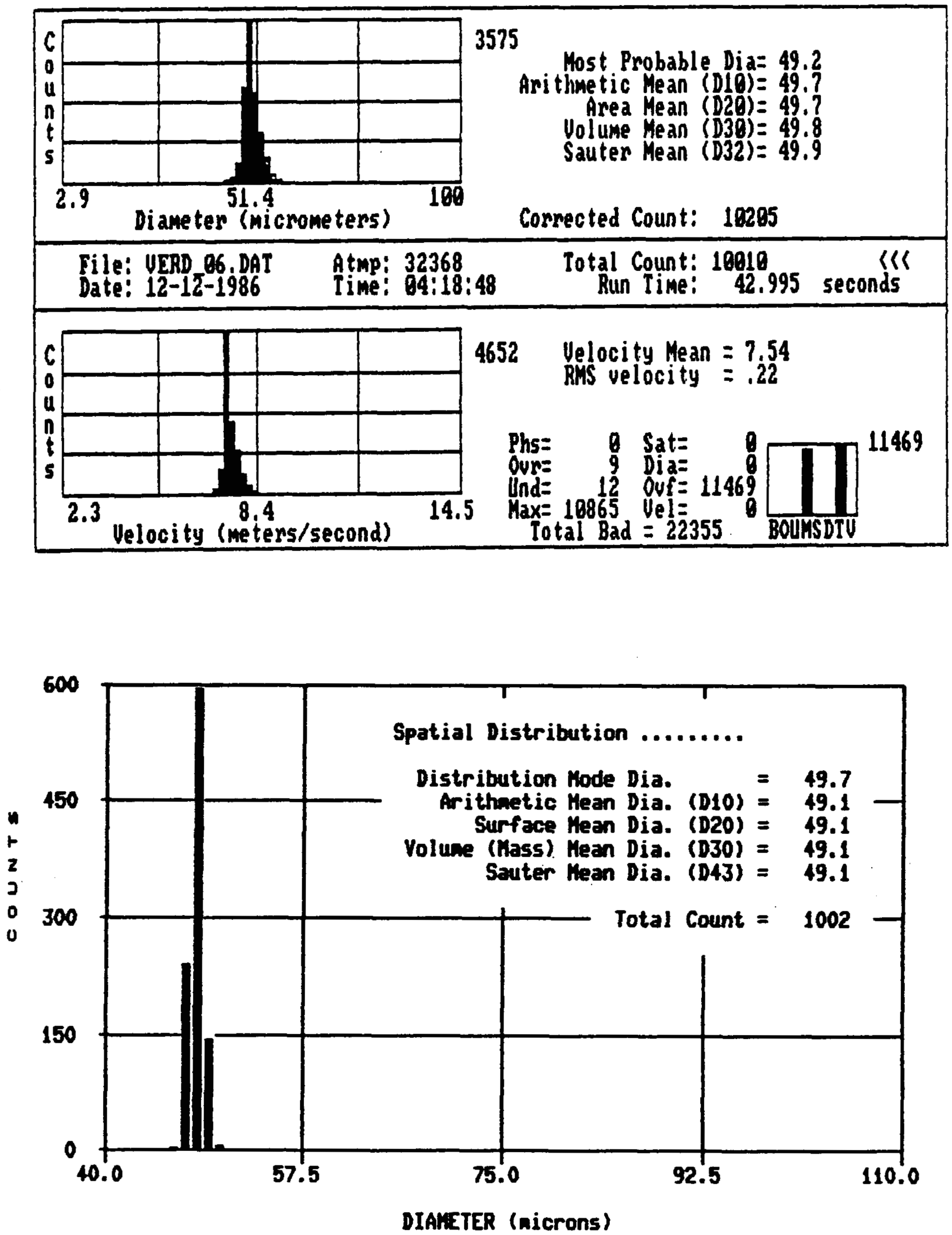


Theoretical Diameter = 47.5 $\mu$m
Diameter of Orifice = 20 $\mu$m
Liquid Feedrate = 0.139 $cm^3$/min.
Vibration Frequency = 41.6 kHz

Figure 3.19: VOAG Verification w/ Dispersion Cup

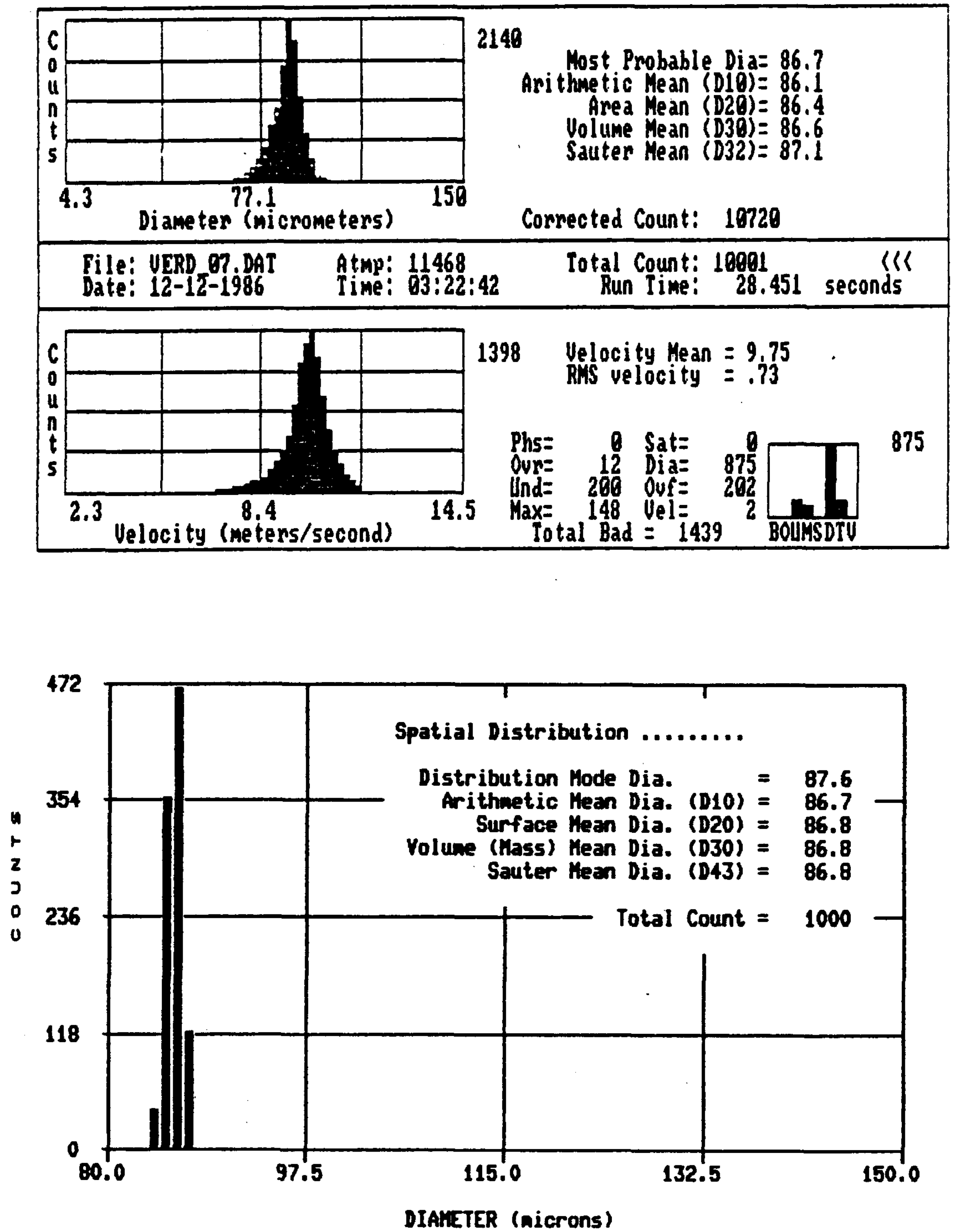


Theoretical Diameter = 85.6 $\mu$m
Diameter of Orifice = 50 $\mu$m
Liquid Feedrate = 0.59 cm$^3$/min.
Vibration Frequency = 30.1 kHz

Figure 3.20: VOAG Verification w/ Dispersion Cup

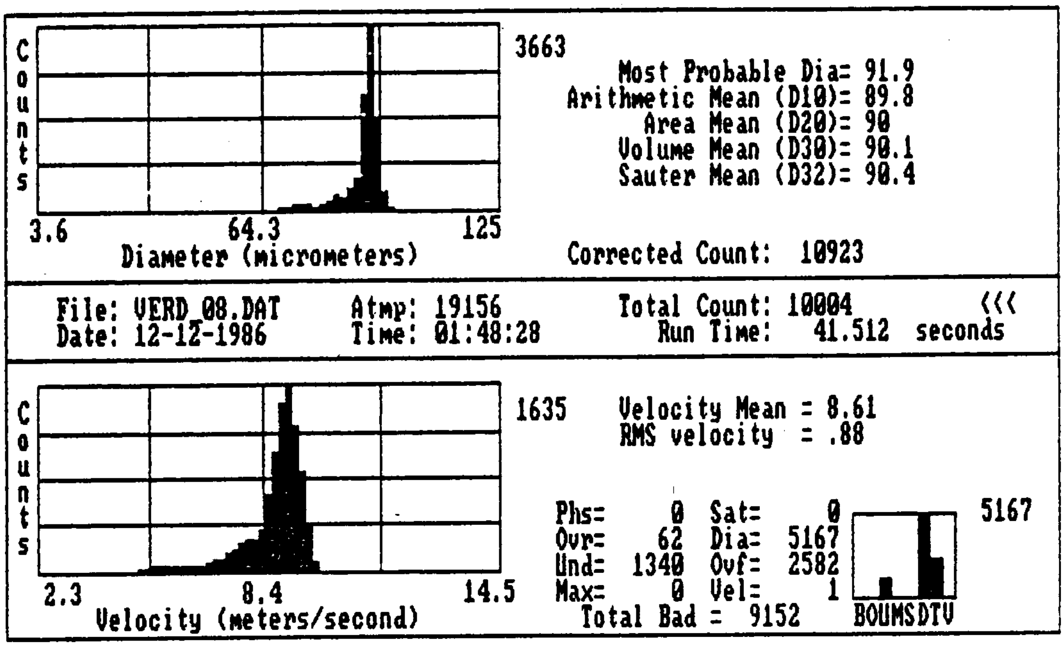


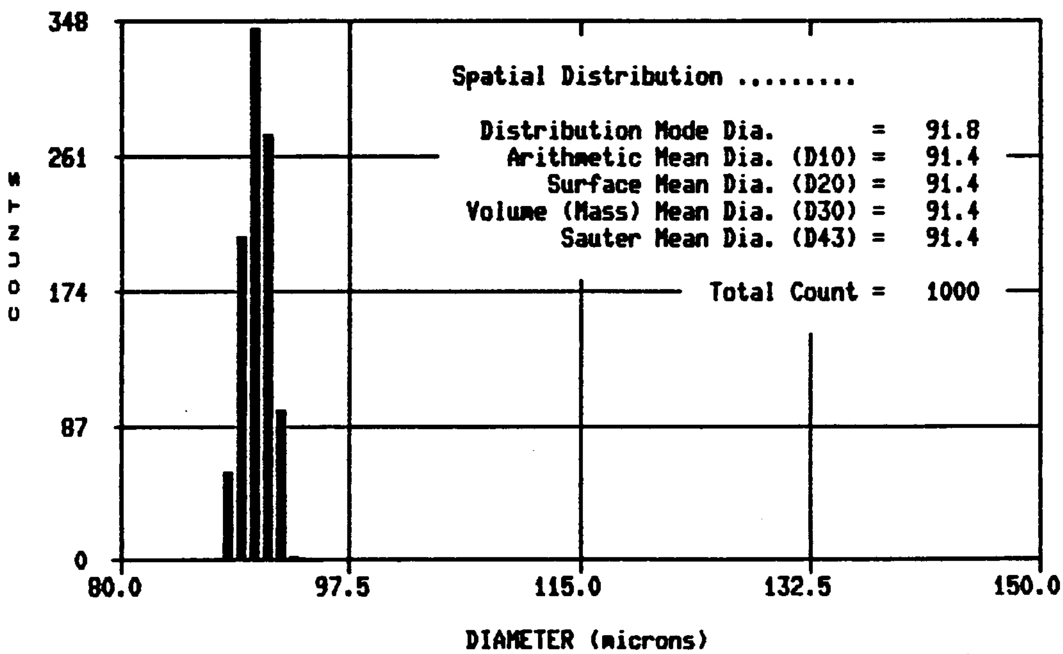


Theoretical Diameter = 90.4 $\mu$m
Diameter of Orifice = 50 $\mu$m
Liquid Feedrate = 0.59 $cm^3$/min.
Vibration Frequency = 25.5 kHz

Figure 3.21: VOAG Verification w/ Dispersion Cup

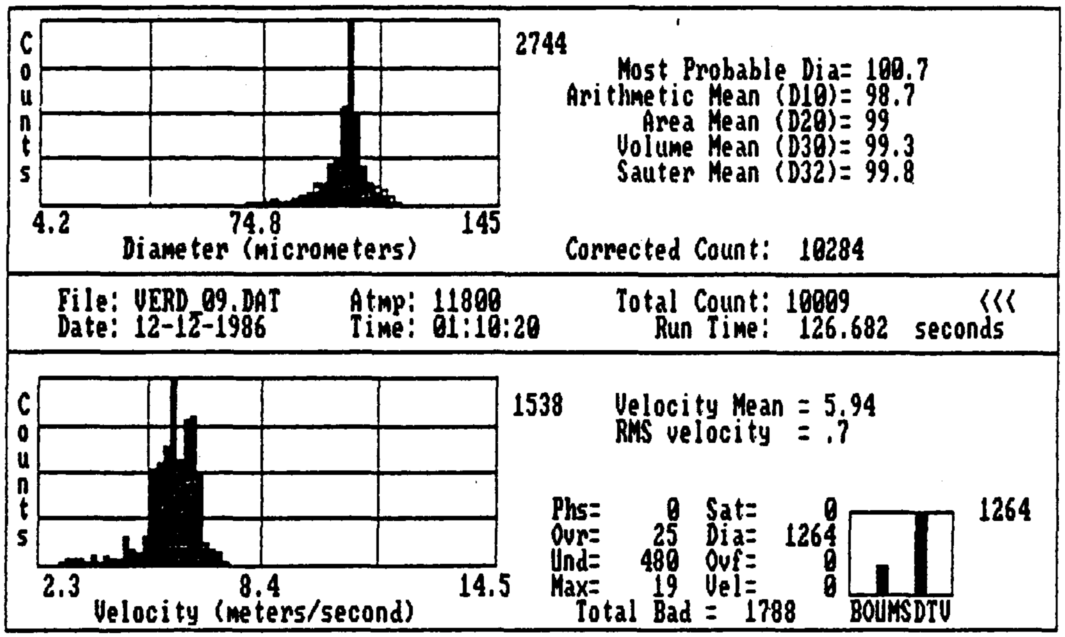


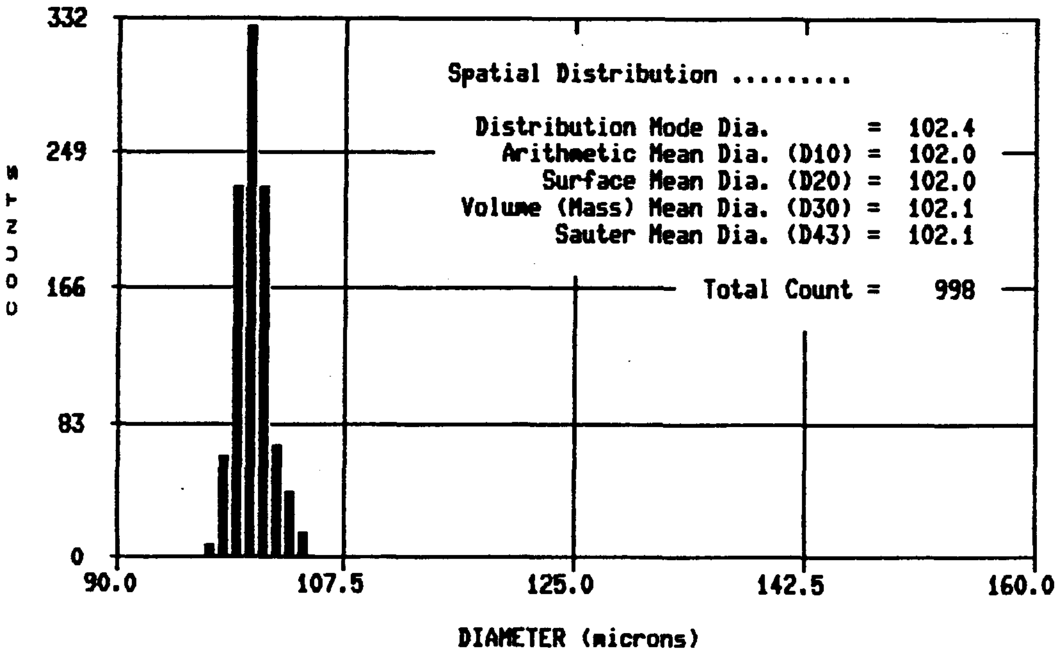


Theoretical Diameter = 99.6 $\mu$m
Diameter of Orifice = 50 $\mu$m
Liquid Feedrate = 0.59 cm$^3$/min.
Vibration Frequency = 19.0 kHz

Figure 3.22: VOAG Verification w/ Dispersion Cup

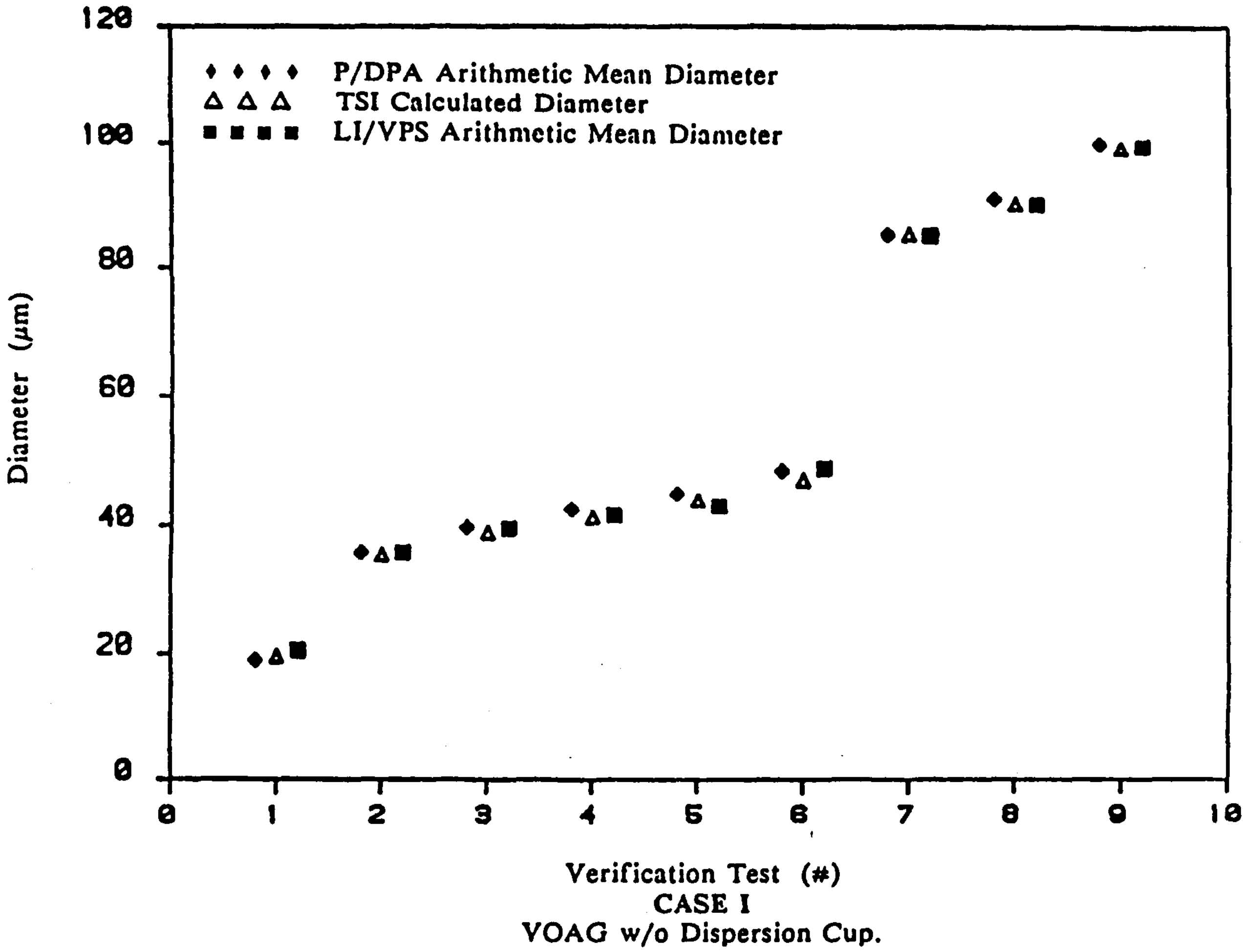


Figure 3.23: Comparison of Arithmetic Mean Diameters for CASE I VOAG Verification w/o Dispersion Cup Results

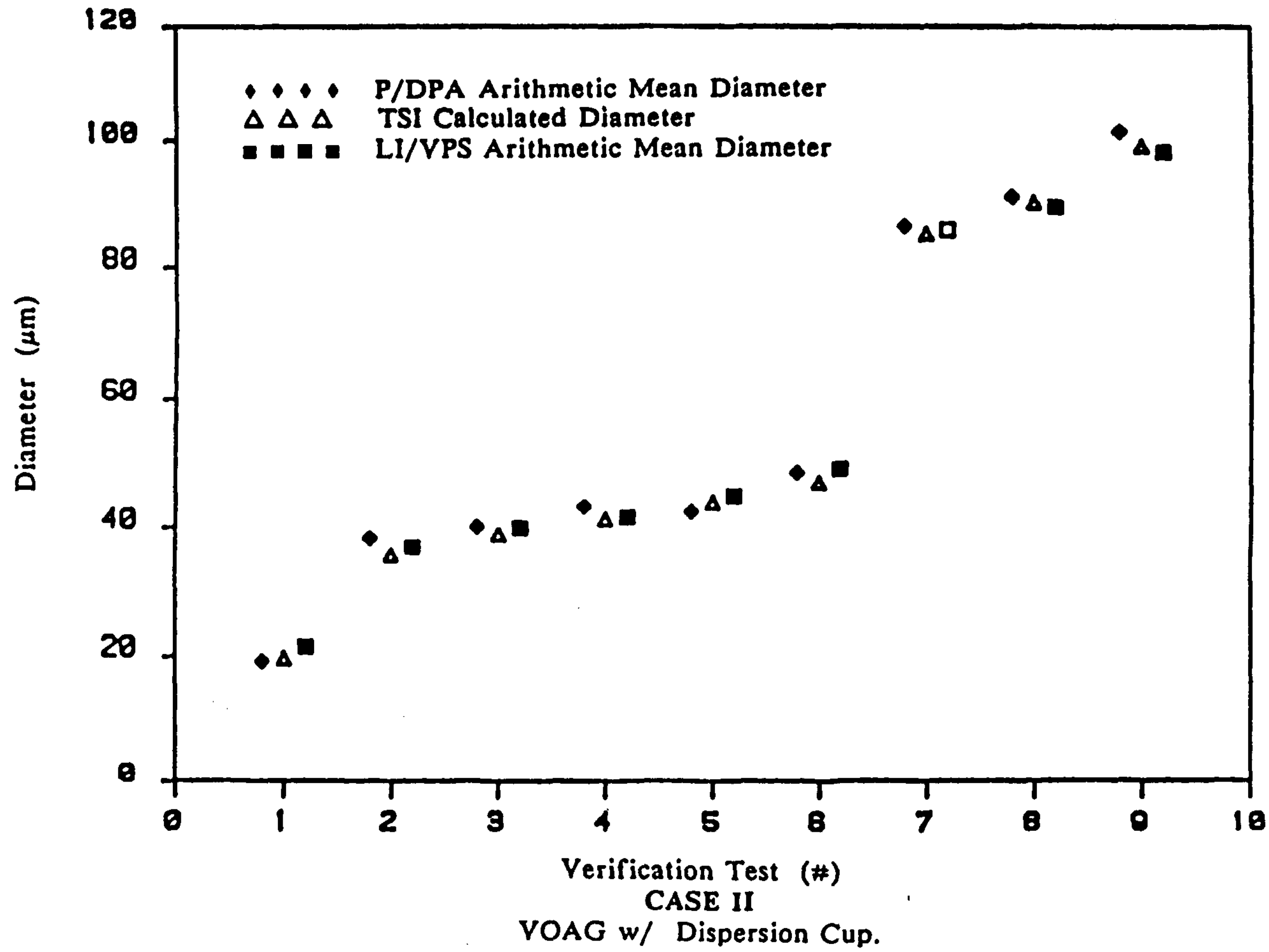


Figure 3.24: Comparison of Arithmetic Mean Diameters for CASE II VOAG Verification w/ Dispersion Cup Results

Table 3.4: VOAG Verification Results

## CASE I

Vibrating Orifice Aerosol Generator w/o Dispersion Cup.

| TEST (#) | TSI DIAMETER (μm) | LI/VPS Results: ARITHMETIC MEAN DIAMETER (μm) | LI/VPS Results: STANDARD DEVIATION (μm) | P/DPA Results: ARITHMETIC MEAN DIAMETER (μm) | P/DPA Results: STANDARD DEVIATION (μm) |
|---|---|---|---|---|---|
| 1 | 19.8 | 19.1 | 0.101 | 20.5 | 2.073 |
| 2 | 35.5 | 35.9 | 0.818 | 35.8 | 1.020 |
| 3 | 39.0 | 39.8 | 0.047 | 39.6 | 0.060 |
| 4 | 41.5 | 42.7 | 0.176 | 41.8 | 0.128 |
| 5 | 44.2 | 45.2 | 0.150 | 43.3 | 0.045 |
| 6 | 47.5 | 48.8 | 0.153 | 49.2 | 0.076 |
| 7 | 85.6 | 85.6 | 0.108 | 89.4 | 0.270 |
| 8 | 90.4 | 91.2 | 0.142 | 90.3 | 0.399 |
| 9 | 99.6 | 100.3 | 0.340 | 99.9 | 0.436 |

## CASE II

Vibrating Orifice Aerosol Generator with Dispersion Cup.

| TEST (#) | TSI DIAMETER (μm) | LI/VPS Results: ARITHMETIC MEAN DIAMETER (μm) | LI/VPS Results: STANDARD DEVIATION (μm) | P/DPA Results: ARITHMETIC MEAN DIAMETER (μm) | P/DPA Results: STANDARD DEVIATION (μm) |
|---|---|---|---|---|---|
| 1 | 19.8 | 19.2 | 0.325 | 21.5 | 2.063 |
| 2 | 35.5 | 38.3 | 0.432 | 36.8 | 1.560 |
| 3 | 39.0 | 40.2 | 1.355 | 40.0 | 0.566 |
| 4 | 41.5 | 43.5 | 1.063 | 41.9 | 0.120 |
| 5 | 44.2 | 42.7 | 1.109 | 45.5 | 0.379 |
| 6 | 47.5 | 49.1 | 0.541 | 49.7 | 0.275 |
| 7 | 85.6 | 86.7 | 0.139 | 86.1 | 2.080 |
| 8 | 90.4 | 91.4 | 0.175 | 89.8 | 0.844 |
| 9 | 99.6 | 102.0 | 0.420 | 98.7 | 0.155 |

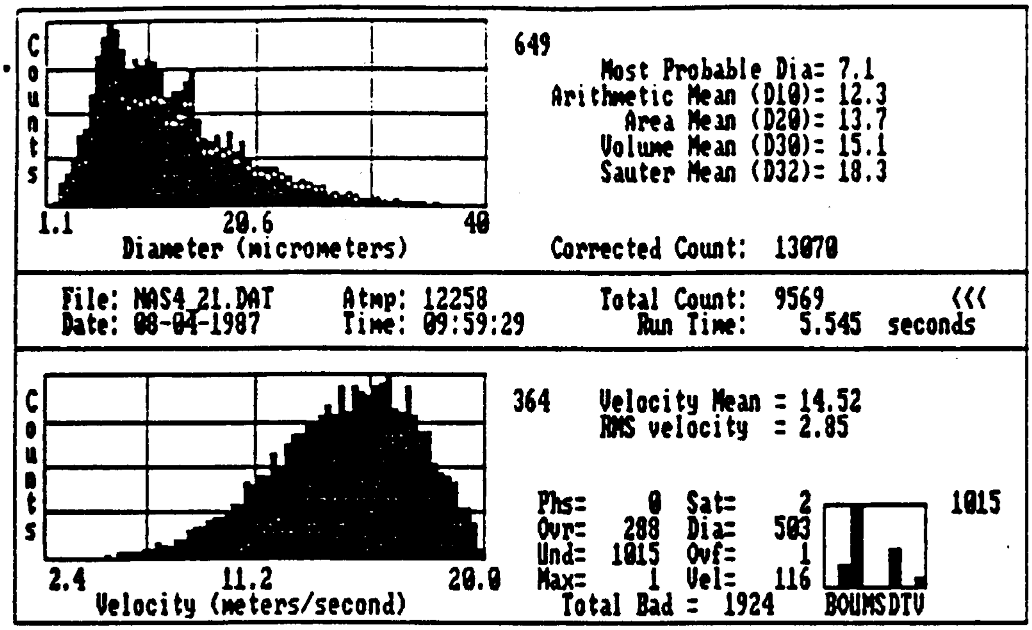


a. P/DPA Results

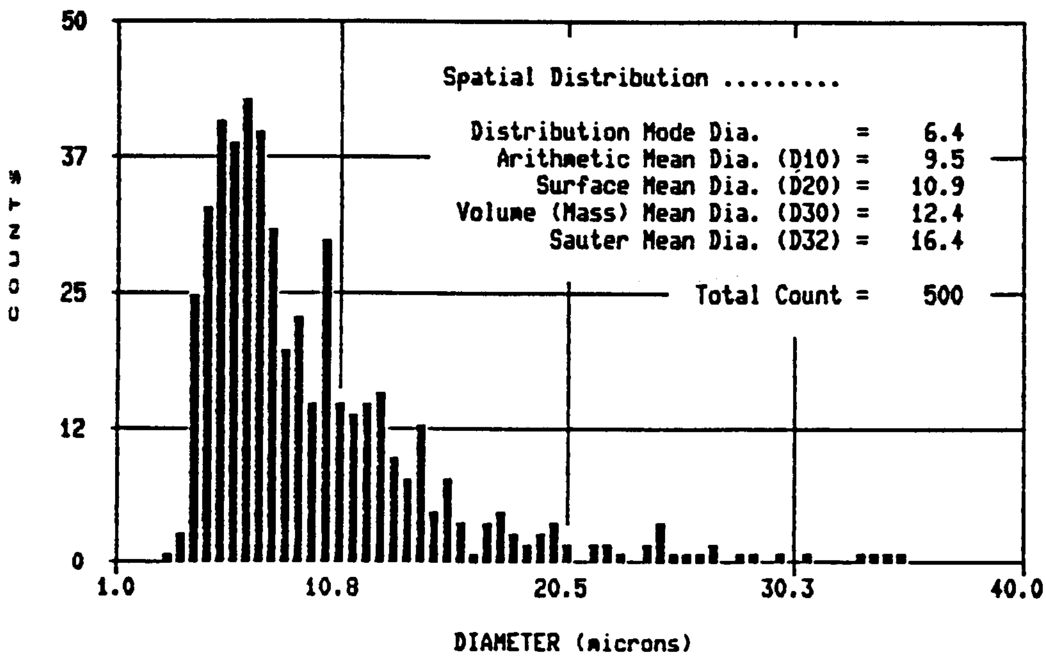


b. LI/VPS Results

(CASE I)

Test Conditions: Radial Position = $C_L$

Air Pressure = 65 psia

Water Pressure = 105 psia

Water Flowrate = 0.038 gal/min.

Axial Position from Nozzle = 2 ft.

Figure 3.25: MOD-1 Nozzle Comparison

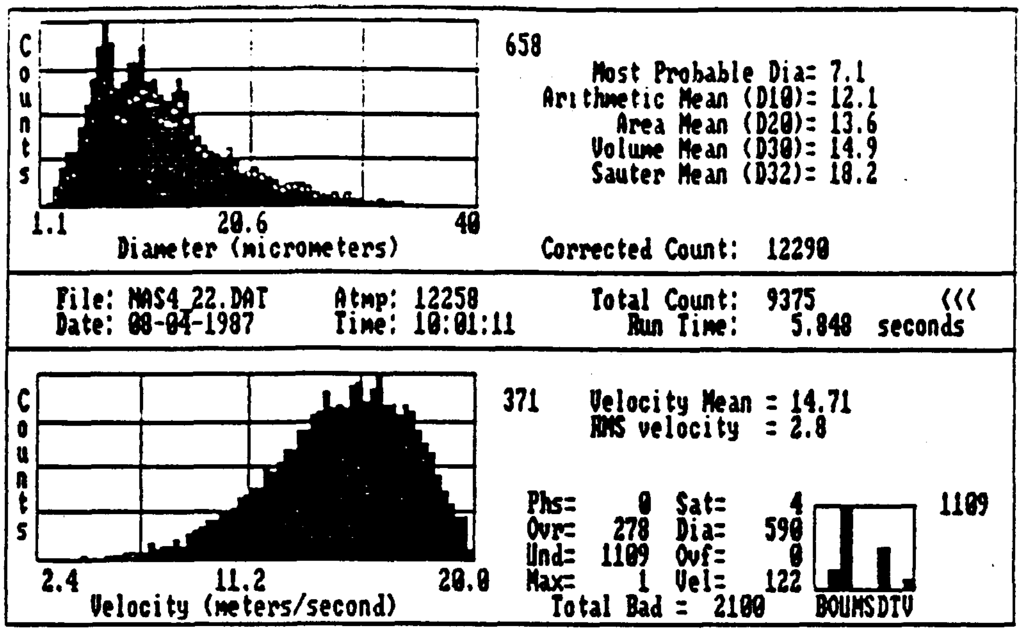


a. P/DPA Results

ORIGINAL PAGE IS
OF POOR QUALITY

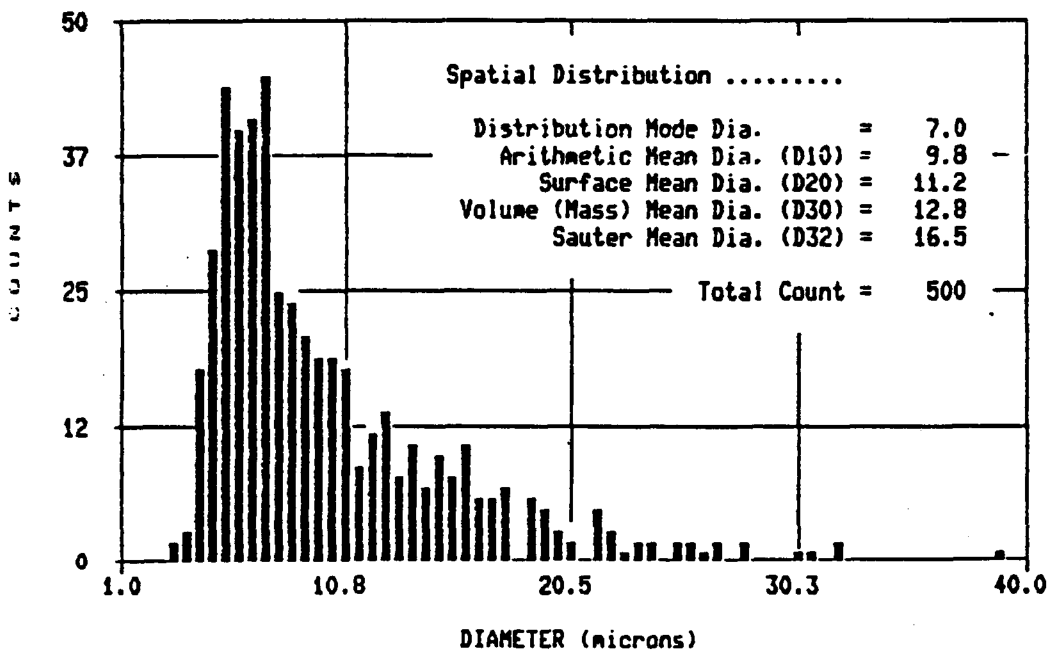


b. LI/VPS Results

(CASE I)

Test Conditions: Radial Position = $\frac{1}{2}$ in.
Air Pressure = 65 psia
Water Pressure = 105 psia
Water Flowrate = 0.038 gal/min.
Axial Position from Nozzle = 2 ft.

Figure 3.26: MOD-1 Nozzle Comparison

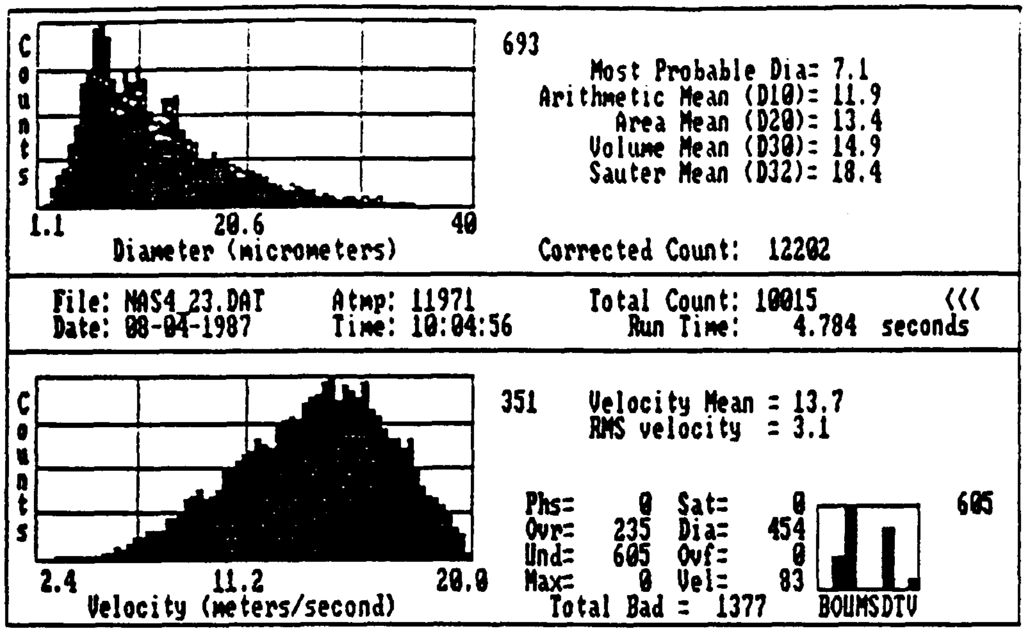


a. P/DPA Results

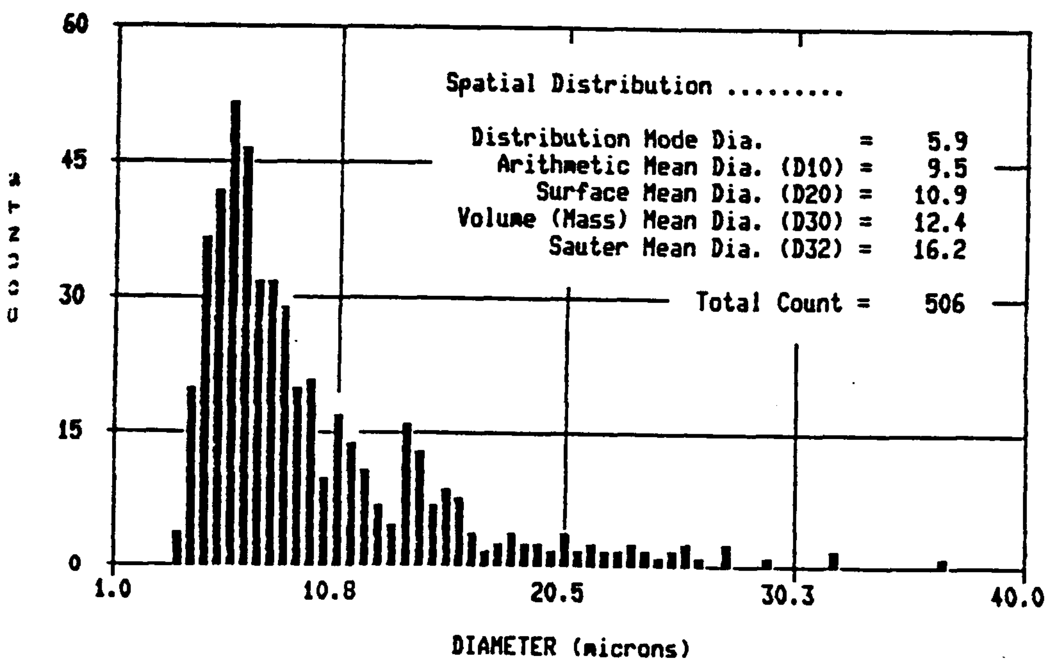


b. LI/VPS Results

(CASE I)

Test Conditions: Radial Position = 1 in.
Air Pressure = 65 psia
Water Pressure = 105 psia
Water Flowrate = 0.038 gal/min.
Axial Position from Nozzle = 2 ft.

Figure 3.27: MOD-1 Nozzle Comparison



ORIGINAL PAGE IS
OF POOR QUALITY

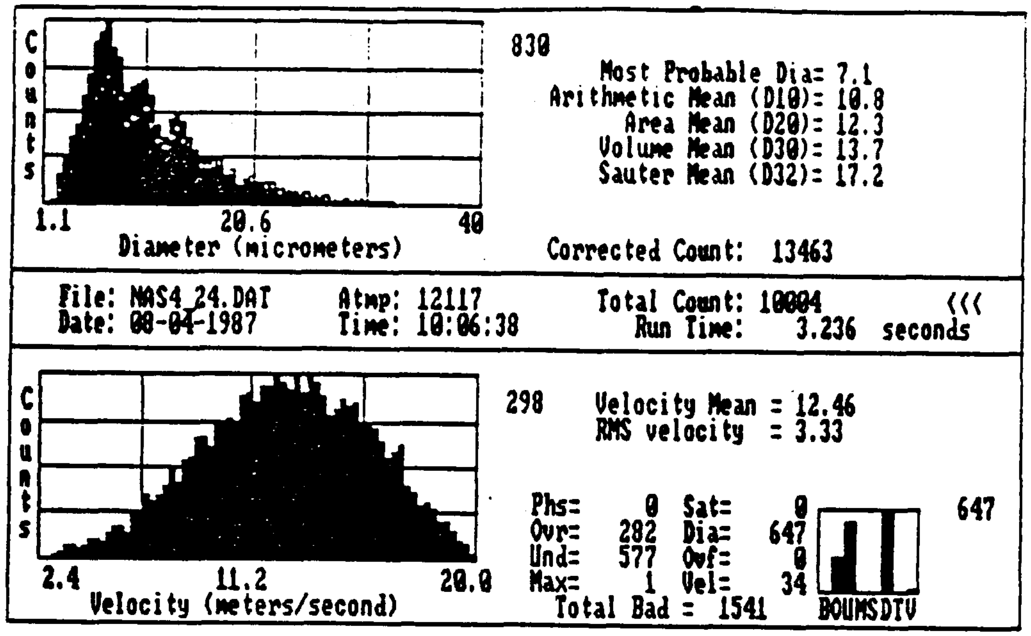


a. P/DPA Results

ORIGINAL PAGE IS
OF POOR QUALITY

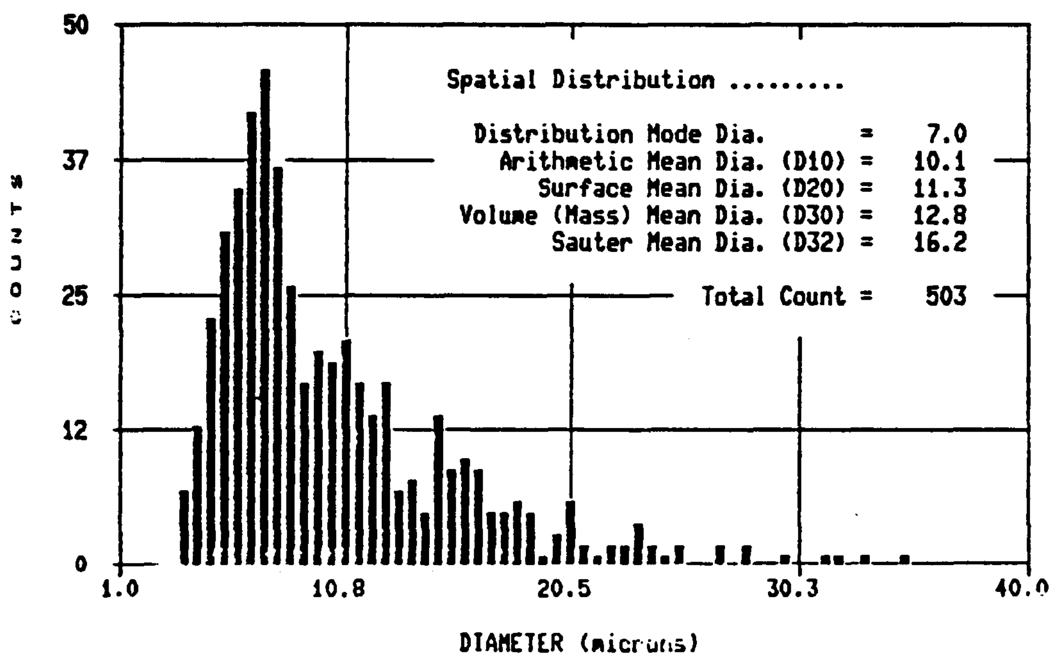


b. LI/VPS Results

(CASE I)

Test Conditions: Radial Position = $1\frac{1}{2}$ in.
Air Pressure = 65 psia
Water Pressure = 105 psia
Water Flowrate = 0.038 gal/min.
Axial Position from Nozzle = 2 ft.

Figure 3.28: MOD-1 Nozzle Comparison

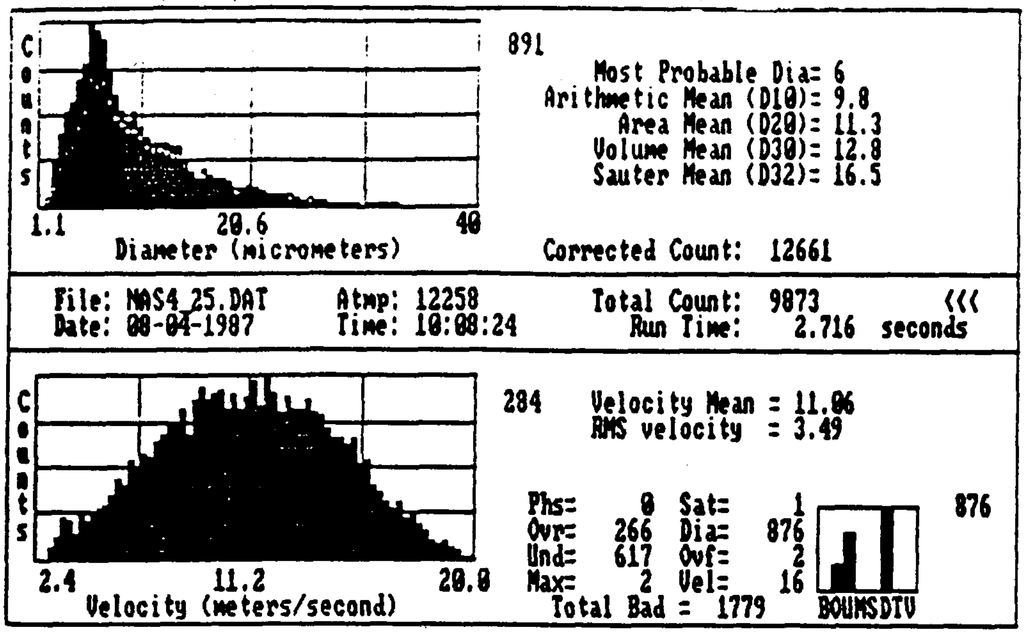


a. P/DPA Results

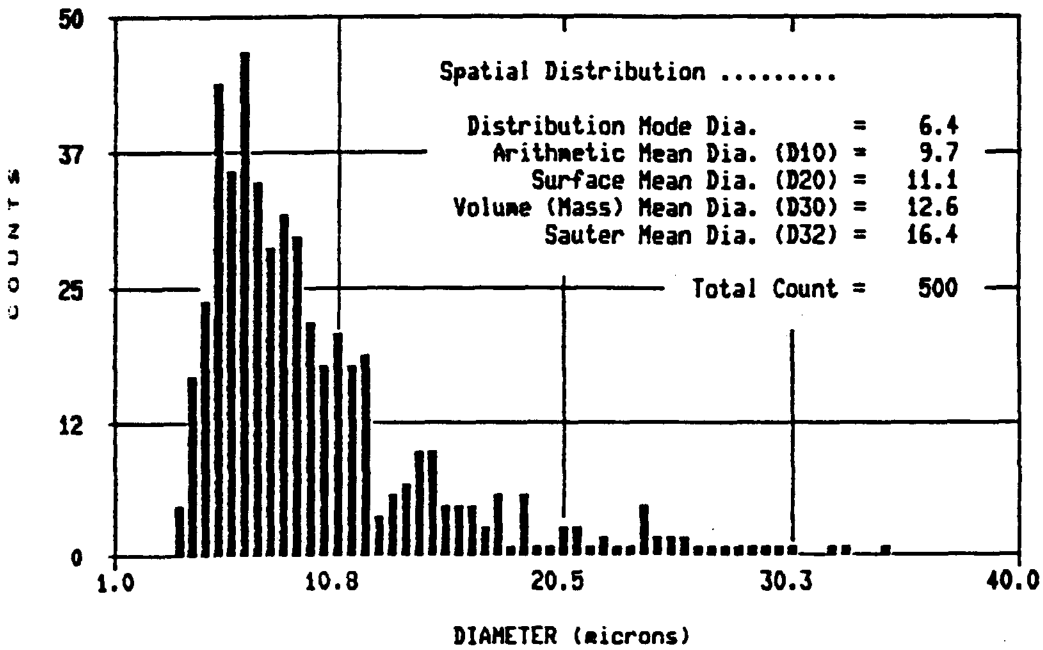


b. LI/VPS Results

(CASE I)

Test Conditions: Radial Position = 2 in.
Air Pressure = 65 psia
Water Pressure = 105 psia
Water Flowrate = 0.038 gal/min.
Axial Position from Nozzle = 2 ft.

Figure 3.29: MOD-1 Nozzle Comparison

ORIGINAL PAGE IS OF POOR QUALITY

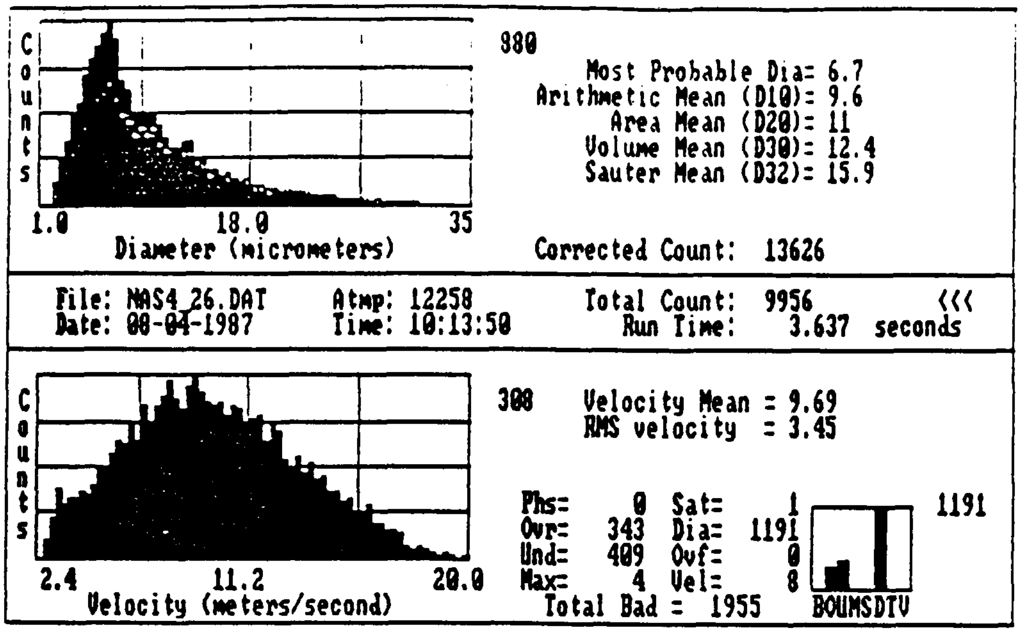


a. P/DPA Results

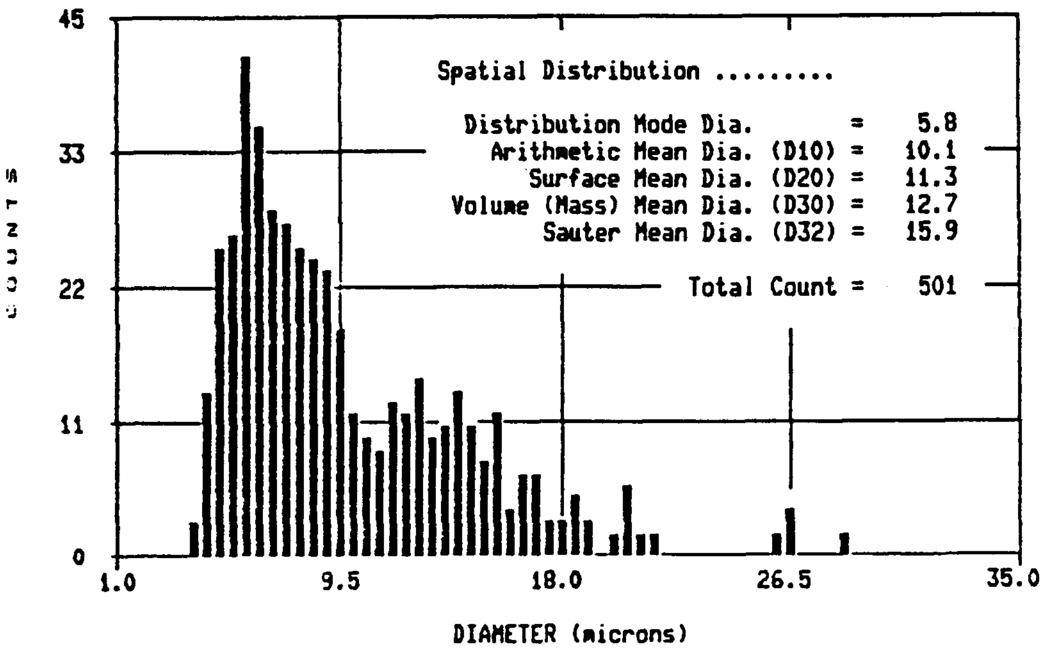


b. LI/VPS Results

(CASE I)

Test Conditions: Radial Position = $2\frac{1}{2}$ in.
Air Pressure = 65 psia
Water Pressure = 105 psia
Water Flowrate = 0.038 gal/min.
Axial Position from Nozzle = 2 ft.

Figure 3.30: MOD-1 Nozzle Comparison

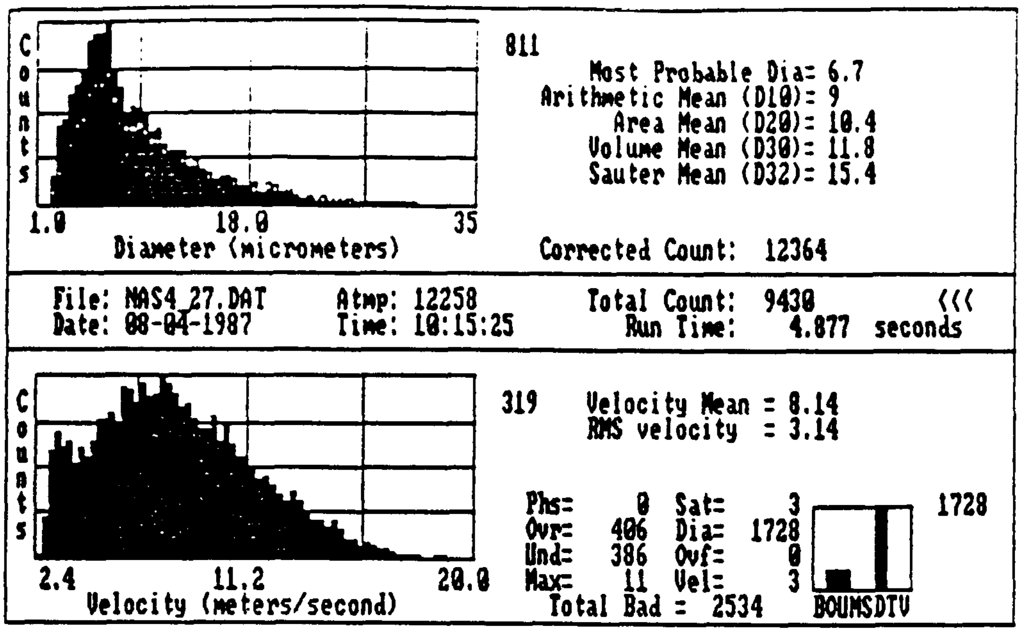


a. P/DPA Results

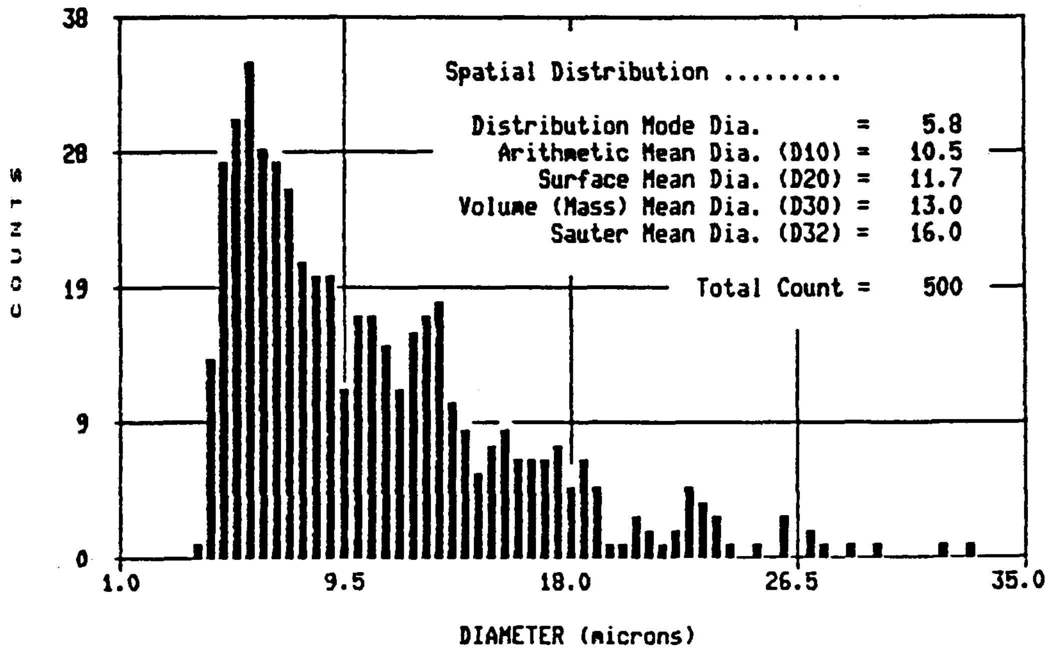


b. LI/VPS Results

(CASE I)

Test Condtions: Radial Position = 3 in.

Air Pressure = 65 psia

Water Pressure 105 psia

Water Flowrate = 0.038 gal/min.

Axial Position from Nozzle = 2 ft.

Figure 3.31: MOD-1 Nozzle Comparison

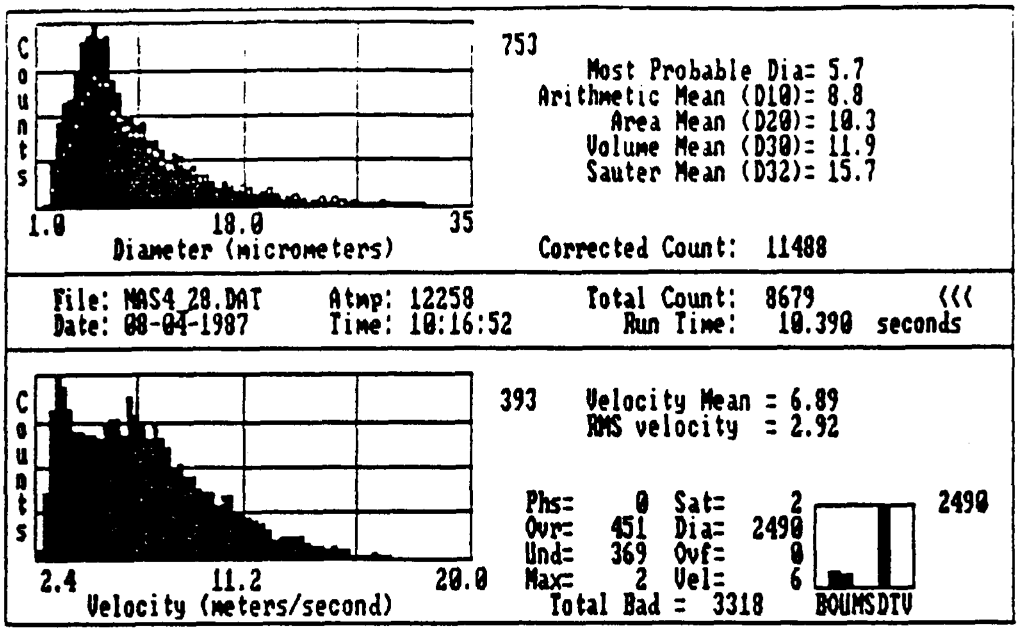


a. P/DPA Results

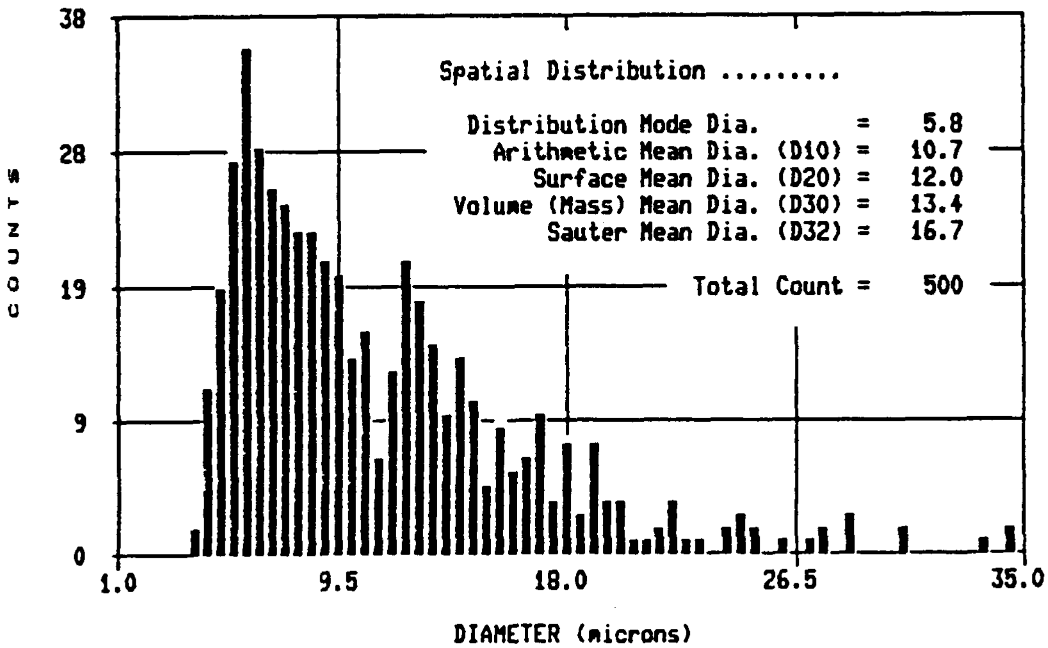


b. LI/VPS Results

(CASE I)

Test Condtions: Radial Position = $3\frac{1}{2}$ in.
Air Pressure = 65 psia
Water Pressure = 105 psia
Water Flowrate = 0.038 gal/min.
Axial Position from Nozzle = 2 ft.

ORIGINAL PAGE IS OF POOR QUALITY

Figure 3.32: MOD-1 Nozzle Comparison

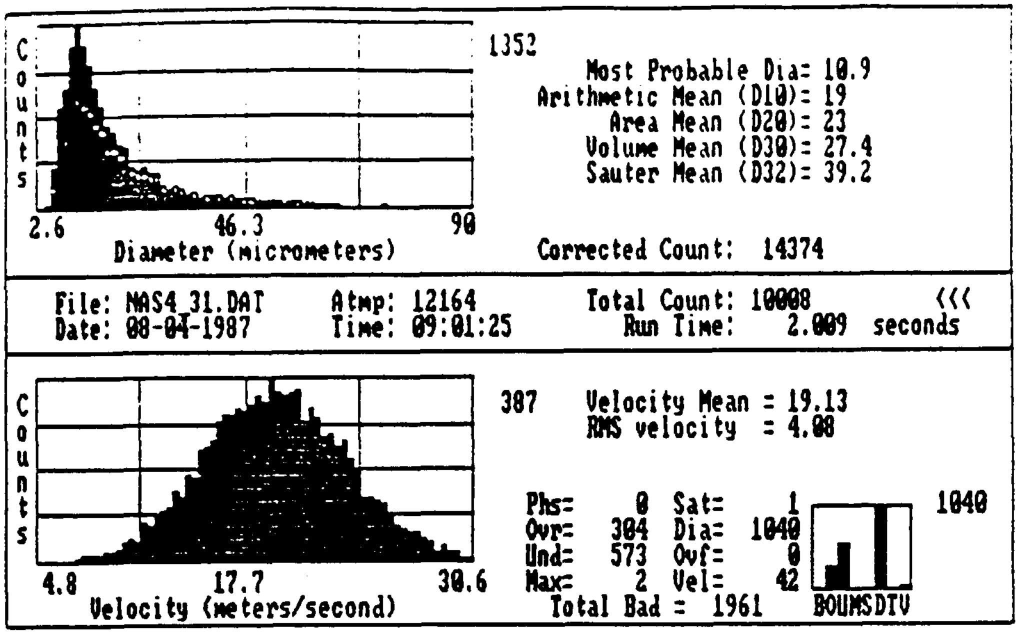


a. P/DPA Results

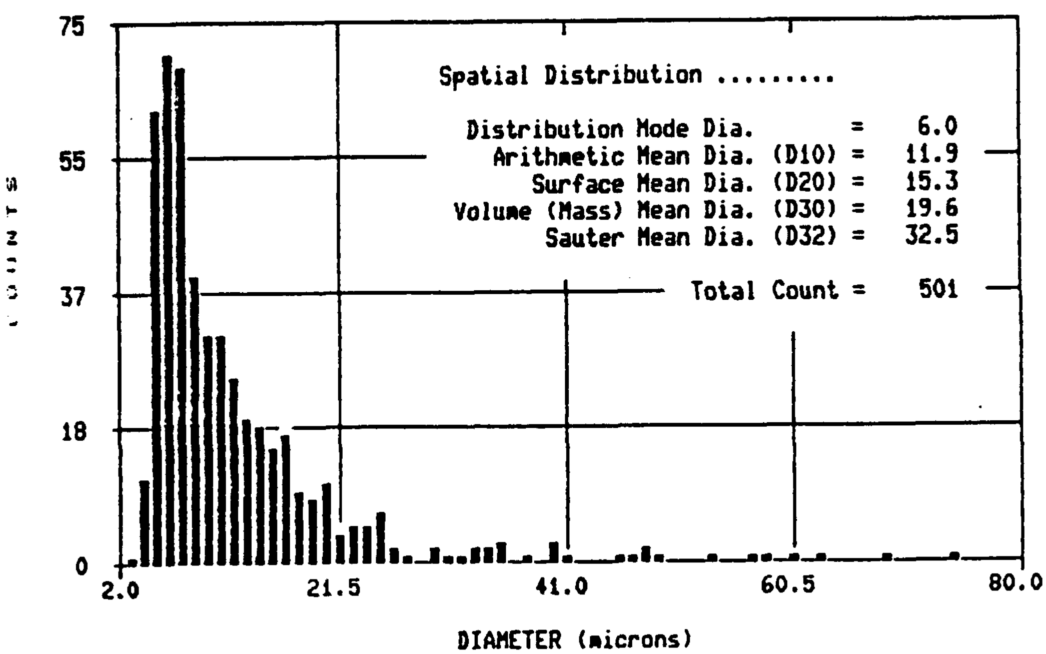


b. LI/VPS Results

(CASE II)

Test Conditions: Radial Position = $C_L$

Air Pressure = 45 psia

Water Pressure = 115 psia

Water Flowrate = 0.06 gal/min.

Axial Position from Nozzle = 2 ft.

ORIGINAL PAGE IS OF POOR QUALITY

Figure 3.33: MOD-1 Nozzle Comparison

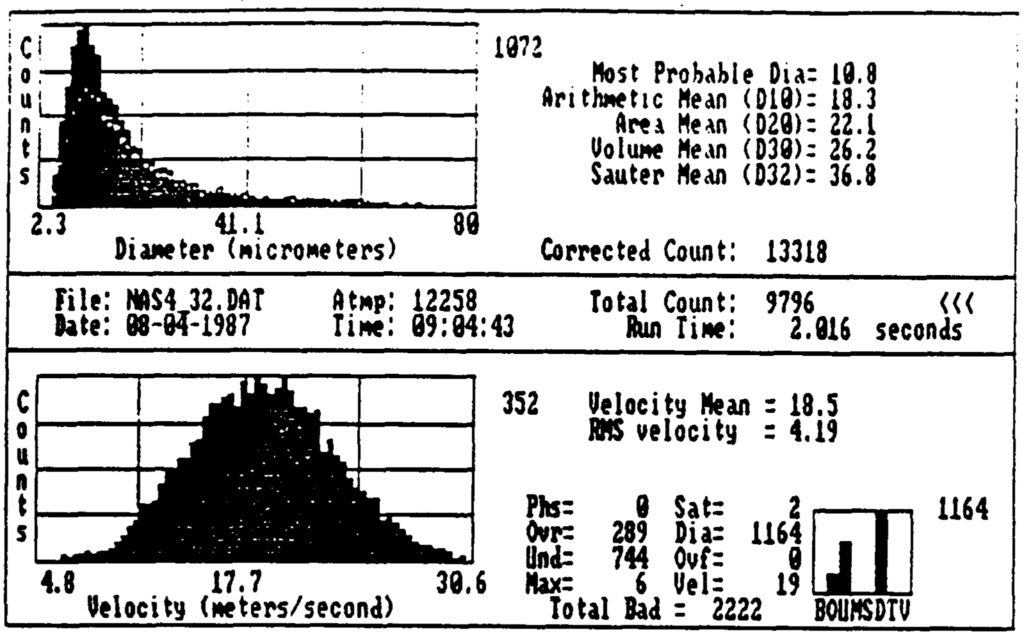


a. P/DPA Results

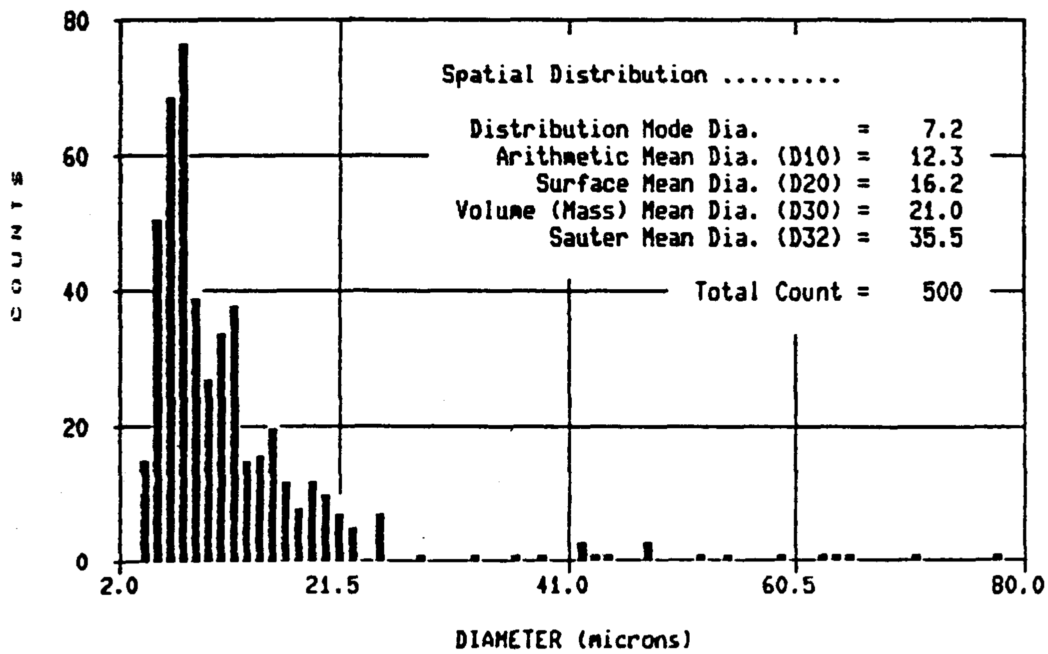


b. LI/VPS Results

(CASE II)

Test Conditions: Radial Position = $\frac{1}{2}$ in.

Air Pressure = 45 psia

Water Pressure = 115 psia

Water Flowrate = 0.06 gal/min.

Axial Position from Nozzle = 2 ft.

Figure 3.34: MOD-1 Nozzle Comparison

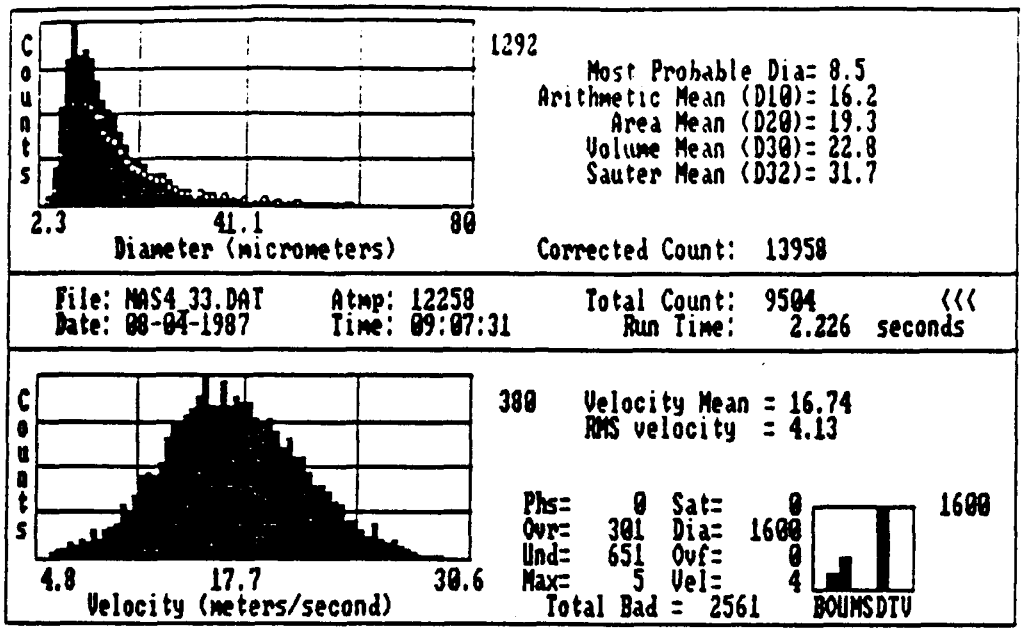


a. P/DPA Results

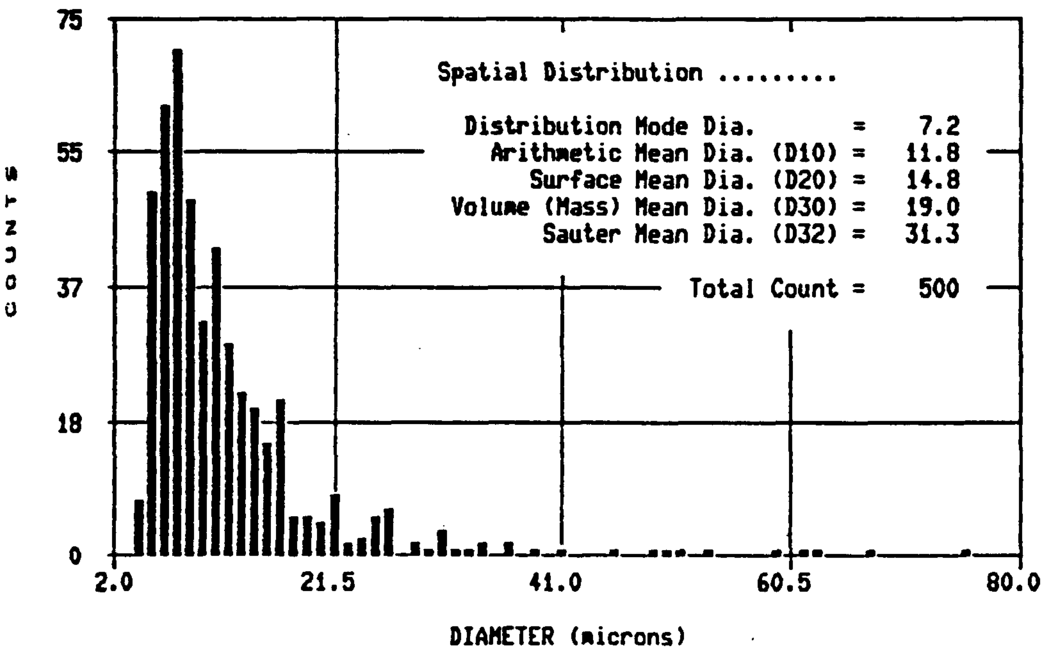


b. LI/VPS Results

(CASE II)

Test Conditions: Radial Position = 1 in.
Air Pressure = 45 psia
Water Pressure = 115 psia
Water Flowrate = 0.06 gal/min.
Axial Position from Nozzle = 2 ft.

Figure 3.35: MOD-1 Nozzle Comparison

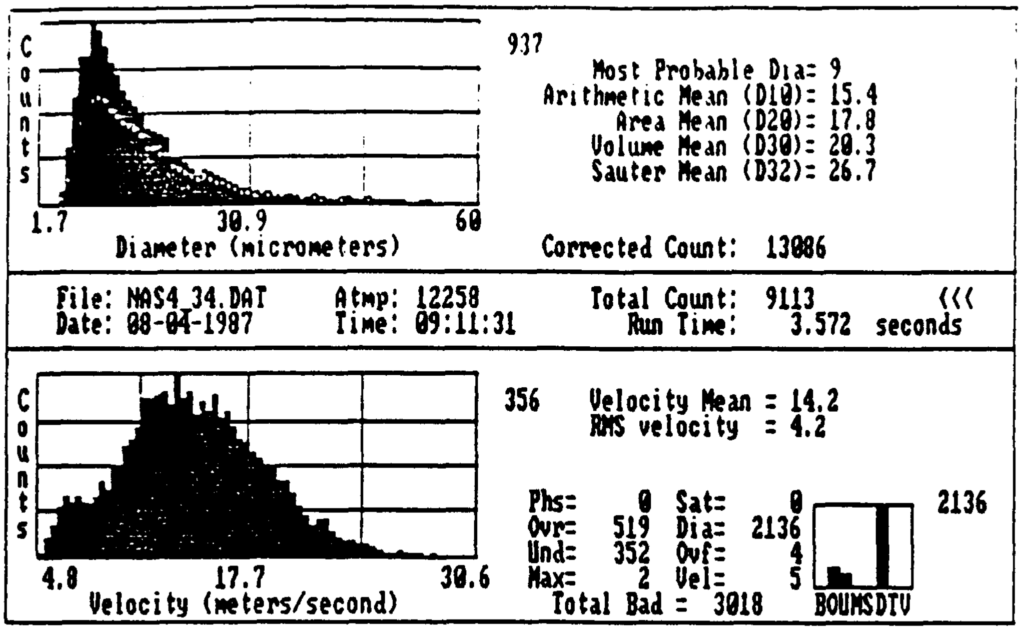


a. P/DPA Results

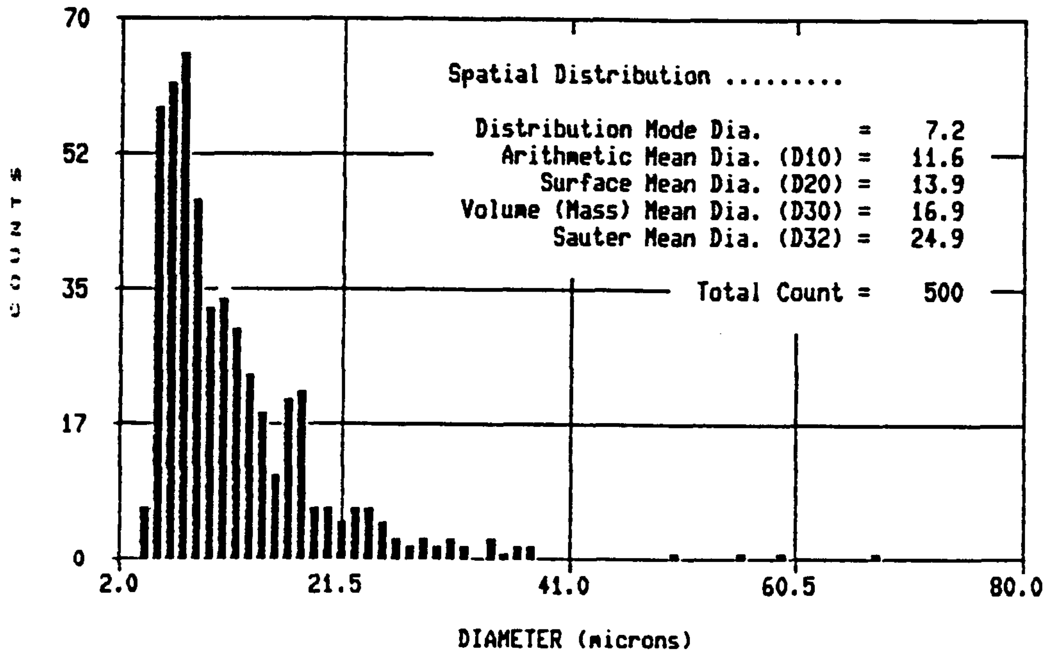


b. LI/VPS Results

(CASE II)

Test Conditions: Radial Position = $1\frac{1}{2}$ in.
Air Pressure = 45 psia
Water Pressure = 115 psia
Water Flowrate = 0.06 gal/min.
Axial Position from Nozzle = 2 ft.

Figure 3.36: MOD-1 Nozzle Comparison

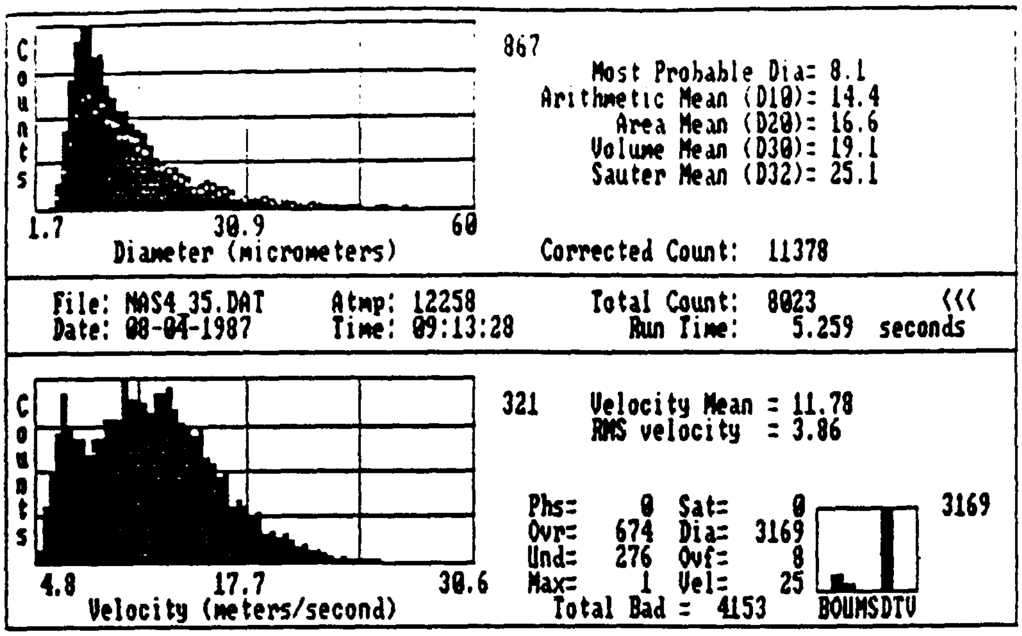


a. P/DPA Results

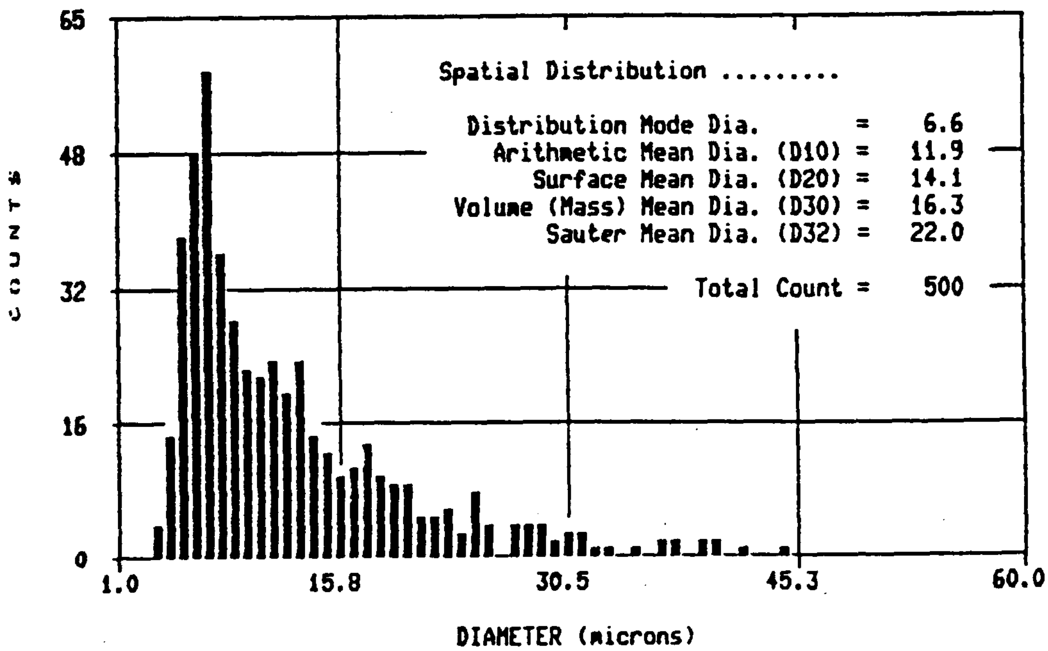


b. LI/VPS Results

(CASE II)

Test Conditions: Radial Position = 2 in.
Air Pressure = 45 psia
Water Pressure = 115 psia
Water Flowrate = 0.06 gal/min.
Axial Position from Nozzle = 2 ft.

Figure 3.37: MOD-1 Nozzle Comparison

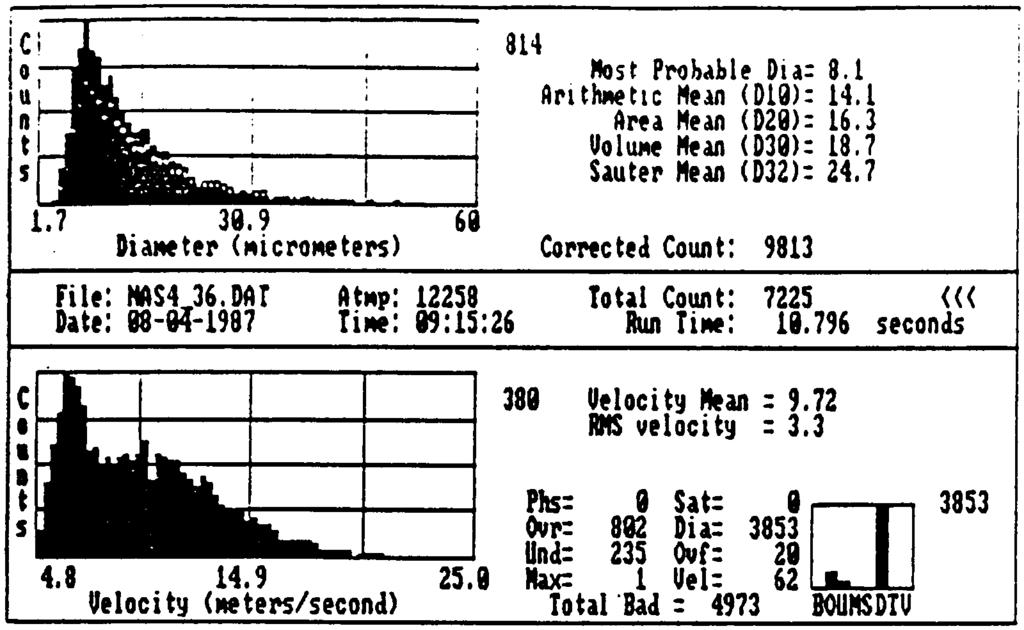


a. P/DPA Results

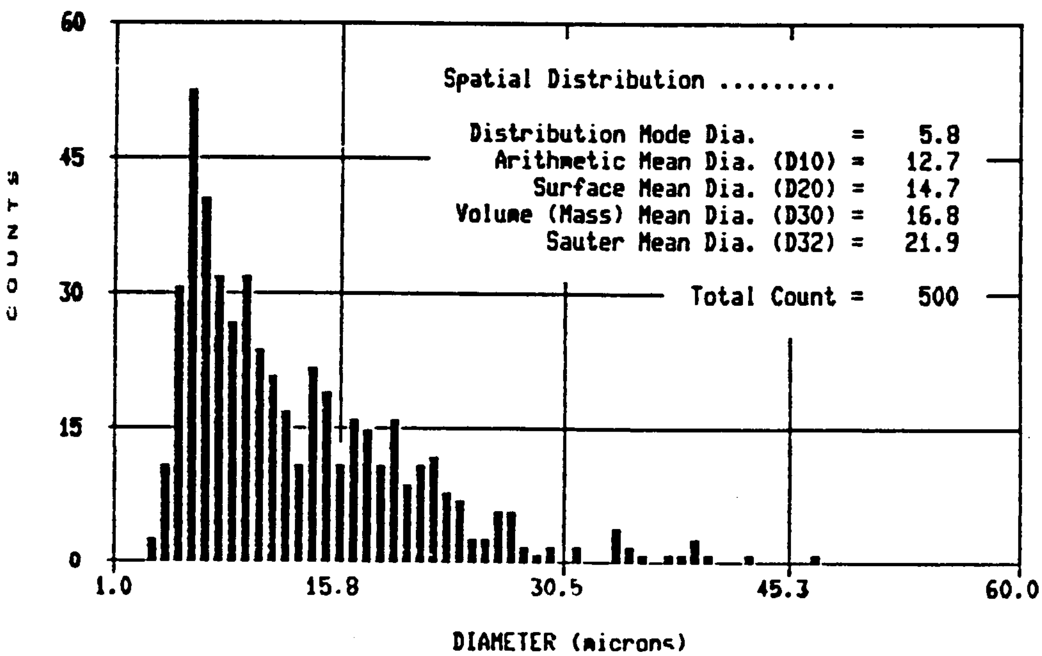


b. LI/VPS Results

(CASE II)

Test Conditions: Radial Position = $2\frac{1}{2}$ in.
Air Pressure = 45 psia
Water Pressure = 115 psia
Water Flowrate = 0.06 gal/min.
Axial Position from Nozzle = 2 ft.

Figure 3.38: MOD-1 Nozzle Comparison

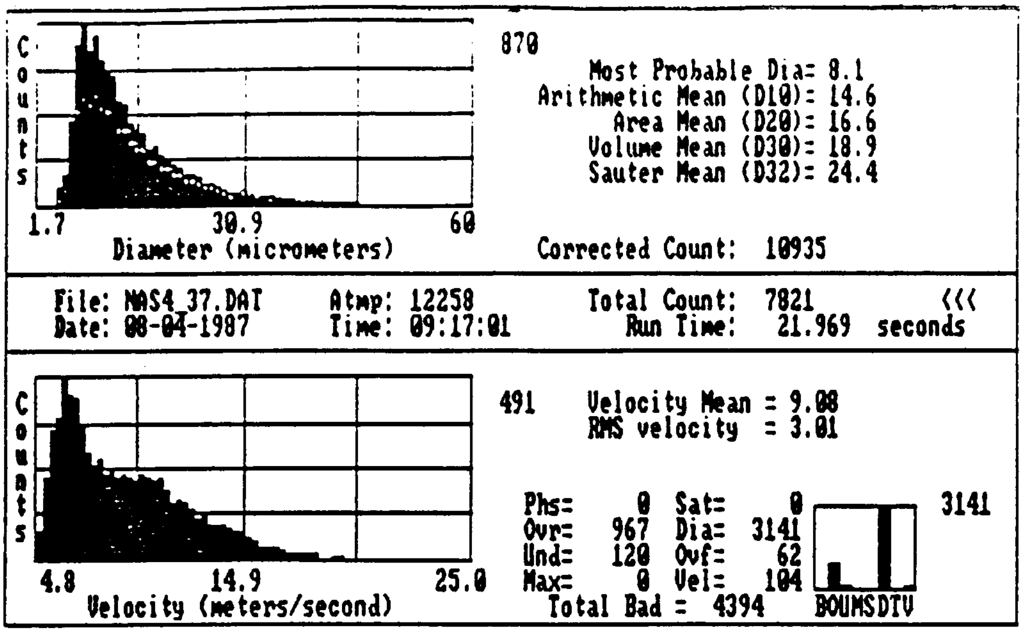


a. P/DPA Results

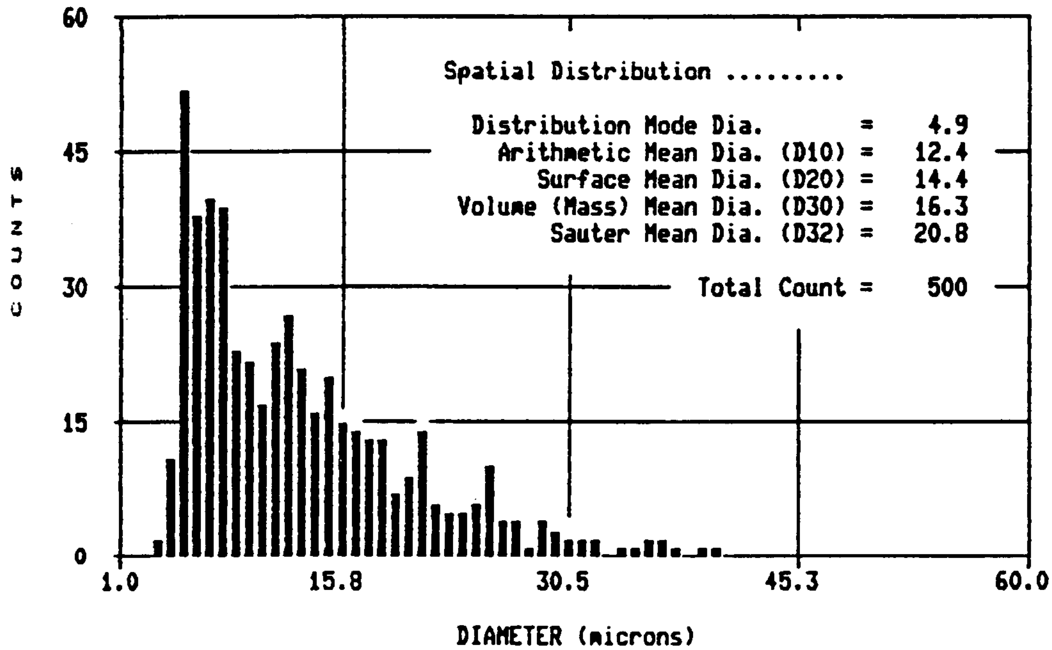


b. LI/VPS Results

(CASE II)

Test Conditions: Radial Position = 3 in.

Air Pressure = 45 psia

Water Pressure = 115 psia

Water Flowrate = 0.06 gal/min.

Axial Position from Nozzle = 2 ft.

Figure 3.39: MOD-1 Nozzle Comparison

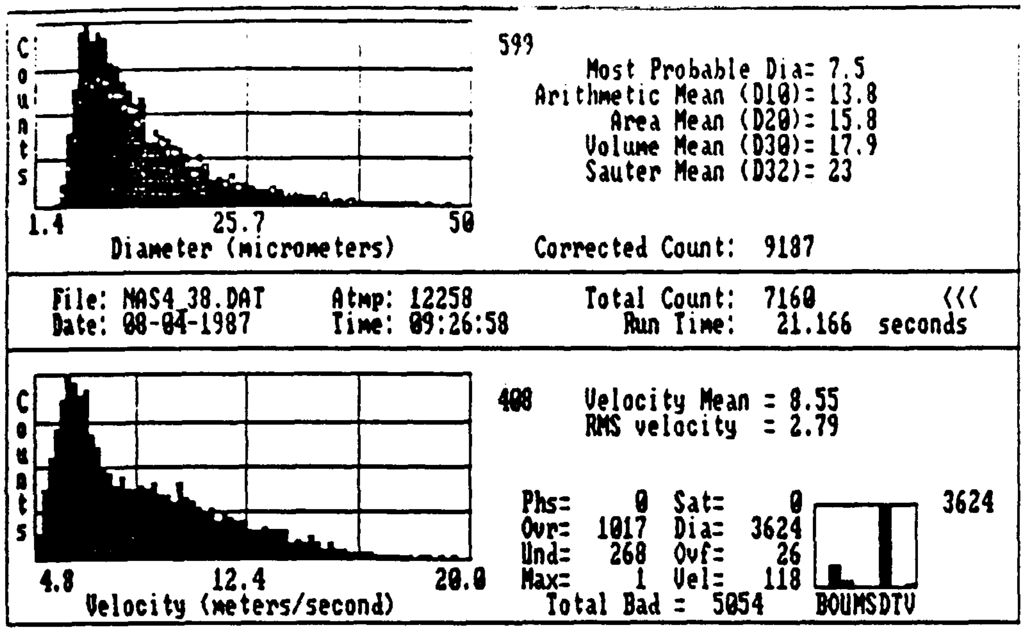


a. P/DPA Results

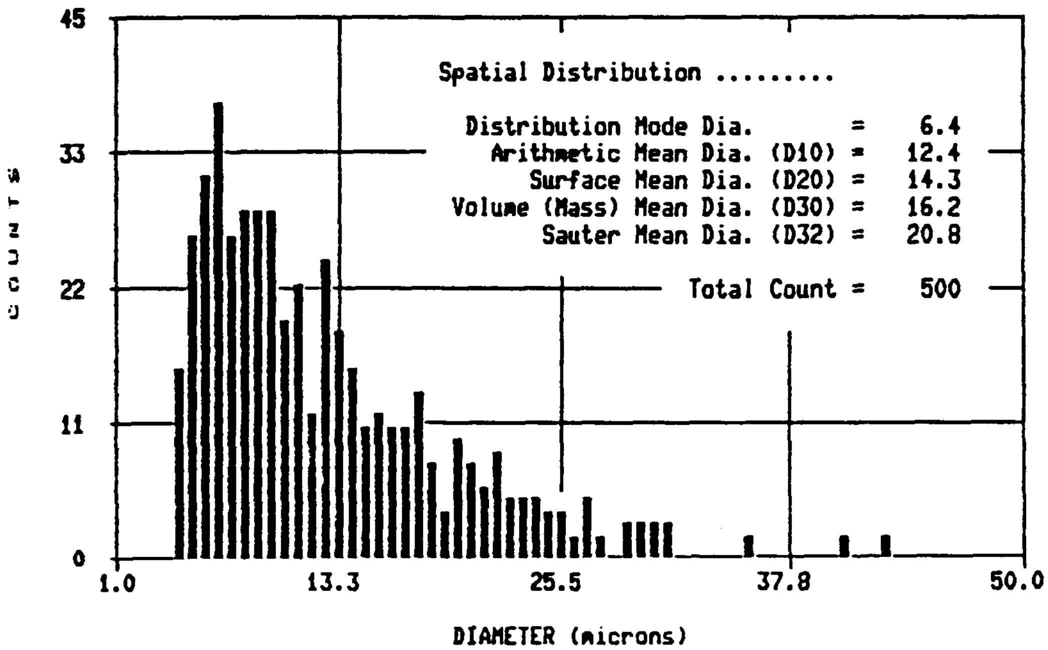


b. LI/VPS Results

(CASE II)

Test Conditions: Radial Position = $3\frac{1}{2}$ in.

Air Pressure = 45 psia

Water Pressure = 115 psia

Water Flowrate = 0.06 gal/min.

Axial Position from Nozzle = 2 ft.

Figure 3.40: MOD-1 Nozzle Comparison

To study the aforementioned results, the arithmetic mean diameter and Sauter mean diameter from each test were graphed as functions of radial position (Figs. 3.41 and 3.44) for each case. The choice of the arithmetic and Sauter mean diameters in the graphs was made to examine the count vs. particle size distribution. The distribution shape most associated with aerosol spray analysis is similar to a log-normal distribution where the distribution mode leans toward the low side of the distribution and conversely the distribution tail shifts to the high side of the distribution. The distribution is reproduced by the fact, that the arithmetic mean diameter is proportional to the mode of the distribution and the Sauter mean diameter is indicative of the distribution's tail. With the above technique, the comparison of results from the P/DPA and the LI/VPS was performed.

### 3.2.1 Discussion of Results for Comparison - CASE I

Referring to Table 3.5, the arithmetic mean diameters measured by the LI/VPS remained approximately constant from 9.5 $\mu$m at the centerline to 10.7 $\mu$m at the edge of the spray, while the P/DPA values varied from 12.3 $\mu$m at the centerline to 8.8 $\mu$m at the edge of the spray. Figure 3.41 shows the general trend in the LI/VPS and P/DPA arithmetic mean diameter to be very similar with a maximum deviation of 2.8 $\mu$m at the centerline and a minimum deviation of 0.1 $\mu$m at the 2.0 inch location. Figure 3.42 shows the trend in the Sauter mean diameter to be also similar for both instruments. The maximum deviation is 2.2 $\mu$m at the 1.0 inch radial position while the minimum deviation is 0.0 for the 2.5 inch position. The maximum deviation of 2.8 $\mu$m for the arithmetic mean diameter, and 2.2 $\mu$m for the Sauter mean diameter can be explained as a result of the difference in instrument operation (automatic imaging vs light scattering and spatial vs temporal), the depth of field correction used by the P/DPA and no correction for the LI/VPS system, and to the LI/VPS instrument calibration error calculated to be $\pm$ 2.6 $\mu$m with a standard deviation of $\pm$ 2.0 $\mu$m.

### 3.2.2 Discussion of Results for Comparison - CASE II

Referring to Fig. 3.43 and Table 3.5, the maximum deviation in arithmetic mean diameter of 7.1 $\mu$m occurred at the centerline with the minimum deviation of 1.4 $\mu$m at the edge of the spray. As in CASE I, the LI/VPS arithmetic mean diameters remained approximately constant from 11.9 $\mu$m at the centerline to 12.4 $\mu$m at the edge of the spray, and the P/DPA values varied from 19.0 $\mu$m at the centerline to 13.8 $\mu$m at the outer edge. Figure 3.44 showed a very similar trend in Sauter mean diameters as a function of the radial location for both instruments. A maximum deviation of 6.7 $\mu$m occurred at the centerline of the spray and a minimum deviation of 0.4 $\mu$m at the 1.0 inch location.

In CASE II, the increase in water pressure may increase the turbulence in the outer region of the spray plume, which in turn caused recirculation of particles through the overlapping probe volumes. In addition to the explanations given in CASE I for the the differences in the arithmetic mean diameters we believe that since the trend for both cases is very similar (i.e., LI/VPS values remained approximately constant across the spray plume, while the P/DPA values decreased as the measurements approached the outer edge of the spray), some of the differences is due to the more difficult test conditions of CASE II. As we approach the outer edge of the spray, there is better agreement in the arithmetic mean diameter for both instruments. A possible explanation is the way the P/DPA operates. Recalling from Section 2.1, for proper operation of the P/DPA, the drops must pass through the probe volume perpendicular to Doppler fringes. Drops exactly at the centerline of the spray will almost always be perpendicular to these fringes and as we approach the outer edge, the drops at these locations will have different directions. The result is an increase in run time which for CASE II varies from 2.0 sec at the centerline to 21.2 sec at the edge of the spray. The increase in time is an indication that more particles were rejected; therefore, the system becomes more selective and perhaps explains the smaller arithmetic mean diameter as the edge of the spray is approached. The difference in arithmetic mean diameters in the inner region of the spray is attributed to the loss of small particles due to the presence of high number of liquid particles per volume of air which produces overlapping signals in the P/DPA. The number density at the center of the spray was 6970 particles/$cm^3$ compared to 1070 particles/$cm^3$ at the edge. According to Dodge et al[22], by comparing the AMD with the SMD for each case, the differences in the shape of the distribution can be observed. Studying Figures 3.41, 3.42, 3.43, and 3.44 it is observed that the Sauter mean diameter compared more closely than the arithmetic mean diameter which suggests a difference in distribution shape for each case.

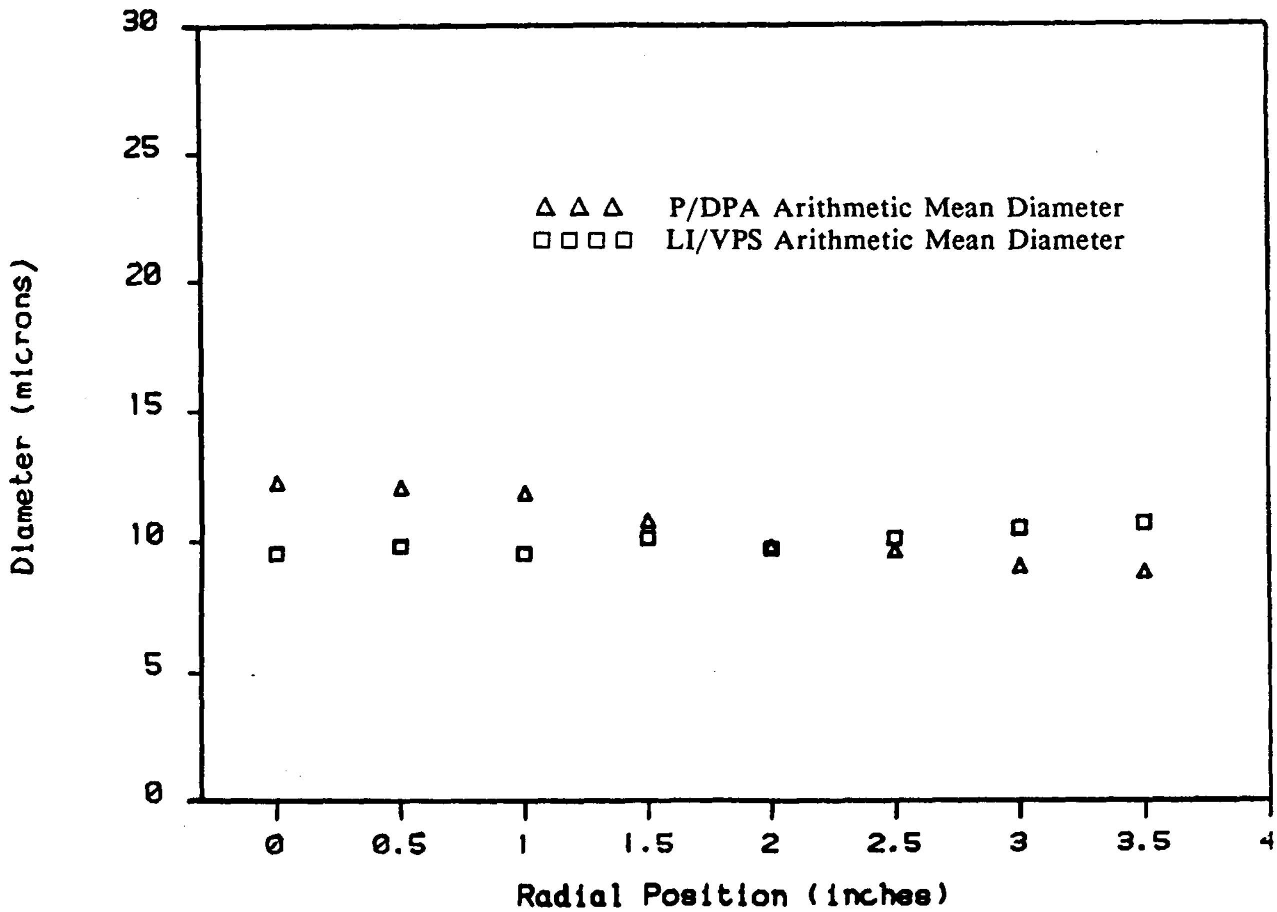


(CASE I)

Test Conditions:

Air Pressure = 65 psia.
Water Pressure = 105 psia.
Water Flow-rate = 0.069 gal/min.

Figure 3.41: Comparison of Arithmetic Mean Diameters for MOD-1 Nozzle Comparison Test - CASE I

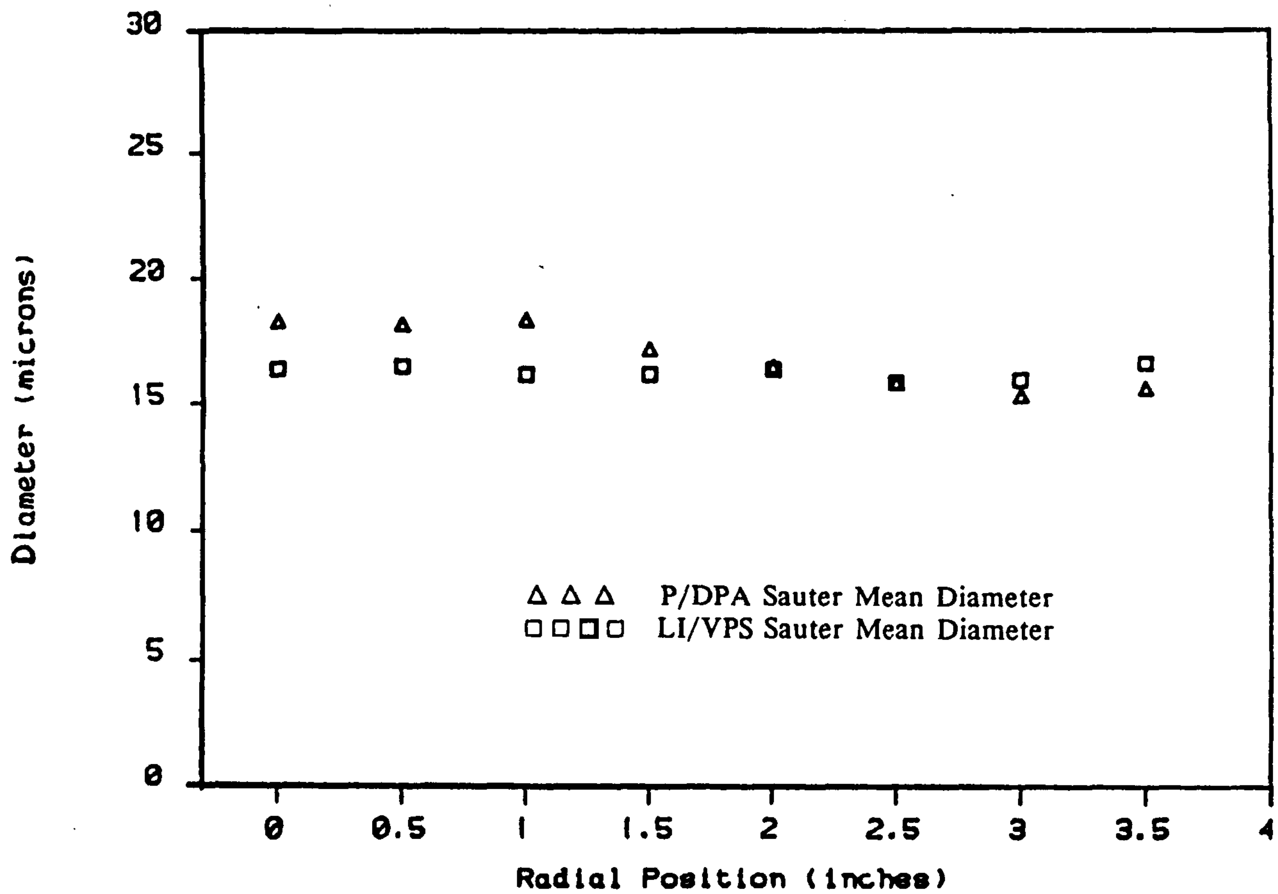


(CASE I)

Test Conditions:

Air Pressure = 65 psia.
Water Pressure = 105 psia.
Water Flow-rate = 0.069 gal/min.

Figure 3.42: Comparison of Sauter Mean Diameters for MOD-1 Nozzle Comparison Test - CASE I

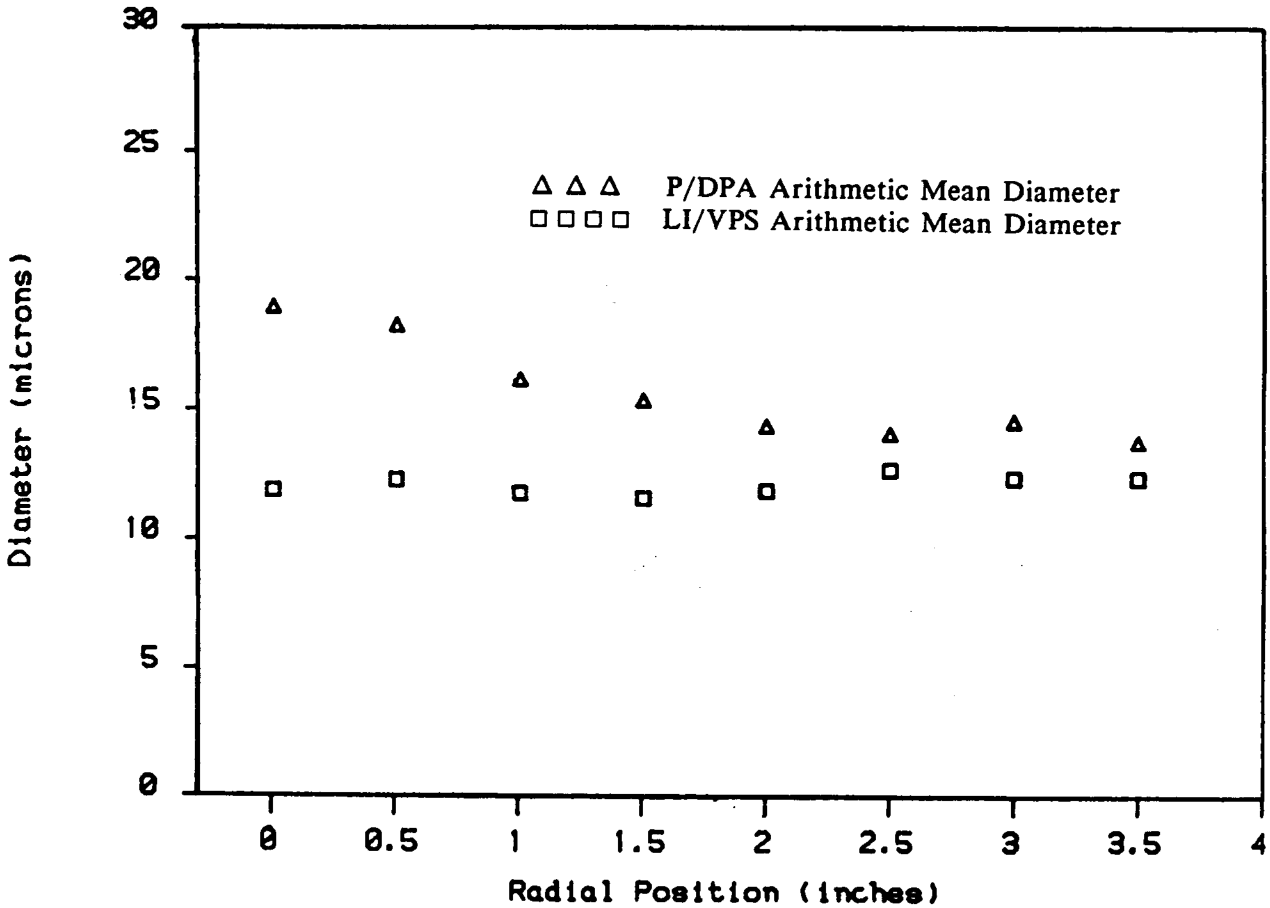


(CASE II)

Test Conditions:

Air Pressure = 45 psia.
Water Pressure = 115 psia.
Water Flow-rate = 0.094 gal/min.

Figure 3.43: Comparison of Arithmetic Mean Diameters for MOD-1 Nozzle Comparison Test - CASE II

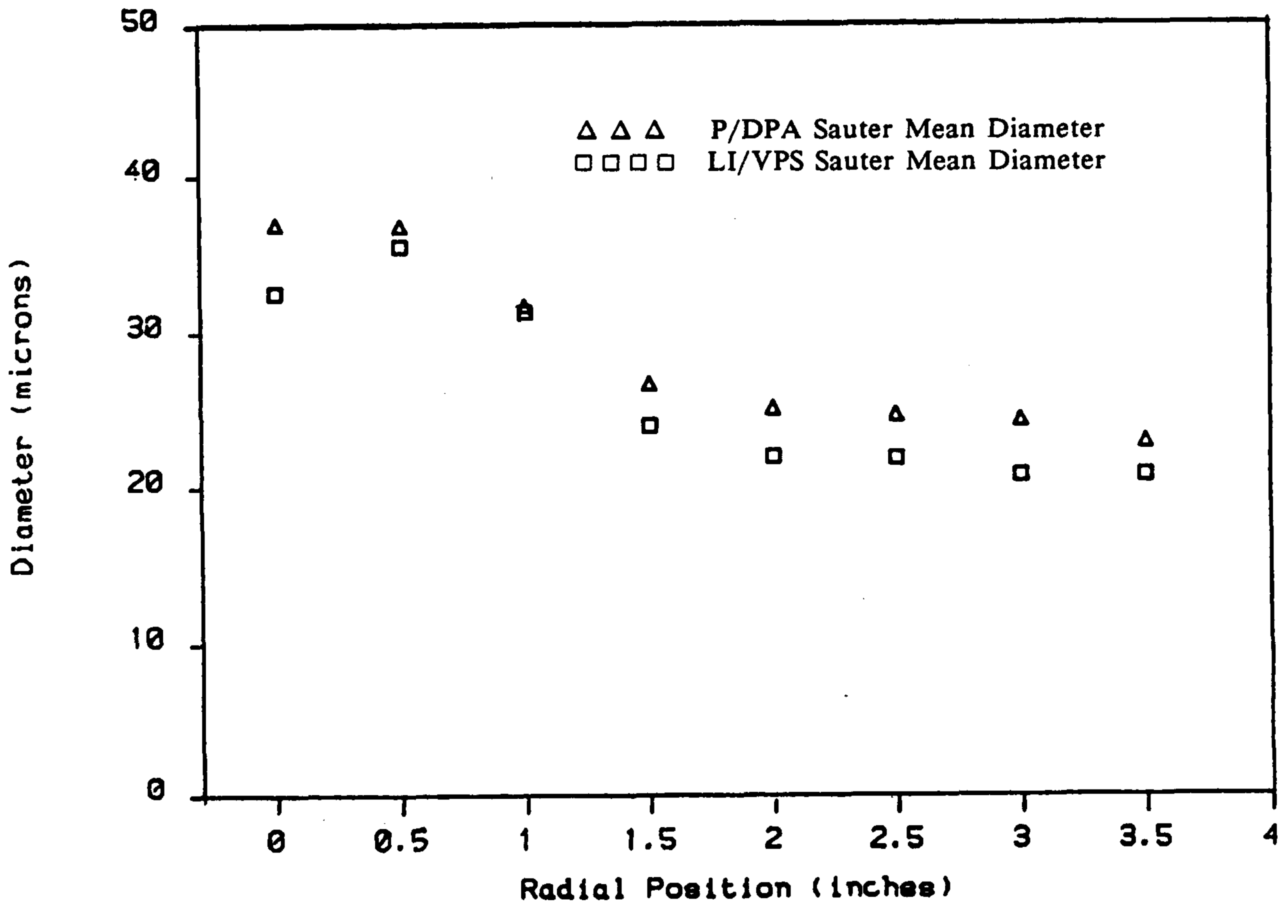


**(CASE II)**

Test Conditions:

Air Pressure = 45 psia.
Water Pressure = 115 psia.
Water Flow-rate = 0.094 gal/min.

Figure 3.44: Comparison of Sauter Mean Diameters for MOD-1 Nozzle Comparison Test - CASE II

C-2

Table 3.5: MOD-1 Nozzle Comparison Results

**CASE I**

| | Water Pressure = 105 psia | | Air Pressure = 65 psia | |
|---|---|---|---|---|
| | LI/VPS Results | | P/DPA Results | |
| RADIAL POSITION (inches) | ARITHMETIC MEAN DIAMETER ($\mu$m) | SAUTER MEAN DIAMETER ($\mu$m) | ARITHMETIC MEAN DIAMETER ($\mu$m) | SAUTER MEAN DIAMETER ($\mu$m) |
| CL | 9.5 | 16.4 | 12.3 | 18.3 |
| 0.5 | 9.8 | 16.5 | 12.1 | 18.2 |
| 1.0 | 9.5 | 16.2 | 11.9 | 18.4 |
| 1.5 | 10.1 | 16.2 | 10.8 | 17.2 |
| 2.0 | 9.7 | 16.4 | 9.8 | 16.5 |
| 2.5 | 10.1 | 15.9 | 9.6 | 15.9 |
| 3.0 | 10.5 | 16.0 | 9.0 | 15.4 |
| 3.5 | 10.7 | 16.7 | 8.8 | 15.7 |

**CASE II**

| | Water Pressure = 115 psia | | Air Pressure = 45 psia | |
|---|---|---|---|---|
| | LI/VPS Results | | P/DPA Results | |
| RADIAL POSITION (inches) | ARITHMETIC MEAN DIAMETER ($\mu$m) | SAUTER MEAN DIAMETER ($\mu$m) | ARITHMETIC MEAN DIAMETER ($\mu$m) | SAUTER MEAN DIAMETER ($\mu$m) |
| CL | 11.9 | 32.5 | 19.0 | 39.2 |
| 0.5 | 12.3 | 35.5 | 18.3 | 36.8 |
| 1.0 | 11.8 | 31.3 | 16.2 | 31.7 |
| 1.5 | 11.6 | 24.9 | 15.4 | 26.7 |
| 2.0 | 11.9 | 22.0 | 14.4 | 25.1 |
| 2.5 | 12.7 | 21.9 | 14.1 | 24.7 |
| 3.0 | 12.4 | 20.8 | 14.6 | 24.4 |
| 3.5 | 12.4 | 20.8 | 13.8 | 23.0 |

Section 4

# CONCLUSIONS AND RECOMMENDATIONS

This section presents the conclusions of the experimental findings and suggestions for utilizing the experimental apparatus and drop-sizing instrumentation in future studies. The first section deals with the revisions to the LI/VPS, including the upgrade to dynamic particle sizing, the development of the calibration procedure, and the software updates. The second section deals with the comparison of the LI/VPS and the P/DPA, and observations concerning their proper operation, set-up, and limitations. The final section of pertains to the improvement of the LI/VPS to a more complete drop-sizing instrument, the continuation of aerosol spray analysis on the MOD-1 nozzle, and general observations concerning the continuing work in aerosol drop-sizing.

## 4.1 LI/VPS

The LI/VPS has been upgraded to a system capable of performing drop-sizing analysis on dynamic particles. With the addition of the AD/DA converter board to the control computer, the PSP has shown the capability to distinguish drop-size and focus on dynamic particles in the SPM (i.e., freeze frame analysis). Therefore, the LI/VPS' drop-sizing method and focus criteria, developed prior to this work, remains essentially intact with minor modifications.

A two-dimensional calibration procedure for LI/VPS has been developed which allows for a straight-forward, step-by-step process in determining the micron/pixel correction factors associated with the lens magnification and camera tube non- linearities. With the developed calibration procedure and the availability of a f/8 lens (i.e., approximate LI/VPS magnification of 1000), the lower-limit on the measurable, focus- dependent size-span of the LI/VPS has been reduced from 9 $\mu$m to 3 $\mu$m.

Included in the LI/VPS upgrade has been the development of the PSP set-up sub-program and a drop-size distribution graphics display package. Due to the variability of conditions in aerosol spray analysis and the flexibility of the LI/VPS, the set-up sub- program was developed to aid the operator in his decision process and allow for utilization of the full capabilities of the LI/VPS. The addition of the graphic package was necessary to further the LI/VPS' ability to characterize aerosol sprays. The graphical representation of the drop-size data was used as a diagnostic tool in specifying the proper drop-size range and a tool in the comparison of the LI/VPS and the P/DPA.

## 4.2 LI/VPS and P/DPA Comparison

The LI/VPS and the P/DPA compared favorably in the tests performed on the VOAG as well as tests performed on the MOD-1 nozzle. Assuming count vs. drop-size distributions were Gaussian in shape, the monodisperse drops generated by the VOAG, with and without the dispersion cup, were accurately measured by LI/VPS and the P/DPA within ± 2.6 $\mu$m. The standard deviation of the test samples were all under 2.0 $\mu$m which implies the LI/VPS and the P/DPA probe volumes are consistent in size and boundaries. The MOD-1 nozzle tests also showed similar results for both instruments. Results from CASE I shows substantial agreement in the trend of AMD and SMD values from instrument to instrument with a maximum deviation of 2.8 $\mu$m for the AMD,and 2.2 $\mu$m for the SMD. In CASE II, the AMD values determined for CASE II show a higher deviation than CASE I (7.1 $\mu$m and 2.8 $\mu$m respectively). The AMD values agree quite well for the outer region of the spray where the system becomes more selective as explained in section 3.3.2. The SMD for both instruments follows the same trend across the spray with a maximum deviation of 6.7 $\mu$m. In icing studies, as well as in combustion and in many other areas, the most important and used diameter is the SMD. Considering the differences in sizing methods employed by the two instruments and the given test conditions, the LI/VPS and the P/DPA comparative measurements were surprisingly close especially for the SMD.

Proper operation and set-up of the LI/VPS and the P/DPA depend on the operating conditions of the tested nozzle or device. For this discussion, the MOD-1 nozzle will be considered. The operating conditions of the MOD-1 nozzle for the aforementioned cases, were not ideal for either instrument. Due to the limited size span available to the LI/VPS, the AMD values determined in CASE I may be slightly higher than the actual values. Considering the turbulent nature of the spray in the outer regions, the P/DPA started to reject counts when collecting data. Therefore, each instrument's capabilities must be tested a priori in any unknown aerosol spray conditions. Even though the LI/VPS and the P/DPA compared very well and have similar probe volume size, each instrument performs better under different test conditions. The LI/VPS performs well in a high density aerosol spray, whereas the P/DPA under similar conditions, has difficulties due to the overlap of signals or loss of dead-time between signal on the PMTs. The P/DPA has a greater overall size span than the LI/VPS which allows for more versatility. Also, the P/DPA is capable of making velocity measurements concurrently with the drop-size measurement, but as is shown for the MOD-1 comparison, the recirculation of drops associated with the turbulent spray resulted in numerous rejections.

## 4.3 Suggestions and Recommendation for Future Work

The LI/VPS, as particle sizing instrument, has progressed in stages of development. The next stage of development should be in the area of off-line analysis (e.g., frame storage on the laser disk recorder), as well as increasing the program speed through hardware and software modifications. A study should be performed to determine the feasibility of frame storage, and if necessary, the error associated with such storage. The control computer, the behavior of imaging laser, and the PSP program structure should be studied to increase the operating speed of the LI/VPS. With the addition of the Micro-VAX computer, the control computer should not be the limiting parameter in program speed. The PSP trigger to the imaging laser doesn't function consistently which makes it necessary to check for appropriate background level before processing. Therefore, with proper operation of the imaging trigger, unnecessary processing time can be avoided. Finally, to increase the speed of the LI/VPS, the PSP should be stream-lined. For example, the double-threshold used to determine BGL parameter for particle focus should be consolidated into a single threshold.

The research on the MOD-1 nozzle and the comparison of the LI/VPS and the P/DPA should be continued. Operating conditions for the current work were specified by NASA. Future work on the MOD-1 nozzle should involve tests performed at lower water and air nozzle pressures. These operating conditions would produce a larger drop-size and reduce turbulence in the spray. Also, a position closer to the nozzle would produce a higher number density spray which would be ideal for the LI/VPS. The use of the P/DPA 200 mm transmitter lens would reduce the probe volume which, in turn, would reduce the probability of multiple particles in the probe volume produced by the high number density of droplets. The above suggestions are included to improve the functionality of the two instruments in future studies.

The current research and other comparison work by Dodge et al. [22] and Jackson et al. [23] improve the understanding of the various types of sizing techniques and assist in the development of accurate sizing instrumentation. The selection of a calibration/verification method or standard should be found for all drop-sizing instruments. The selection should be a priority for researchers and instrument manufacturers.

Section 5

## REFERENCES


1. Proceedings - Particle Sizing Instrument Development Group, 1986 Droplet Technology Workshop, NASA Lewis Research Center, Cleveland, Ohio, May 1986.

2. Malvern Instruments Limited, Malvern Worcestershire WR14 1AQ, England.

3. Bachalo, W. D., "Method for Measuring the Size and Velocity of Spheres by Dual- Beam Light-Scatter Interferometry," Applied Optics, Vol. 19, 1980.

4. Bachalo, W. D., and Houser, M. J., "Development of the Phase/Doppler Spray Analyzer for Liquid Drop Size and Velocity Characterizations," AIAA/SAE/ASME 20th Joint Propulsion Conference, Cincinnati, Ohio, AIAA paper No. 841199, June 1984.

5. Farmer, W. M., "Measurement of Particle Size, Number Density, and Velocity Using a Laser Interferometer," Applied Optics, Vol. 11, No. 11, 1972.

6. Alexander, D. R., and Morrison, M. J., "Particle Concentration Measurements by Laser Imaging for a Turbulent Dispersion," Particulate Science and Technology, Vol. 2, No. 4, p. 379, 1984.

7. Ahlers, K. D., "A Microcomputer-Based Digital Image Processing System Developed to Count and Size Laser-Generated Small Particle Images," M.S. Thesis, Mechanical Engineering Dept., University of Nebraska–Lincoln, 1984.

8. Alexander, D. R., and Ahlers, K. D., "A Microcomputer- Based Digital Image Processing System Developed to Count and Size Laser-Generated Small Particle Images," Optical Engineering, Vol. 24, No. 6, p. 1060, 1985.

9. Ahlers, K. D., and Alexander, D. R., "A Flexible High- Speed Digital Image Processing System, " SPIE 29th Annual Meeting, Paper No. 573-11, SPIE Proceedings, Vol. 573, San Diego, CA, 1985.

10. Wiles, K. J., "Development of a System for Secondary Liquid Injection into a Mach 2 Supersonic Flow to Study Drop Size and Distribution by Video Imaging Techniques," M.S. Thesis, Mechanical Engineering Dept., University of Nebraska–Lincoln, 1985.

11. Weiss, B. A., Derov, P., DeBiase, D., Simmons, H. C., "Fluid Particle Sizing Using a Fully Automated Optical Imaging System," Optical Engineering, Vol. 23, No. 5, 1984.

12. Hirleman, E. D., "On-Line Calibration Technique for Laser Diffraction Droplet Sizing Instruments," ASME paper No. 83-GT-232, 1983.

13. Tishkoff, J. M., "Spray Characterization: Practices and Requirements," Optical Engineering, Vol. 23, No. 5, 1984.

14. Alexander, D. R., Wiles, K. J., Schaub, S. A., Seeman, M. P., "Effects of Non-spherical Drops on a Phase Doppler Spray Analyzer," Proceedings of SPIE - The International Society of Optical Engineering, Volume 573, August 21, 1985.

15. ASTM Standard E799-81 (1981).

16. Supplied by NASA Lewis Research Center.

17. Berglund, R. N., and Liu, B. Y. H., "Generation of Monodisperse Aerosol Standards," Environmental Science and Technology, Vol. 7, 1973.

18. Available from TSI Inc., St. Paul, MN.

19. Bachalo, W. D., and Houser, M. J., "Phase/Doppler Particle Analyzer Operations Manual," Aerometrics Inc., Mountain View, CA., Release 1.0, 1985.

20. Interview, Bachalo, W. D., Concerning PMT voltage gain voltage, Dec. 9, 1985.

21. Bachalo, W. D., and Houser, M. J., "Measurements of Drop Dynamics and Mass Flux in Sprays," Presented, 1986 Meeting of the Central States Section/The Combustion Institute, NASA Lewis Space Center, Cleveland, Ohio, May, 1986.

22. Dodge, L. G., Rhodes, D. J., and Reitz, R. D., "Comparison of Drop-size Measurement Techniques in Fuel Sprays: Malvern Laser-Diffraction and Aerometrics Phase/Doppler," Presented, 1986 Meeting of the Central States Section/The Combustion Institute, NASA Lewis Space Center, Cleveland, Ohio, May, 1986.

23. Jackson, T. A., and Samuelson, G. S., "An Evaluation of the Performance of Visibility/Intensity Validation and Phase/Doppler Techniques in Characterizing the Spray of an Air- Assist Nozzle," Presented, 1986 Meeting of the Central States Section/The Combustion Institute, NASA Lewis Space Center, Cleveland, Ohio, May, 1986.

Section 6

## APPENDIX A: EQUIPMENT LISTING

| Device | Manufacturer | Model # | Serial # |
|---|---|---|---|
| P/DPA Transmitter | Aerometrics Inc. | 1100 | 101 |
| P/DPA Receiver | Aerometrics Inc. | 2100 | 101 |
| P/DPA Signal Processor | Aerometrics Inc. | PDP 3100 | 103 |
| P/DPA Control Computer | IBM Corp. | AT-5170 | 01619045170 |
| P/DPA Output Printer | Hewlett Packard Corp. | 2225A | 2617S31411 |
| LI/VPS Imaging Laser | Energy Systems Inc. | N2-50 | |
| LI/VPS Imaging Laser Power Supply | Laser Systems Inc. | N2-50 | |
| LI/VPS Imaging Laser Control Module | Laser Holography Inc. | N2-50 | |
| LI/VPS Laser Sync Generator | Laser Holography Inc. | N2-50 | |
| LI/VPS (back-up) Imaging Laser | Molectron Corp. | UV-12 | 198 |
| LI/VPS (back-up) Imaging Laser Vacuum Pump | Busch Inc. | V-20 | 116 |
| LI/VPS Video Camera | COHU Inc. | 2006-011 | 625810 |
| LI/VPS Video Camera Control Unit | COHU Inc. | 7910B-011 | 112698 |
| LI/VPS Control Computer | Digital Equipment Corp. | PDP11/73 | |
| LI/VPS Output Printer | Digital Equipment Corp. | LA75-A2 | 03555 |
| LI/VPS Video Processor | Recognition Concepts Inc. | TRAPIX 55/32Q | 134 |
| Computer Terminal | Digital Equipment Corp. | VT-240 | HK14705 |
| Computer Terminal | CIE Terminals Inc. | CIT-220+ | 8471C6916 |

| | | | |
|---|---|---|---|
| Video Monitor | Sanyo Corp. | AVM255 | 55805757 |
| Video Monitor | SONY Corp. | CKV-1900F | 204071 |
| Video Cassette Recorder | RCA Corp. | VET650 | 1032FM243 |
| Video Cassette Recorder | Panasonic Corp. | NV-8950 | B5HL00491 |
| Laser/optical Disk Recorder | Panasonic Corp. | TQ-2320F(A) | EH4669001 |
| Decwriter | Digital Equipment Corp. | LA120AA | PNE1366 |
| Digital Oscilloscope | Hewlett-Packard Corp. | 54200A | 2511A-00639 |
| Measurement Plotting System | Hewlett-Packard Corp. | 7090A | 2430A00344 |
| Real-time Oscilloscope | Tektronix Inc. | 549 | 7365 |
| Digital Multimeter | John Fluke Mfg. Co., Inc. | 8024B | 3715516 |
| Pressure Transducer | OMEGA Eng., Inc. | PX304-150 | 850502 |
| Pressure Transducer | OMEGA Eng., Inc. | PX304-150 | 850311 |
| Direct Current Power Supply | Hewlett-Packard Corp. | 6200B | 2411A-12365 |
| Flowmeter-regulator | Cole-Palmer Inc. | PR004 | FM044-40G |
| Monodisperse Drop Generator | TSI Inc. | 345000 | 167 |
| Test Nozzle | NASA Lewis Space Center | MOD-1 | |
| Air and Water Supply | University of Nebraska | | |
| Pressure Regulator | WATTS Regulator Co. | 2-26A | 8305 |
| Water Pressure Vessel | Brunswick Corp. | 6121020-024 | 1003 |
| Isolation Table | Newport Research Corp. | | |
| High-pressure Charging Hose | Yellow Jacket Inc. | WPP0031A | |
| Dead Weight Pressure Tester | American Steam Gage Co. | | |
| Balance Scale | HOWE Inc. | 3074131 | |

Section 7

## APPENDIX B Design and Implementation of the PSP Laser Trigger

Due to the availability of the existing laser sync circuit (LSC) and the AD/DA converter board, the development of the PSP software generated trigger was simplified. With the aforementioned hardware, the PSP software, utilizing available FORTRAN callable commands, directs a digital value to the AD/DA board. The AD/DA board converts the digital value to the appropriate analog signal. The analog signal is then sent to the LSC. The analog signal from the control computer is paralleled with the sync signal from the CCU, and the resulting signal triggers the imaging laser. The above process was used as the basis for LI/VPS conversion from the CPM to the SPM. Except for cabling, the majority of work in the modification dealt with the LSC. Figure B7.1 shows the overall circuitry of the LSC with special attention given to the source of the LSC laser trigger and the position marked by the Xs. The major addition to the LSC circuitry was the two AND gates (Appendix B, Fig. B7.2. Therefore an analog signal from the control computer must be present at the first AND gate before the imaging laser can be triggered. The above method, therefore, facilitates SPM operation for the LI/VPS.

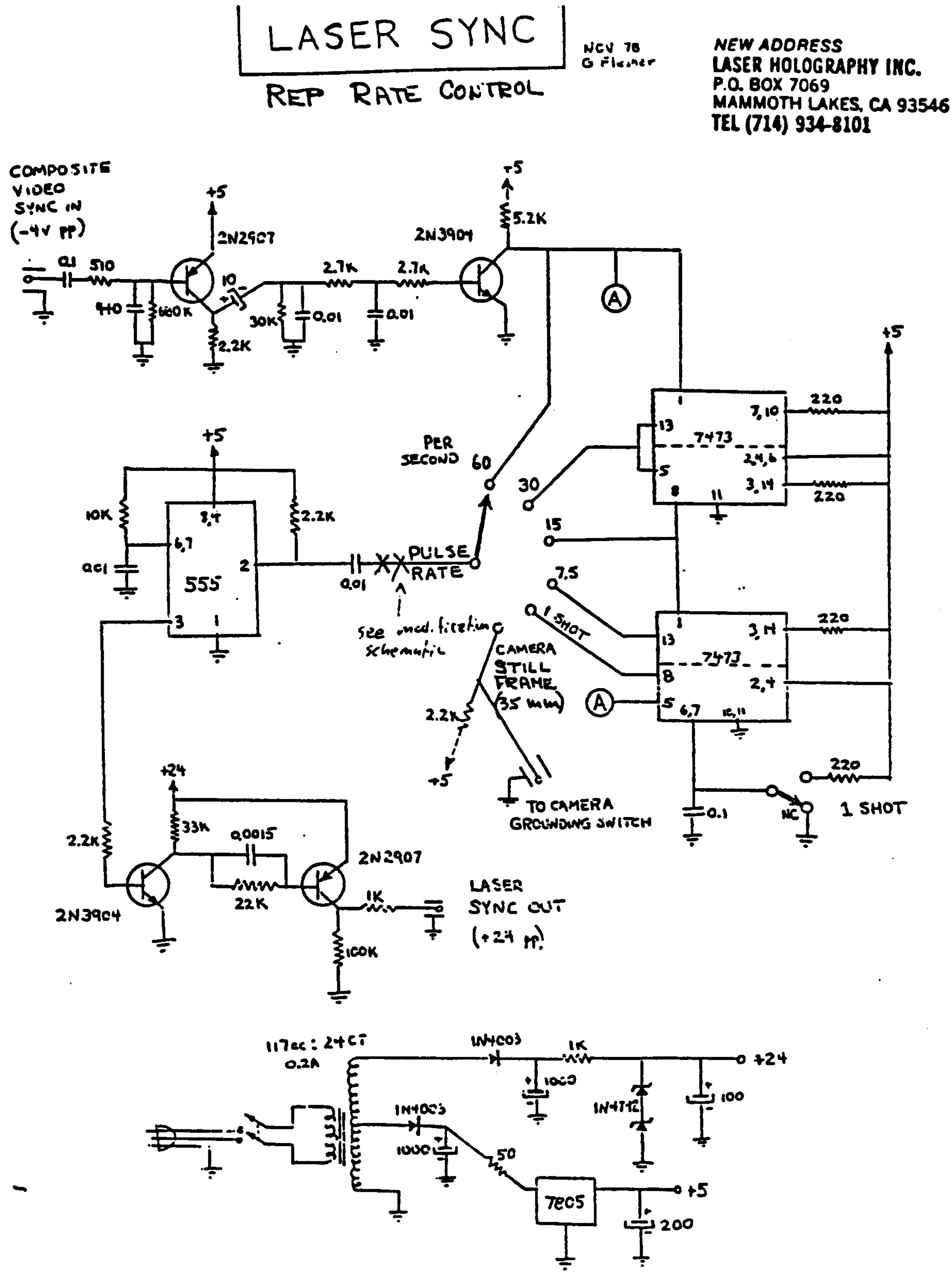

NEW ADDRESS
LASER HOLOGRAPHY INC.
P.O. BOX 7069
MAMMOTH LAKES, CA 93546
TEL (714) 934-8101

Figure 7.1: LSG Schematic

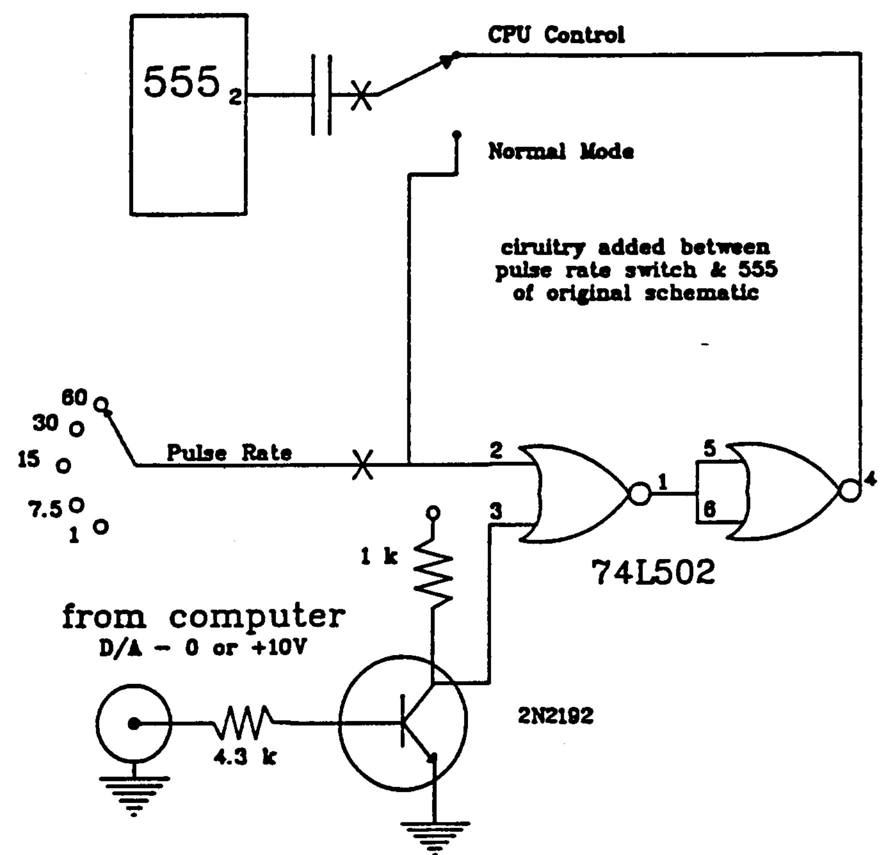


Figure 7.2: LSG Modification Schematic

Section 8

## APPENDIX C.1: PSP Set-up Program

```
C
        PROGRAM MENU
C
C+++++++++++++++++++++++++++++++++++++++++++++++++++++++++++++-
++++++++++++ C
C       PROGRAM DEVELOPED TO SET-UP OPERATING PARAMETERS FOR THE
C       THE PARTICLE SIZING PROGRAM UTILIZING A MENU-TYPE FORMAT.
C
C+++++++++++++++++++++++++++++++++++++++++++++++++++++++++++++-
+++++++++++ C
      REAL*8 PROCESS(2), YESNO(2), ADVANCE(2), LIMIT(3),
BOUNDRY(2)       REAL*8 MAG(2), A, B, C, D, F, G, H, I, J, V, W
      INTEGER TOD(4), DOY(5)
      CHARACTER*10 NUMBER
      CHARACTER*6 FILE1, FILE2
      CHARACTER*1 L(6), M(6)
      LOGICAL*1 IKEY
      BYTE ESC, LINE(50,4)
      DATA ESC / 27 /
      DATA PROCESS, YESNO / 'STATIC', 'DYNAMC', 'YES   ', 'NO
' /       DATA ADVANCE, FILE1 / 'SINGLE', 'AUTO  ', 'TEMP01' /
   DATA LIMIT, FILE2 / 'TIME  ', 'FRAME ', 'PARTCL', 'TEMP01' /
    DATA BOUNDRY, MAG / 'PROCSS', 'REJECT', 'LOW   ', 'HIGH  ' /
      DATA IGPST, WIDTH, NGRPS, ITHRSH, LIMVAL / 5, 5.0, 50, 90,
2000 /       DATA JXSTR, JXDST, JYSTR, JYDST / 50, 400, 50, 400 /
      DATA A, B, C, D / 'DYNAMC', 'YES   ', 'AUTO  ', 'PARTCL'  /
      DATA F, G, H, I / 'REJECT', 'YES   ', 'YES   ', 'YES   '  /
      DATA J, V, W / 'NO    ', 'LOW   ','NO    '  /
      DATA LINE / 200*' ' /
      DATA NUMBER / '1234567890' /
      EQUIVALENCE(L,FILE1)
      EQUIVALENCE(M,FILE2)
      CALL DATE(DOY)
      CALL TIME(TOD)
      WRITE(7,1) ESC, ESC, ESC, ESC
```

```
1     FORMAT(1X,A1,'[81',A1,'[?251',A1,'[H',A1,'[2J')
C
C*** IF DATE NOT SET, INSERT "NO DATE" INTO DATE FIELD
C
      IF( DOY(1) .EQ. '00' ) DOY(5) = '  '
      IF( DOY(1) .EQ. '00' ) DOY(4) = 'TE'
      IF( DOY(1) .EQ. '00' ) DOY(3) = 'DA'
      IF( DOY(1) .EQ. '00' ) DOY(2) = 'O '
      IF( DOY(1) .EQ. '00' ) DOY(1) = ' N'
C
C
C...   INPUT PREVIOUSLY STORED PSP PARAMETERS.
C
      OPEN(UNIT=1, FILE='SETUP.MNU',STATUS='OLD',ERR= 5)
      READ(1,10) A,. B, C, D, LIMVAL, F, G, H, FILE1, I, J, FILE2,
     & IGPST, WIDTH, NGRPS, JXSTR, JXDST, JYSTR, JYDST, ITHRSH,
V, W       READ(1,2)
2     FORMAT(2(/))
      DO 4 II=1,4
      READ(1,3) (LINE(JJ,II), JJ=1,50)
3     FORMAT(3X,50A1)
4     CONTINUE
      GOTO 9 5 OPEN(UNIT=1, FILE='SETUP.MNU',STATUS='NEW')
WRITE(1,10) A, B, C, D, LIMVAL, F, G, H, FILE1, I, J, FILE2,
 & IGPST, WIDTH, NGRPS, JXSTR, JXDST, JYSTR, JYDST, ITHRSH, V, W
      WRITE(1,2)
      DO 6 II=1,4
      WRITE(1,3) (LINE(JJ,II), JJ=1,50)
6     CONTINUE
9     WRITE(7,10) A, B, C, D, LIMVAL, F, G, H, FILE1, I, J,
FILE2,      & IGPST, WIDTH, NGRPS, JXSTR, JXDST, JYSTR, JYDST,
ITHRSH, V, W       CLOSE(UNIT=1)
10    FORMAT('+',T39,'SETUP'/T26,'PARTICLE SIZING PROGRAM (ver.
4)'//      & 33('-'),' PROCESSING OPTIONS',T54,25('-')/
     & T3,'(A)',T9,A6,T19,'Type of Processing',T49,
     & '(STATIC/DYNAMIC)',/
     & T3,'(B)',T9,A6,T19,'Focus Criteria',T49,
     & '(YES/NO)',/
     & T3,'(C)',T9,A6,T19,'Type of Frame Advance',T49,
     & '(AUTO/SINGLE)',/
     & T3,'(D)',T9,A6,T19,'Processing Limit',T49,
     & '(TIME/FRAME/PARTICLE)',/
     & T3,'(E) (',T9,I6,T15,') Limiting Value',T49,
     & '(seconds/frames/particles)',/
     & T3,'(F)',T9,A6,T19,'Boundary Particles',T49,
     & '(PROCESS/REJECT)',/
```

```
     & 36('-'),' OUTPUT OPTIONS ',26('-')/
     & T3,'(G)',T9,A6,T19,'General Results (to PRINTER)
(YES/NO)'/      & T19,'WRITE TO FILE (YES/NO)',T49,
     & '(K) FILE HEADER (4 lines)',/
     & T3,'(H)',T9,A6,T19,'Average Particle size data -- ',T49,
   & '(L) FILE: (',A6,').OUT',/
     & T3,'(I)',T9,A6,T19,'Group Breakdown data ',9('-'),'/'/
 & T3,'(J)',T9,A6,T19,'Per Frame data ',13('-'),'>',T49,      &
'(M) FILE: (',A6,').DAT',/
     & 35('-'),' GENERAL OPTIONS ',26('-')/
     & T3,'(N) Group Start =( ',I3,') '
     & T29,'(O) Group Width =(',F4.1,') '
     & T55,'(P) # of Groups =( ',I3,')'/
     & T3,'(Q) X Window Start = (',I3,')',
     & T49,'(R) X Window Width = (',I3,')'/
     & T3,'(S) Y Window Start = (',I3,')',
     & T49,'(T) Y Window Width = (',I3,')'/
     & T3,'(U) Threshold = (',I3,')'
     & T29,'(V) Lens = ',A6,
     & T49,'(W) Markers = ',A6,'(YES/NO)'/78('-'))
      WRITE(7,20) ESC, ESC
20    FORMAT('+',A1,'[23;2H',A1,'[0J','(X) to exit SETUP menu or
     & (Z) to begin Particle Sizing Program ...,  '/
     & T3,'Enter Letter to change specific Parameter ??')
C
C
C ...    SPECIFY PSP PARAMETER W/ KEY TOGGLE OR KEYBOARD ENTRY.
C
30    CALL IPOKE("44,"10000 .OR.  IPEEK("44))
      IKEY = ITTINR()
      IF(IKEY.LT.0)     GOTO 30
      IF(IKEY.EQ.'A')   GOTO  100
      IF(IKEY.EQ.'B')   GOTO  200
      IF(IKEY.EQ.'C')   GOTO  300
      IF(IKEY.EQ.'D')   GOTO  400
      IF(IKEY.EQ.'E')   GOTO  500
      IF(IKEY.EQ.'F')   GOTO  600
      IF(IKEY.EQ.'G')   GOTO  700
      IF(IKEY.EQ.'H')   GOTO  800
      IF(IKEY.EQ.'I')   GOTO  900
      IF(IKEY.EQ.'J')   GOTO 1000
      IF(IKEY.EQ.'K')   GOTO 1100
      IF(IKEY.EQ.'L')   GOTO 1200
      IF(IKEY.EQ.'M')   GOTO 1300
      IF(IKEY.EQ.'N')   GOTO 1400
      IF(IKEY.EQ.'O')   GOTO 1500
```

```
      IF(IKEY.EQ.'P')   GOTO 1600
      IF(IKEY.EQ.'Q')   GOTO 1700
      IF(IKEY.EQ.'R')   GOTO 1800
      IF(IKEY.EQ.'S')   GOTO 1900
      IF(IKEY.EQ.'T')   GOTO 2000
      IF(IKEY.EQ.'U')   GOTO 2100
      IF(IKEY.EQ.'V')   GOTO 2200
      IF(IKEY.EQ.'W')   GOTO 2400
      IF(IKEY.EQ.'X')   GOTO 2600
C      IF(IKEY.EQ.'Y') GOTO 2500
      IF(IKEY.EQ.'Z')   GOTO 2600
      GO TO 30
90    FORMAT('+',A1,'[23;2H',A1,'[0J',
     & 'Enter new value for (',A1,') here ==>',$)
C
C...  (A) SPECIFY PROCESS TYPE (DYNAMIC/STATIC)
C
100   CALL IPOKE("44,"167777 .AND.  IPEEK("44))
      IF(A.EQ.PROCESS(1)) GOTO 150
      A = PROCESS(1)
      GOTO 180
150   A = PROCESS(2)
180   WRITE(7,190) ESC, A
190   FORMAT('+',A1,'[5;8H',A6)
      GOTO 30 C
C...  (B) SPECIFY FOCUS (YES/NO)
C
200   CALL IPOKE("44,"167777 .AND.  IPEEK("44))
      IF(B.EQ.YESNO(1)) GOTO 250
      B = YESNO(1)
      GOTO 280
250   B = YESNO(2)
280   WRITE(7,290) ESC, B
290   FORMAT('+',A1,'[6;8H',A6)
      GOTO 30
C
C...  (C) TYPE OF FRAME ADVANCE (SINGLE/AUTO)
C
300   CALL IPOKE("44,"167777 .AND.  IPEEK("44))
      IF(C.EQ.ADVANCE(1)) GOTO 350
      C = ADVANCE(1)
      GOTO 380
350   C = ADVANCE(2)
380   WRITE(7,390) ESC, C
390   FORMAT('+',A1,'[7;8H',A6)
      GOTO 30
```

```
C
C...  (D) PROCESSING LIMIT (TIME/PARTICLE/FRAME)
C...  NOTE: DUE TO COMPUTER LIMITATIONS TIME IS NOT INCLUDED C
400   CALL IPOKE("44,"167777 .AND.  IPEEK("44))
      IF(D.EQ.LIMIT(1).OR.D.EQ.LIMIT(2)) GOTO 450
      D = LIMIT(1)
      GOTO 480
450   IF(D.EQ.LIMIT(2)) GOTO 470
      D = LIMIT(2)
      GOTO 480
470   D = LIMIT(3)
480   WRITE(7,490) ESC, D
490   FORMAT('+',A1,'[8;8H',A6)
      GOTO 30
C
C...  (E) SPECIFY LIMITING VALUE
C
500   CALL IPOKE("44,"167777 .AND.  IPEEK("44))
      WRITE(7,90) ESC, ESC, 'E'
      READ(5,*) LIMVAL
580   WRITE(7,590) ESC, LIMVAL
590   FORMAT('+',A1,'[9;8H',I6)
      WRITE(7,20) ESC, ESC
      GOTO 30
C
C...  (F) BOUNDARY ANALYSIS
C...  NOTE: UNAVAILABLE
C
600   CALL IPOKE("44,"167777 .AND. IPEEK("44))
      IF(F.EQ.BOUNDRY(1)) GOTO 650
      F = BOUNDRY(1)
      GOTO 680
650   F = BOUNDRY(2)
680   WRITE(7,690) ESC, F
690   FORMAT('+',A1,'[10;8H',A6)
      GOTO 30
C
C...  (G) OUTPUT GENERAL RESULTS TO PRINTER
C
700   CALL IPOKE("44,"167777 .AND. IPEEK("44))
      IF(G.EQ.YESNO(1)) GOTO 750
      G = YESNO(1)
      GOTO 780
750   G = YESNO(2)
780   WRITE(7,790) ESC, G
790   FORMAT('+',A1,'[12;8H',A6)
```

```
      GOTO 30
C
C...  (H) WRITE TO FILE: ANALYSIS SUMMARY (YES/NO)
C
800   CALL IPOKE("44,"167777 .AND. IPEEK("44))
      IF(H.EQ.YESNO(1)) GOTO 850
      H = YESNO(1)
      GOTO 880
850   H = YESNO(2)
880   WRITE(7,890) ESC, H
890   FORMAT('+',A1,'[14;8H',A6)
      GOTO 30
C
C...  (I) WRITE TO FILE: GROUP BREAKDOWN (YES/NO)
C
900   CALL IPOKE("44,"167777 .AND. IPEEK("44))
      IF(I.EQ.YESNO(1)) GOTO 950
      I = YESNO(1)
      GOTO 980
950   I = YESNO(2)
980   WRITE(7,990) ESC, I
990   FORMAT('+',A1,'[15;8H',A6)
      GOTO 30
C
C...  (J) WRITE TO FILE: PER FRAME DATA (YES/NO)
C
1000  CALL IPOKE("44,"167777 .AND. IPEEK("44))
      IF(J.EQ.YESNO(1)) GOTO 1050
      J = YESNO(1)
      GOTO 1080
1050  J = YESNO(2)
1080  WRITE(7,1090) ESC, J
1090  FORMAT('+',A1,'[16;8H',A6)
      GOTO 30
C
C...  (K) SPECIFY FILE HEADER
C
1100  CALL IPOKE("44,"167777 .AND. IPEEK("44))
      WRITE(7,1110) ESC, ESC, ESC, ESC
1110  FORMAT(1X,A1,'[81',A1,'[?251',A1,'[H',A1,'[2J')
      WRITE(7,1111) ((LINE(JJ,II), JJ=1,50), II=1,4)
1111  FORMAT('+',T39,'SETUP'/T35,'FOR FILE HEADER'//
     & T36,'CHANGE (Y/N)'///T16,54('*'),/T16,'*',T69,'*',
     & 4(/,T16,'* '50A1,' *'),/T16,'*',T69,'*',
     & /T16,54('*')//T31,'(4 LINES/50 SPACES each)')
      CALL IPOKE("44,"10000 .OR. IPEEK("44))
```

```
1115  IKEY = ITTINR()
      IF(IKEY.LT.0) GOTO 1115
      IF(IKEY.EQ.'Y') GOTO  1120
      IF(IKEY.EQ.'N') GOTO 1190
      GOTO 1115
1120  CALL IPOKE("44,"167777 .AND. IPEEK("44))
      DO 1140 II=1,4
      WRITE(7,1125) ESC, ESC, II
1125  FORMAT('+',A1,'[17;3H',A1,'[0J',
     & 'Change Line (',I1,'), (Y/N)')
      CALL IPOKE("44,"10000 .OR. IPEEK("44))
1126  IKEY = ITTINR()
      IF(IKEY.LT.0) GOTO 1126
      IF(IKEY.EQ.'Y') GOTO  1127
      IF(IKEY.EQ.'N') GOTO 1140
      GOTO 1126
1127  CALL IPOKE("44,"167777 .AND. IPEEK("44))
      WRITE(7,1130) ESC, ESC, ESC, II
1130  FORMAT('+',A1,'[22;1H',A1,'[0J',A1,'[?8h',
     & ' Line (',I1,') ==>',$)
      IF(II.EQ.1) GOTO 1141
      IF(II.EQ.2) GOTO 1143
      IF(II.EQ.3) GOTO 1145
      IF(II.EQ.4) GOTO 1147
1140  CONTINUE
      GOTO 1180
1141  READ(5,1170) (LINE(JJ,1), JJ=1,50)
      WRITE(7,1142) ESC, (LINE(JJ,1), JJ=1,50)
1142  FORMAT('+',A1,'[9;15H','* ',50A1,' *')
      GOTO 1140
1143  READ(5,1170) (LINE(JJ,2), JJ=1,50)
      WRITE(7,1144) ESC, (LINE(JJ,2), JJ=1,50)
1144  FORMAT('+',A1,'[10;15H','* ',50A1,' *')
      GOTO 1140
1145  READ(5,1170) (LINE(JJ,3), JJ=1,50)
      WRITE(7,1146) ESC, (LINE(JJ,3), JJ=1,50)
1146  FORMAT('+',A1,'[11;15H','* ',50A1,' *')
      GOTO 1140
1147  READ(5,1170) (LINE(JJ,4), JJ=1,50)
      WRITE(7,1148) ESC, (LINE(JJ,4), JJ=1,50)
1148  FORMAT('+',A1,'[12;15H','* ',50A1,' *')
      GOTO 1140
1170  FORMAT(50A1)
1180  GOTO 1100
1190  WRITE(7,1) ESC, ESC, ESC, ESC
      GOTO 9
```

```
C
C...  (L) FILE SPECIFICATION: GENERAL & GROUP DATA
C
1200  CALL IPOKE("44,"167777 .AND. IPEEK("44))
      WRITE(7,1220) ESC, ESC, 'L'
1220  FORMAT('+',A1,'[23;2H',A1,'[0J',
     & 'File Name (',A1,') (4 letters) here ==>',$)
      READ(5,1230) (L(II), II=1,4)
1230  FORMAT(4A1)
      WRITE(7,1240) ESC, (L(II), II=1,4)
1240  FORMAT('+',A1,'[14;60H',4A1)
      WRITE(7,1250) ESC, ESC, 'L'
1250  FORMAT('+',A1,'[23;2H',A1,'[0J',
     & 'File Number (',A1,') (2 numbers) here ==>',$)
      READ(5,1260) L1
1260  FORMAT(I2)
      I1 = L1/10
      I0 = L1-I1*10
      IF(L1.LT.10)  I1=10
      IF(I0 .EQ. 0) I0=10
      L(5) = NUMBER(I1:I1)
      L(6) = NUMBER(I0:I0)
      IF(L1.LT.10) GOTO 1280
      WRITE(7,1270) ESC, L1
1270  FORMAT('+',A1,'[14;64H',I2)
      WRITE(7,20) ESC, ESC
      GOTO 30
1280  WRITE(7,1290) ESC, L1
1290  FORMAT('+',A1,'[14;64H0',I1)
      WRITE(7,20) ESC, ESC
      GOTO 30
C
C...  (M) FILE SPECIFICATION: PER FRAME DATA
C
1300  CALL IPOKE("44,"167777 .AND. IPEEK("44))
      WRITE(7,1320) ESC, ESC, 'M'
1320  FORMAT('+',A1,'[23;2H',A1,'[0J',
     & 'File Name (',A1,') (4 letters) here ==>',$)
      READ(5,1330) (M(II), II=1,4)
1330  FORMAT(4A1)
      WRITE(7,1340) ESC, (M(II), II=1,4)
1340  FORMAT('+',A1,'[16;60H',4A1)
      WRITE(7,1350) ESC, ESC, 'M'
1350  FORMAT('+',A1,'[23;2H',A1,'[0J',
     & 'File Number (',A1,') (2 numbers) here ==>',$)
      READ(5,1360) M1
```

```
1360  FORMAT(I2)
      I1 = M1/10
      I0 = M1-I1*10
      IF(M1.LT.10)  I1=10
      IF(I0 .EQ. 0) I0=10
      M(5) = NUMBER(I1:I1)
      M(6) = NUMBER(I0:I0)
      IF(M1.LT.10) GOTO 1380
      WRITE(7,1370) ESC, M1
1370  FORMAT('+',A1,'[16;64H',I2)
      WRITE(7,20) ESC, ESC
      GOTO 30
1380  WRITE(7,1390) ESC, M1
1390  FORMAT('+',A1,'[16;64H0',I1)
      WRITE(7,20) ESC, ESC
      GOTO 30
C
C...  (N) DROP-SIZE GROUP BREAKDOWN: STARTING VALUE
C
1400  CALL IPOKE("44,"167777 .AND. IPEEK("44))
      WRITE(7,90) ESC, ESC, 'N'
      READ(5,*) IGPST
1480  WRITE(7,1490) ESC, IGPST
1490  FORMAT('+',A1,'[18;21H',I3)
      WRITE(7,20) ESC, ESC
      GOTO 30
C
C...  (O) DROP-SIZE GROUP BREAKDOWN: INTERVAL WIDTH
C
1500  CALL IPOKE("44,"167777 .AND. IPEEK("44))
      WRITE(7,90) ESC, ESC, 'O'
      READ(5,*) WIDTH
1580  WRITE(7,1590) ESC, WIDTH
1590  FORMAT('+',A1,'[18;46H',F4.1)
      WRITE(7,20) ESC, ESC
      GOTO 30
C
C...  (P) DROP-SIZE GROUP BREAKDOWN: # OF GROUPS
C
1600  CALL IPOKE("44,"167777 .AND. IPEEK("44))
      WRITE(7,90) ESC, ESC, 'P'
      READ(5,*) NGRPS
1680  WRITE(7,1690) ESC, NGRPS
1690  FORMAT('+',A1,'[18;73H',I3)
      WRITE(7,20) ESC, ESC
      GOTO 30
```

```
C
C...  (Q) SIZING WINDOW (PIXEL SPEC): X STARTING VALUE
C
1700  CALL IPOKE("44,"167777 .AND. IPEEK("44))
      WRITE(7,90) ESC, ESC, 'Q'
      READ(5,*) JXSTR
1780  WRITE(7,1790) ESC, JXSTR
1790  FORMAT('+',A1,'[19;24H',I3)
      WRITE(7,20) ESC, ESC
      GOTO 30
C
C...  (R) SIZING WINDOW (PIXEL SPEC): X SCREEN WIDTH
C
1800  CALL IPOKE("44,"167777 .AND. IPEEK("44))
      WRITE(7,90) ESC, ESC, 'R'
      READ(5,*) JXDST
1880  WRITE(7,1890) ESC, JXDST
1890  FORMAT('+',A1,'[19;72H',I3)
      WRITE(7,20) ESC, ESC
      GOTO 30
C
C...  (S) SIZING WINDOW (PIXEL SPEC): Y STARTING VALUE
C
1900  CALL IPOKE("44,"167777 .AND. IPEEK("44))
      WRITE(7,90) ESC, ESC, 'S'
      READ(5,*) JYSTR
1980  WRITE(7,1990) ESC, JYSTR
1990  FORMAT('+',A1,'[20;26H',I3)
      WRITE(7,20) ESC, ESC
      GOTO 30
C
C...  (T) SIZING WINDOW (PIXEL SPEC): Y SCREEN WIDTH
C
2000  CALL IPOKE("44,"167777 .AND. IPEEK("44))
      WRITE(7,90) ESC, ESC, 'T'
      READ(5,*) JYDST
2080  WRITE(7,2090) ESC, JYDST
2090  FORMAT('+',A1,'[20;70H',I3)
      WRITE(7,20) ESC, ESC
      GOTO 30
C
C...  (U) INPUT SIZING THRESHOLD
C
2100  CALL IPOKE("44,"167777 .AND. IPEEK("44))
      WRITE(7,90) ESC, ESC, 'U'
      READ(5,*) ITHRSH
```

```
2180  WRITE(7,2190) ESC, ITHRSH
2190  FORMAT('+',A1,'[21;19H',I3)
      WRITE(7,20) ESC, ESC
      GOTO 30
C
C...  (V) INPUT SYSTEM MAGNIFICATION (HIGH/LOW)
C
2200  CALL IPOKE("44,"167777 .AND. IPEEK("44))
      IF(V.EQ.MAG(1)) GOTO 2250
      V = MAG(1)
      GOTO 2280
2250  V = MAG(2)
2280  WRITE(7,2290) ESC, V
2290  FORMAT('+',A1,'[21;39H',A6)
      GOTO 30
C
C...  (W) DIAGNOSTIC MARKERS PLACED ON COUNTED PARTICLES
C
2300  CALL IPOKE("44,"167777 .AND. IPEEK("44))
      IF(W.EQ.YESNO(1)) GOTO 2350
      W = YESNO(1)
      GOTO 2380
2350  W = YESNO(2)
2380  WRITE(7,2390) ESC, W
2390  FORMAT('+',A1,'[21;62H',A6)
      GOTO 30
C
C...  (Z) STORE SET-UP PARAMETERS AND START PSP
C
2600  CALL IPOKE("44,"167777 .AND. IPEEK("44))
      OPEN(UNIT=1, FILE='SETUP.MNU',STATUS='NEW')
      WRITE(1,10) A, B, C, D, LIMVAL, F, G, H, FILE1, I, J,
FILE2,      & IGPST, WIDTH, NGRPS, JXSTR, JXDST, JYSTR, JYDST,
ITHRSH, V, W       WRITE(1,2605)
2605  FORMAT(2(/))
      DO 2650 II=1,4
      WRITE(1,2610) (LINE(JJ,II), JJ=1,50)
2610  FORMAT(3X,50A1)
2650  CONTINUE
      CLOSE(UNIT=1)
      WRITE(7,2690) ESC, ESC, ESC, ESC
2690  FORMAT(1X,A1,'[8h',A1,'[?25h',A1,'[H',A1,'[2J')
      IF(IKEY.EQ.'Z') CALL SETCMD('RUN PSP1')
      CALL EXIT
2700  STOP
      END
```

Section 9

## APPENDIX C.2: PSP Graphical Presentation of Results

```
C
        PROGRAM GRAPH
C+++++++++++++++++++++++++++++++++++++++++++++++++++++++++++++++++-
+++++++++++ C
C       PROGRAM DEVELOPED FOR THE PSP TO GRAPHICALLY REPRESENT C
     THE GROUP BREAK-DOWN DATA ON A DEC COMPATIBLE TERMINAL. C
C+++++++++++++++++++++++++++++++++++++++++++++++++++++++++++++++++-
+++++++++++ C
        DIMENSION X(1000), Y(1000), Y1(70), X1(70)
        BYTE ESC, CSI, TIM(9), DAY(9)
        CHARACTER*1 A, B, C, H, II, NUMXO, NUMYO, NUMX1, NUMY1
     CHARACTER*11 CO
        CHARACTER*1 NAME(7), JUNK
        CHARACTER*10 NUMBER, FILE
        DATA  A, ESC, CSI /'*', 27, 155 /
        DATA B, C, H /'[', ';', 'f'/
        DATA NUMBER / '1234567890' /
        DATA CO, PI    / '           ', 3.1415926 /
        EQUIVALENCE (NAME(1),B)
        EQUIVALENCE (NAME(2),NUMX1)
        EQUIVALENCE (NAME(3),NUMXO)
        EQUIVALENCE (NAME(4),C)
        EQUIVALENCE (NAME(5),NUMY1)
        EQUIVALENCE (NAME(6),NUMYO)
        EQUIVALENCE (NAME(7),H)
1       DO 5 I=1,1000
        X(I)=0.0
        Y(I)=0.0
5       CONTINUE
        DAVSUM = 0.0
        DSSUM  = 0.0
        DVSUM  = 0.0
        DWSUM  = 0.0
        SUMN   = 0.0
        SUM    = 0.0
```

```
      WEIGHT = 0.0
      COUNT  = 0.0
      DO 6 I=1,70
      X1(I)=0.0
      Y1(I)=0.0
6     CONTINUE
C
C...  INPUT DATA FILE NAME.
C
      WRITE(7,10)
10    FORMAT(1X,'INPUT DATA FILE ==> ',$)
      READ(5,20,ERR=200)FILE
20    FORMAT(A10)
      OPEN(UNIT=2,NAME=FILE,STATUS='OLD')
      DO 30 I=1,1000
      READ(2,*,END=40) X(I),Y(I)
30    CONTINUE
40    INDEX = I-1
      IF(INDEX.EQ.68) GO TO 94
      YMAX = -1.0E+30
      XMIN = 1.0E+30
      XMAX = -1.0E+30
      DO 50 K=1,INDEX
      XMIN = AMIN1(XMIN,Y(K))
50    XMAX = AMAX1(XMAX,Y(K))
      XCEN = (XMIN+XMAX)/2.0
      XSCALE = (XMAX-XMIN)/67.0
      DO 60 J=1,67
      X1(J)=XMIN+XSCALE*FLOAT(J)
60    CONTINUE
      DO 90 L=1,INDEX
      DO 70 M=1,67
      IF(Y(L).GT.X1(M)) GO TO 70
      GO TO 80
70    CONTINUE
      M=68
80    Y1(M)=Y1(M)+1.0
90    CONTINUE
C
C...  STATISTICAL MEAN DIAMETERS DETERMINED
C
      DO 93 I=1,67
      IF(I.EQ.1) GRPAVG = X1(I)/2.0
      IF(I.NE.1) GRPAVG = (X1(I)+X1(I-1))/2.0
      DIAMAX = YMAX
      DAVSUM = DAVSUM + Y1(I)*GRPAVG
```

```
      DSSUM  = DSSUM  + Y1(I)*GRPAVG**2
      DVSUM  = DVSUM  + Y1(I)*GRPAVG**3
      DWSUM  = DWSUM  + Y1(I)*GRPAVG**4
      SUMN   = SUMN   + Y1(I)
      SUM    = SUM    + Y1(I)
      WEIGHT = WEIGHT + (4./3.*PI*(GRPAVG/2.)**3)*Y1(I)
93    CONTINUE
      DAV = DAVSUM/SUMN
      DS  = SQRT(DSSUM/SUM)
      DV  = (DVSUM/SUMN)**(1./3.)
      DVS = DVSUM/DSSUM
      DW  = DWSUM/DVSUM
      NSUM = IFIX(SUM)
      GOTO 97
94    REWIND (2)
      READ(2,*) GCD,DAV,DS,DV,DVS,DW
      DO 95 K=1,67
      X1(K) = X(K+1)
      Y1(K) = Y(K+1)
95    CONTINUE
      XMAX = X1(67)
      XMIN = X1(1)-(X1(67)-X1(66))
      XCEN = (XMIN+XMAX)/2.0
      XQUA = (XCEN-XMIN)/2.0
      X14  = XMIN + XQUA
      X34  = XCEN + XQUA
      COUNT=0.0
97    DO 100 K=1,67
      COUNT=COUNT + Y1(K)
      YMAX = AMAX1(YMAX,Y1(K))
100   CONTINUE
      NSUM = IFIX(COUNT)
      YSCALE = YMAX/21.0
      YSCAL1 = YMAX/199.0
      IYMAX = IFIX(YMAX)
      IYCEN = IFIX(.50*YMAX)
      IY14  = IYCEN/2
      IY34  = IYCEN + IY14
C
C...  UTILIZING THE PSEUDO-GRAPHIC CAPABILITIES OF
C...  DEC COMPATIBLE TERMINALS: INITIATE GRID.
C
      CALL CHARGR
      WRITE(7,105) ESC, ESC
105   FORMAT('+',A1,'*0',A1,'n')
      WRITE(7,110) ESC, ESC, ESC, ESC
```

```
110     FORMAT(1X,A1,'[H',A1,'[2J',A1,'[?3h',A1,'[?25l')
        WRITE(7,115) CO(1:1),IYMAX
115     FORMAT('+',1X,A1,2X,I4,2X,'w',16('q'),'w',16('q'),'w',
  & 16('q'),'w',16('q'),'k')
117     FORMAT(2X,A1,2X,I4,2X,'n',16('q'),'n',16('q'),'n',      &
16('q'),'n',16('q'),'u')
120     FORMAT(2X,A1,8X,'n',16('q'),'n',16('q'),'n',
     & 16('q'),'n',16('q'),'u')
        DO 130 M=1,19
        M1=M
        IF(M.EQ. 5)WRITE(7,117) CO(M1:M1), IY34
        IF(M.EQ. 5) GOTO 130
        IF(M.GT. 5) GOTO 122
        GOTO 128
122     IF(M.EQ.10)WRITE(7,117) CO(M1:M1), IYCEN
        IF(M.EQ.10) GOTO 130
        IF(M.GT.10) GOTO 124
        GOTO 128
124     M1=1
        IF(M.EQ.15)WRITE(7,117) CO(M1:M1), IY14
        IF(M.EQ.15) GOTO 130
128     WRITE(7,140) CO(M1:M1)
130     CONTINUE
140     FORMAT(2X,A1,8X,'x',16X,'x',16X,'x',
     & 16X,'x',16X,'x')
        WRITE(7,120) CO(1:1)
        WRITE(7,145) ESC, ESC, ESC
145     FORMAT('+',A1,'*B',A1,'n',A1,'[0m')
        WRITE(7,146) XMIN, X14, XCEN, X34, XMAX
146     FORMAT(8X,F5.1,12X,F5.1,12X,F5.1,12X,F5.1,12X,F5.1,
& //37X,'DIAMETER [microns]')
        WRITE(7,161) ESC, ESC
        WRITE(7,147) ESC, ESC, ESC, ESC, ESC, ESC
147     FORMAT('+',A1,'[7;2f 5',
     & A1,'[8;2f 6',
     & A1,'[9;2f 7',
     & A1,'[10;2f 8',
     & A1,'[11;2f 9',
     & A1,'[12;2f :')
161     FORMAT('+',A1,'* @',A1,'n')
        DO 168 J = 12,78
        J1 = J/10
        J0 = J - J1*10
        IF(J.LT.10)J1=10
        IF(J0.EQ.0)J0=10
        NUMY0 = NUMBER(J0:J0)
```

```
      NUMY1 = NUMBER(J1:J1)
C
C...  HISTOGRAM SCREEN PLOT
C
      J2 = J-11
      IF(Y1(J2).LE.0.0) GOTO 168
      NN2 = 4
      NN1 = IFIX(Y1(J2)/YSCAL1)
      I1 = 2
      I0 = 1
      NUMX0 = NUMBER(I0:I0)
      NUMX1 = NUMBER(I1:I1)
      IF(NN1.GT.4) GOTO 162
      IF(NN1.EQ.1)    WRITE(7,163) ESC, (NAME(K),K=1,7)
      IF(NN1.EQ.2)    WRITE(7,164) ESC, (NAME(K),K=1,7)
      IF(NN1.EQ.3)    WRITE(7,165) ESC, (NAME(K),K=1,7)
      GOTO 168
162   WRITE(7,166) ESC, (NAME(K),K=1,7)
163   FORMAT('+',A1,7A1,'1')
164   FORMAT('+',A1,7A1,'2')
165   FORMAT('+',A1,7A1,'3')
166   FORMAT('+',A1,7A1,'4')
      DO 167 I = 20,1,-1
      NN2 = NN2 + 10
      IF(NN2.GT.NN1) GOTO 250
      I1 = I/10
      I0 = I - I1*10
      IF(I.LT.10)I1=10
      IF(I0.EQ.0)I0=10
      NUMX0 = NUMBER(I0:I0)
      NUMX1 = NUMBER(I1:I1)
      WRITE(7,169) ESC, (NAME(K),K=1,7)
167   CONTINUE
250   NN2 = NN2 - 10
      NN2 = NN1 - NN2
      I1 = I/10
      I0 = I - I1*10
      IF(I.LT.10)I1=10
      IF(I0.EQ.0)I0=10
      NUMX0 = NUMBER(I0:I0)
      NUMX1 = NUMBER(I1:I1)
      IF(NN2.EQ.1)    WRITE(7,301) ESC, (NAME(K),K=1,7)
      IF(NN2.EQ.2)    WRITE(7,302) ESC, (NAME(K),K=1,7)
      IF(NN2.EQ.3)    WRITE(7,303) ESC, (NAME(K),K=1,7)
      IF(NN2.EQ.4)    WRITE(7,304) ESC, (NAME(K),K=1,7)
      IF(NN2.EQ.5)    WRITE(7,305) ESC, (NAME(K),K=1,7)
```

```
        IF(NN2.EQ.6)    WRITE(7,306) ESC, (NAME(K),K=1,7)
        IF(NN2.EQ.7)    WRITE(7,307) ESC, (NAME(K),K=1,7)
        IF(NN2.EQ.8)    WRITE(7,308) ESC, (NAME(K),K=1,7)
        IF(NN2.EQ.9)    WRITE(7,309) ESC, (NAME(K),K=1,7)
168     CONTINUE
301     FORMAT('+',A1,7A1,'A')
302     FORMAT('+',A1,7A1,'B')
303     FORMAT('+',A1,7A1,'C')
304     FORMAT('+',A1,7A1,'D')
305     FORMAT('+',A1,7A1,'E')
306     FORMAT('+',A1,7A1,'F')
307     FORMAT('+',A1,7A1,'G')
308     FORMAT('+',A1,7A1,'H')
309     FORMAT('+',A1,7A1,'I')
169     FORMAT('+',A1,7A1,'J')
C
C...  OUTPUT MEAN DIAMETERS TO SCREEN
C
        WRITE(7,145) ESC, ESC, ESC
        CALL DATE(DAY)
        CALL TIME(TIM)
        WRITE(7,170) ESC
170     FORMAT('+',A1,'[3;85f','Spatial Distribution .........
')         WRITE(7,171) ESC, GCD
171     FORMAT('+',A1,'[5;85f','             Most Probable Dia.
=',F7.1)         WRITE(7,172) ESC, DAV
172     FORMAT('+',A1,'[6;85f','    Arithmetic Mean Dia. (D10)
=',F7.1)         WRITE(7,173) ESC, DS
173     FORMAT('+',A1,'[7;85f','       Surface Mean Dia. (D20)
=',F7.1)         WRITE(7,174) ESC, DV
174     FORMAT('+',A1,'[8;85f',' Volume (Mass) Mean Dia. (D30)
=',F7.1)         WRITE(7,175) ESC, DVS
175     FORMAT('+',A1,'[9;85f','        Sauter Mean Dia. (D32)
=',F7.1)         WRITE(7,176) ESC, NSUM
176     FORMAT('+',A1,'[11;85f','                    Total Count
=',I7)         WRITE(7,177) ESC, FILE
177     FORMAT('+',A1,'[16;85f','            File: ',A10)
        WRITE(7,178) ESC, DAY
178     FORMAT('+',A1,'[17;85f','            Date: ',9A1)
        WRITE(7,179) ESC, TIM
179     FORMAT('+',A1,'[18;85f','            Time: ',9A1)
        READ(7,198) JUNK
198     FORMAT(A1)
        WRITE(7,199) ESC, ESC, ESC, ESC, ESC
199     FORMAT(1X,A1,'[Om',A1,'[H',A1,'[?31',A1,'[2J',A1,'[?25h')
        CLOSE(2)
```

```
      CALL SETCMD('RUN GRAPH')
      CALL EXIT
200   STOP
      END
C
C...  SUBROUTINE UTILIZED TO SET-UP HISTOGRAM SYMBOLS
C
      SUBROUTINE CHARGR
      BYTE ESC
      DATA ESC / 27 /
      WRITE(7,147) ESC, ESC
147   FORMAT('+',A1,'P0;33;1;0;0;0{ @???????/GGGGGGG',A1,'\')
     WRITE(7,148) ESC, ESC
148   FORMAT('+',A1,'P0;34;1;0;0;0{ @???????/KKKKKKK',A1,'\')
     WRITE(7,149) ESC, ESC
149   FORMAT('+',A1,'P0;35;1;0;0;0{ @???????/MMMMMMM',A1,'\')
     WRITE(7,150) ESC, ESC
150   FORMAT('+',A1,'P0;36;1;0;0;0{ @???????/NNNNNNN',A1,'\')
     WRITE(7,151) ESC, ESC
151   FORMAT('+',A1,'P0;37;1;0;0;0{ @_______/NNNNNNN',A1,'\')
      WRITE(7,152) ESC, ESC
152   FORMAT('+',A1,'P0;38;1;0;0;0{ @ooooooo/NNNNNNN',A1,'\')
     WRITE(7,153) ESC, ESC
153   FORMAT('+',A1,'P0;39;1;0;0;0{ @wwwwwww/NNNNNNN',A1,'\')
     WRITE(7,154) ESC, ESC
154   FORMAT('+',A1,'P0;40;1;0;0;0{ @{{{{{{{/NNNNNNN',A1,'\')
     WRITE(7,155) ESC, ESC
155   FORMAT('+',A1,'P0;41;1;0;0;0{ @}}}}}}}/NNNNNNN',A1,'\')
     WRITE(7,156) ESC, ESC
156   FORMAT('+',A1,'P0;42;1;0;0;0{ @~~~~~~~/NNNNNNN',A1,'\')
     WRITE(7,157) ESC, ESC
157   FORMAT('+',A1,'P0;17;1;0;0;0{ @WWWWWWW/???????',A1,'\')
     WRITE(7,158) ESC, ESC
158   FORMAT('+',A1,'P0;18;1;0;0;0{ @[[[[[[[/???????',A1,'\')
     WRITE(7,159) ESC, ESC
159   FORMAT('+',A1,'P0;19;1;0;0;0{ @]]]]]]]/???????',A1,'\')
     WRITE(7,160) ESC, ESC
160   FORMAT('+',A1,'P0;20;1;0;0;0{ @^^^^^^^/???????',A1,'\')
     WRITE(7,161) ESC, ESC
161   FORMAT('+',A1,'P0;21;1;0;0;0{ @NOOM@@]/???????',A1,'\')
     WRITE(7,162) ESC, ESC
162   FORMAT('+',A1,'P0;22;1;0;0;0{ @^CCCCCC/???????',A1,'\')
     WRITE(7,163) ESC, ESC
163   FORMAT('+',A1,'P0;23;1;0;0;0{ @PXTTTRP/???????',A1,'\')
     WRITE(7,164) ESC, ESC
164   FORMAT('+',A1,'P0;24;1;0;0;0{ @PPPPPPM/???????',A1,'\')
```

```
      WRITE(7,165) ESC, ESC
165     FORMAT('+',A1,'P0;25;1;0;0;0{ @MPPPPPM/???????',A1,'\')
      WRITE(7,166) ESC, ESC
166     FORMAT('+',A1,'P0;26;1;0;0;0{ @MP000PM/???????',A1,'\')
      CALL EXIT
        STOP
        END
```

Section 10

## APPENDIX C.3: MOD-1 Nozzle Input Pressure Determination

```
C
       SUBROUTINE PRESSURE(NCHCK)
C+++++++++++++++++++++++++++++++++++++++++++++++++++++++++++++++-
+++++++++++ C
C      SUBROUTINE TO DETERMINE WATER AND AIR PRESSURE FROM C
  THE OMEGA TRANSDUCERS USING THE AXV11-C A-D BOARD. C
C+++++++++++++++++++++++++++++++++++++++++++++++++++++++++++++++-
+++++++++++         LOGICAL*1 IKEY
       BYTE ESC
       DATA ESC / 27 /
       CALL IPOKE("44,"10000.OR.IPEEK("44))
C
C...   THE FOLLOWING ARE THE APPROPRIATE OCTAL VALUES TO
C...  BE STORED IN THE CSRs OF CH.  1 & 2 TO START AN
C...   A TO D CONVERSION OF THE PRESSURE TRANSDUCERS.
C
       ISTRT1 = "415
       ISTRT2 = "1015
C
       IF(NCHCK.EQ.1) GOTO 12
       WRITE(7,10) ESC, ESC, ESC
10     FORMAT('+',A1,'[2J',A1,'[?25l',A1,'[H')
       WRITE(7,11) ESC
11     FORMAT(1X,A1,'#6',' PRESS "C" to continue')
C
C...   17770400 IS THE CSR (CONTROL STATUS REGISTER) FOR CH. 1
C
12     CALL IPOKE("17770400,ISTRT1)
13     ICHK = IPEEK("17770400)
       IF(ICHK.NE."614) GOTO 13
C
C...   17770402 IS THE DBR (DATA BUFFER REGISTER) FOR CH. 1
C...   AND IPW IS THE WATER PRESSURE (DIGITAL VOLTS).
C
       IPW = IPEEK("177770402)
```

```
      CALL IPOKE("17770400,ISTRT2)
14    ICHK = IPEEK("17770400)
      IF(ICHK.NE."1214) GOTO 14
      IPA = IPEEK("17770402)
      IPA = -1.189 + 0.4598*IPA
      IPW = -1.95 + 0.4598*IPW
C
C...  OUTPUT PRESSURE VALUES TO TERMINAL SCREEN
C
      WRITE(7,18) ESC, ESC, IPW, IPA
      WRITE(7,19) ESC, ESC, IPW, IPA
      IF(NCHCK.EQ.1) GOTO 25
      IKEY = ITTINR()
      IF(IKEY.EQ.'C') GOTO 20
      GOTO 12
18    FORMAT('+',A1,'[22;1f',A1,'#3','WATER PRESSURE = ',
& I3,' AIR PRESSURE = ',I3)
19    FORMAT('+',A1,'[23;1f',A1,'#4','#WATER PRESSURE = ',
 & I3,' AIR PRESSURE = ',I3)
20    CALL IPOKE("44,"167777.AND.IPEEK("44))
      WRITE(7,21) ESC,ESC
21    FORMAT('+',A1,'[H',A1,'[2J')
25    RETURN
      END
```

Section 11

## APPENDIX C.4: PSP Magnification Correction Factor Determination

```
C
C+++++++++++++++++++++++++++++++++++++++++++++++++++++++++++++-
++++++++ C
C       FUNCTIONS TO DETERMINE CORRECTION FACTORS FOR
C       MICRON TO PIXEL FACTORS WHICH DEPEND ON X AND Y.
C
C+++++++++++++++++++++++++++++++++++++++++++++++++++++++++++++-
++++++++          FUNCTION   XFACT(MAG,XPOS,YPOS)
        IF(MAG.EQ.500) GOTO 100
C
C...    HIGH MAGNIFICATION X-CORRECTION
C
        IF(XPOS.LE.100.0) XFACT=0.977+YPOS*8.09E-05
        IF(XPOS.GT.100.0.AND.XPOS.LE.150.0)
XFACT=0.974+YPOS*2.60E-05
IF(XPOS.GT.150.0.AND.XPOS.LE.200.0) XFACT=0.967-YPOS*8.12E-07
    IF(XPOS.GT.200.0.AND.XPOS.LE.250.0) XFACT=0.961+YPOS*4.73E-06
        IF(XPOS.GT.250.0.AND.XPOS.LE.300.0) XFACT=0.961-
YPOS*5.46E-05         IF(XPOS.GT.300.0.AND.XPOS.LE.350.0)
XFACT=0.948-YPOS*3.72E-05
IF(XPOS.GT.350.0.AND.XPOS.LE.400.0) XFACT=0.943-YPOS*6.80E-05
    IF(XPOS.GT.400.0) XFACT=0.920-YPOS*2.58E-05
        RETURN
100     IF(XPOS.LE.100.0) XFACT=2.21+YPOS*0.290E-04
C
C...    LOW MAGNIFICATION X-CORRECTION
C
        IF(XPOS.GT.100.0.AND.XPOS.LE.150.0)
XFACT=2.22+YPOS*0.803E-04
IF(XPOS.GT.150.0.AND.XPOS.LE.200.0) XFACT=2.16+YPOS*0.679E-04
    IF(XPOS.GT.200.0.AND.XPOS.LE.250.0) XFACT=2.16+YPOS*0.442E-07
        IF(XPOS.GT.250.0.AND.XPOS.LE.300.0) XFACT=2.16-
YPOS*0.947E-04          IF(XPOS.GT.300.0.AND.XPOS.LE.350.0)
XFACT=2.11-YPOS*0.306E-07
IF(XPOS.GT.350.0.AND.XPOS.LE.400.0) XFACT=2.10-YPOS*0.124E-03
```

```
    IF(XPOS.GT.400.0) XFACT=2.07-YPOS*0.135E-03
        RETURN
        END
C
        FUNCTION   YFACT(MAG,XPOS,YPOS)
        IF(MAG.EQ.500) GOTO 100
C
C...     HIGH MAGNIFICATION Y-CORRECTION
C
        IF(XPOS.LE.100.0) YFACT=0.977-YPOS*9.17E-05
        IF(XPOS.GT.100.0.AND.XPOS.LE.150.0) YFACT=0.981-
YPOS*1.24E-04          IF(XPOS.GT.150.0.AND.XPOS.LE.200.0)
YFACT=0.981-YPOS*1.19E-04
IF(XPOS.GT.200.0.AND.XPOS.LE.250.0) YFACT=0.990-YPOS*1.63E-04
    IF(XPOS.GT.250.0.AND.XPOS.LE.300.0) YFACT=1.000-YPOS*1.96E-04
        IF(XPOS.GT.300.0.AND.XPOS.LE.350.0) YFACT=1.014-
YPOS*2.19E-04          IF(XPOS.GT.350.0.AND.XPOS.LE.400.0)
YFACT=1.027-YPOS*2.63E-04          IF(XPOS.GT.400.0) YFACT=1.029-
YPOS*2.69E-04
        RETURN

100     IF(XPOS.LE.100.0) YFACT=2.10-YPOS*0.183E-03
C
C...     LOW MAGNIFICATION Y-CORRECTION
C
        IF(XPOS.GT.100.0.AND.XPOS.LE.150.0) YFACT=2.15-
YPOS*0.268E-03          IF(XPOS.GT.150.0.AND.XPOS.LE.200.0)
YFACT=2.12-YPOS*0.315E-03
IF(XPOS.GT.200.0.AND.XPOS.LE.250.0) YFACT=2.13-YPOS*0.313E-03
    IF(XPOS.GT.250.0.AND.XPOS.LE.300.0) YFACT=2.15-YPOS*0.397E-03
        IF(XPOS.GT.300.0.AND.XPOS.LE.350.0) YFACT=2.18-
YPOS*0.484E-03          IF(XPOS.GT.350.0.AND.XPOS.LE.400.0)
YFACT=2.19-YPOS*0.505E-03          IF(XPOS.GT.400.0) YFACT=2.18-
YPOS*0.509E-03
        RETURN
        END
```

Section 12

## APPENDIX D: Mean Diameter Calculations

Arithmetic Mean Diameter (AMD)

$$D(10) = \frac{\sum_{i=1}^{N} n_i d_i}{\sum_{i=1}^{N} n_i}$$

Area Mean Diameter (ArMD)

$$D(20) = \sqrt{\frac{\sum_{i=1}^{N} n_i d_i^2}{\sum_{i=1}^{N} n_i}} \tag{12.1}$$

Volume Mean Diameter (VMD)

$$D(30) = \sqrt[3]{\frac{\sum_{i=1}^{N} n_i d_i^3}{\sum_{i=1}^{N} n_i}} \tag{12.2}$$

Sauter Mean Diameter (SMD)

$$D(32) = \frac{\sum_{i=1}^{N} n_i d_i^3}{\sum_{i=1}^{N} n_i d_i^2} \tag{12.3}$$

where
N = total number of bins
ni = counts per bin
di = diameter for size class i

Section 13

## APPENDIX E: Cole-Palmer Flowmeter Calibration Data

| Scale Reading | Flow-rate (gpm)[1] |
|---|---|
| 30 | 0.022 |
| 40 | 0.031 |
| 50 | 0.040 |
| 60 | 0.050 |
| 70 | 0.059 |
| 80 | 0.069 |
| 90 | 0.078 |
| 100 | 0.090 |
| 110 | 0.100 |
| 120 | 0.110 |
| 130 | 0.120 |
| 140 | 0.130 |

*Calibration values were verified by replication.

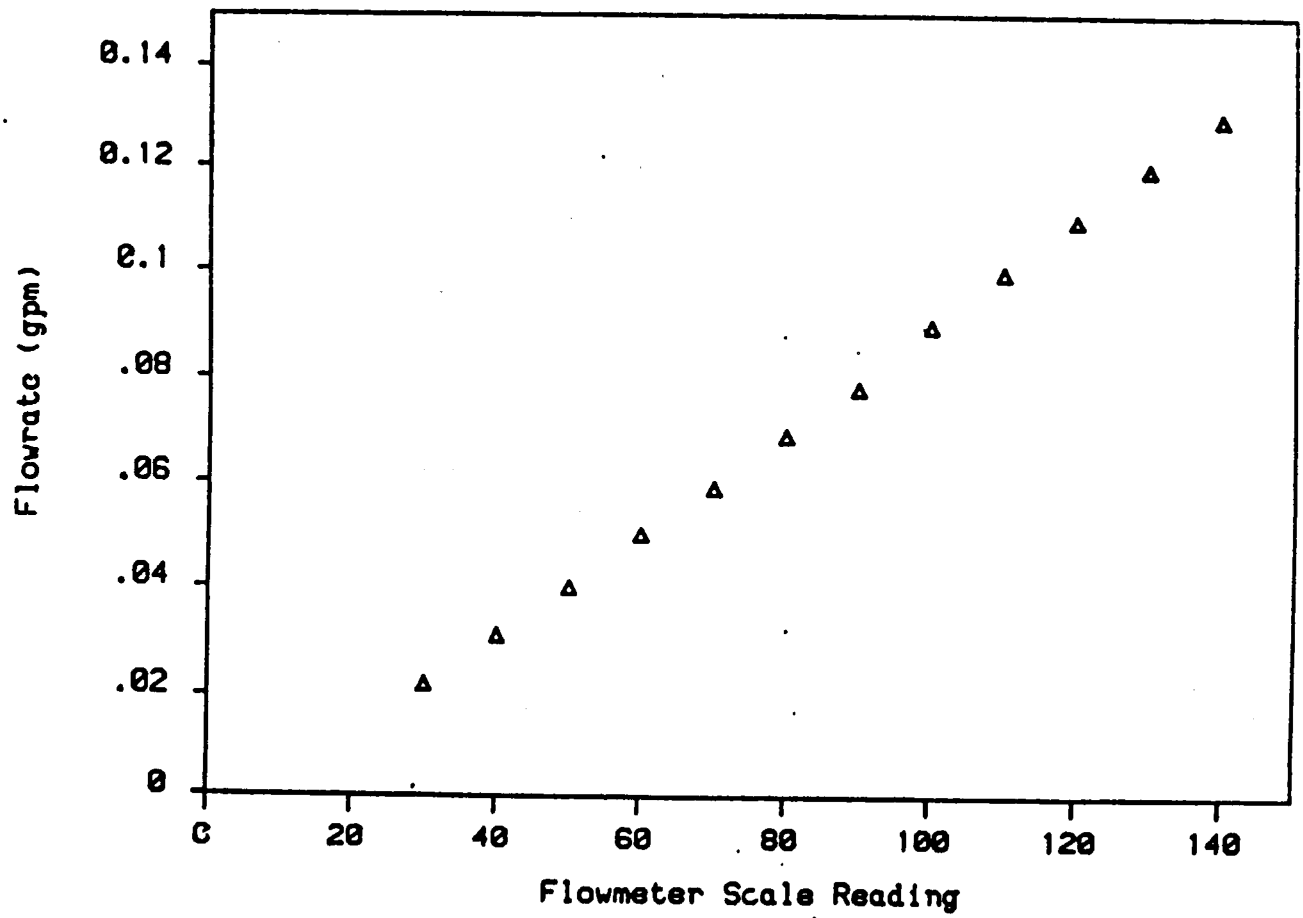


Figure 13.1: Cole-Palmer Flowmeter Calibration

Section 14

## APPENDIX F: OMEGA Pressure Transducer Calibration Data

Table 14.1: S/N: 850502

| Standard Pressure Corrected to psia | Output Voltage (millivolts) |
|---|---|
| 0 | 9.20 |
| 10 | 15.00 |
| 20 | 21.70 |
| 30 | 28.30 |
| 40 | 34.80 |
| 50 | 41.45 |
| 60 | 47.95 |
| 70 | 55.20 |
| 80 | 61.70 |
| 90 | 68.60 |
| 100 | 75.20 |
| 110 | 80.70 |

Table 14.2: OMEGA S/N: 850311

| Standard Pressure Corrected to psia | Output Voltage (millivolts) |
|---|---|
| 0 | 9.80 |
| 10 | 16.00 |
| 20 | 22.90 |
| 30 | 29.10 |
| 40 | 35.75 |
| 50 | 42.60 |
| 60 | 49.10 |
| 70 | 56.20 |
| 80 | 62.60 |
| 90 | 69.40 |
| 100 | 75.80 |
| 110 | 81.50 |

*Calibration values were verified by replication.

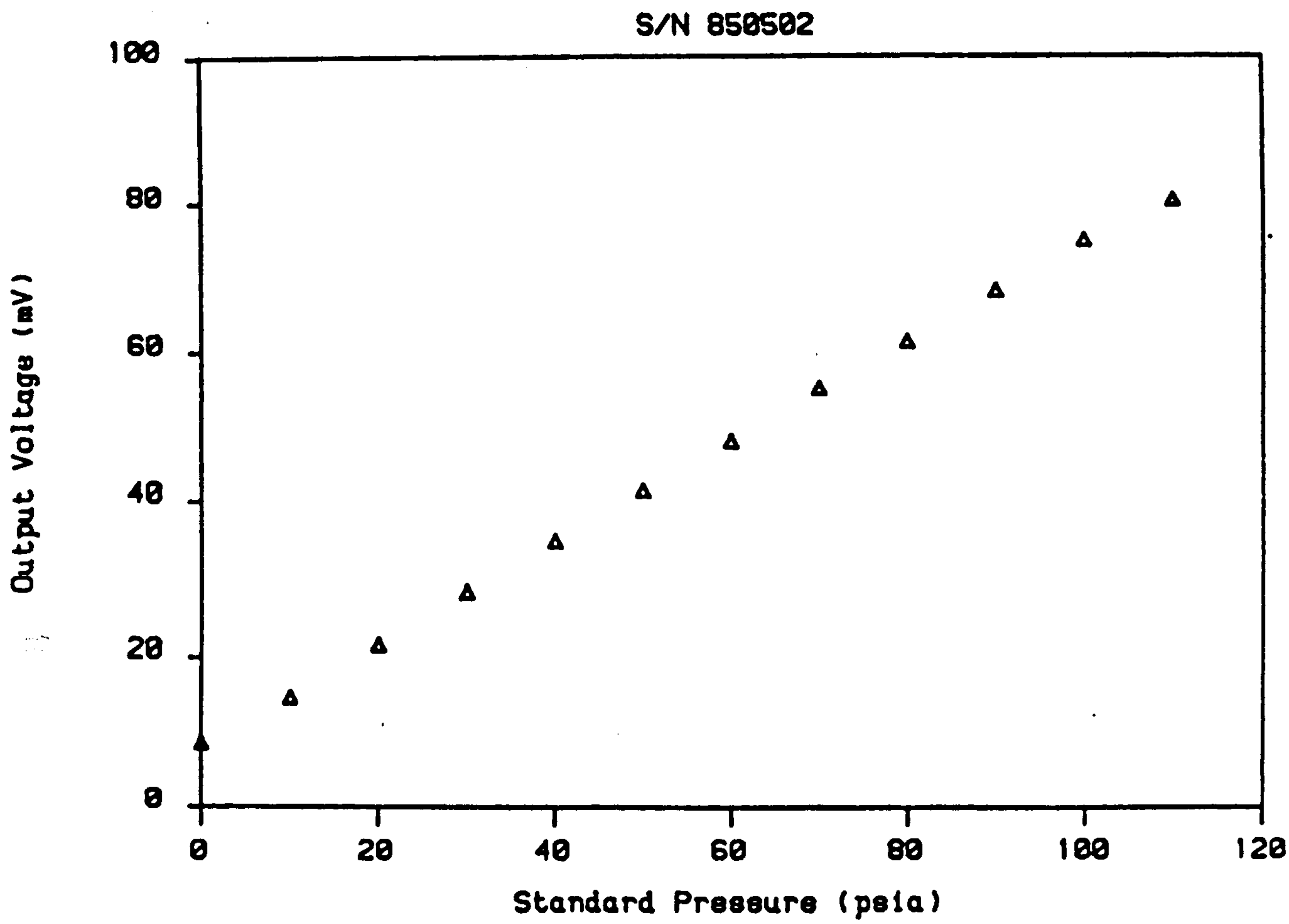


Figure 14.1: OMEGA Pressure Transducer Calibration

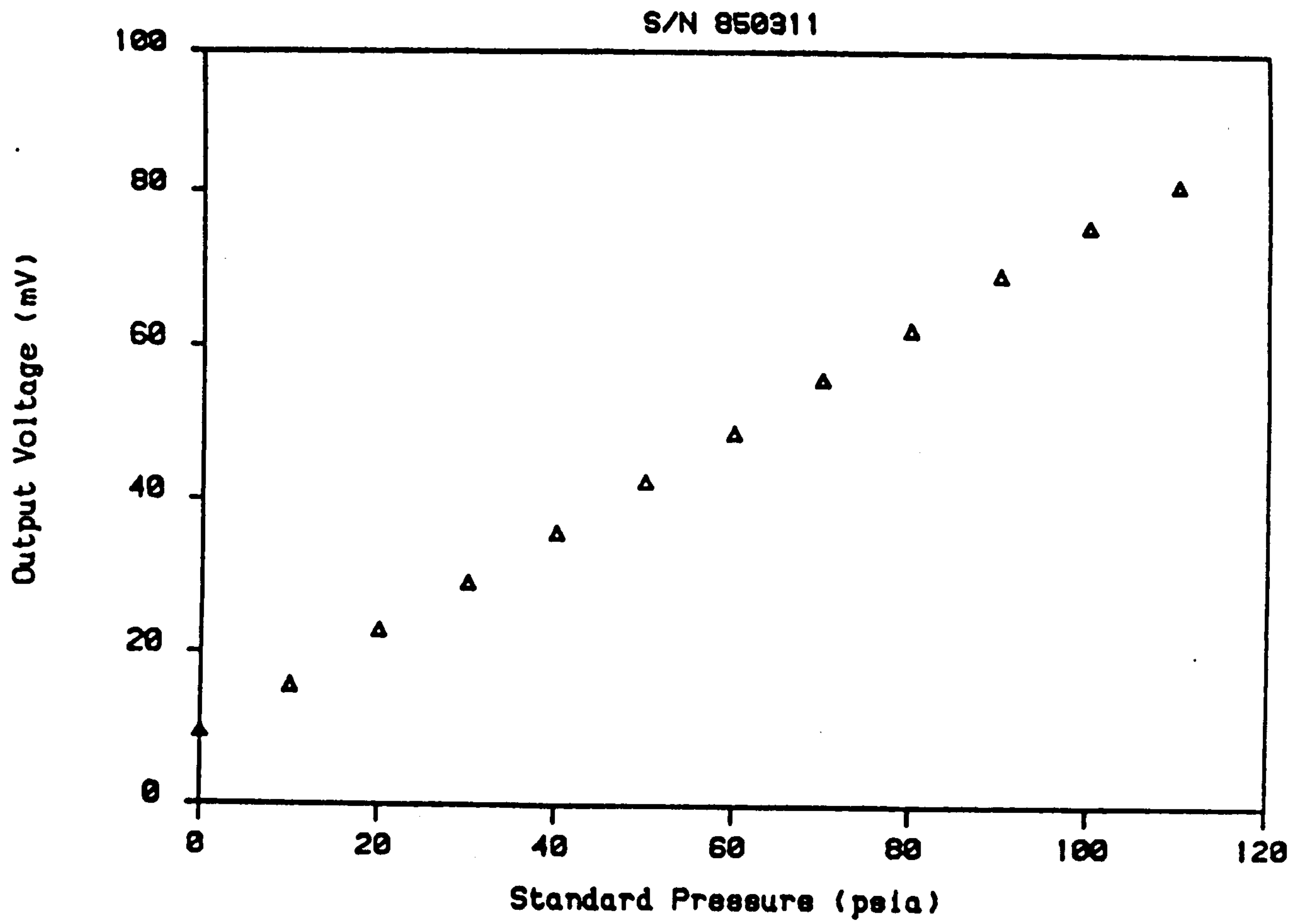


Figure 14.2: OMEGA Pressure Transducer Calibration